The International Journal of Advanced Manufacturing Technology (2022) 121:127–169
https://doi.org/10.1007/s00170-022-09406-7

CRITICAL REVIEW

A comprehensive review on 3D printing advancements in polymer composites: technologies, materials, and applications

Praveenkumara Jagadeesh[1] · Madhu Puttegowda[2] · Sanjay Mavinkere Rangappa[1] · Karfidov Alexey[3] · Sergey Gorbatyuk[3] · Anish Khan[4] · Mrityunjay Doddamani[5] · Suchart Siengchin[1]

Received: 16 December 2021 / Accepted: 22 May 2022 / Published online: 31 May 2022

Abstract

3D printing is a constantly expanding technology that represents one of the most exciting and disruptive production possibilities available today. This technology has gained global recognition and garnered considerable attention in recent years. However, technological breakthroughs, particularly in the field of material science, continue to be the focus of research, particularly in terms of future advancements. The 3D printing techniques are employed for the manufacturing of advanced multifunctional polymer composites due to their mass customization, freedom of design, capability to print complex 3D structures, and rapid prototyping. The advantages of 3D printing with multipurpose materials enable solutions in challenging locations such as outer space and extreme weather conditions where human involvement is not possible. Each year, numerous research papers are published on the subject of imbuing composites with various capabilities such as magnetic, sensing, thermal, embedded circuitry, self-healing, and conductive qualities by the use of innovative materials and printing technologies. This review article discusses the various 3D printing techniques used in the manufacture of polymer composites, the various types of reinforced polymer composites (fibers, nanomaterials, and particles reinforcements), the characterization of 3D printed parts, and their applications in a various industries. Additionally, this review discussed the limitations of 3D printing processes, which may assist future researchers in increasing the utility of their works and overcoming the shortcomings of previous works. Additionally, this paper discusses processing difficulties, anisotropic behavior, stimuli-responsive characteristics (shape memory and self-healing materials), CAD constraints, layer-by-layer appearance, and void formation in printed composites. Eventually, the promise of maturing technology is discussed, along with recommendations for research activities that are desperately required to realize the immense potential of operational 3D printing.

Keywords 3D printing · Technologies · Polymer composites · Additive manufacturing · Multi-functionality · Applications

1 Introduction

3D printing is one of the latest popular technologies of manufacturing, in which it is a process of layer-by-layer deposition of plastics or metals to create a three-dimensional object. This 3D printing is also referred to as rapid prototyping (RP), solid freeform (SFF), or additive manufacturing (AM) technique, and it was invented by Charles Hull in the year of 1986 [1, 2]. AM is distinct from typical manufacturing methods like as casting, forging, and machining, which involve the

✉ Sanjay Mavinkere Rangappa
mavinkere.r.s@op.kmutnb.ac.th; mcemrs@gmail.com

Suchart Siengchin
suchart.s.pe@tggs-bangkok.org

[1] Natural Composites Research Group Lab, Department of Materials and Production Engineering, The Sirindhorn International Thai-German Graduate School of Engineering (TGGS), King Mongkut's University of Technology North Bangkok (KMUTNB), Bangkok, Thailand

[2] Department of Mechanical Engineering, Malnad College of Engineering, Hassan, Visvesvaraya Technological University, Belagavi, Karnataka, India

[3] Department of Engineering of Technological Equipment, National University of Science and Technology MISIS, Moscow, Russia

[4] Chemistry Department, Faculty of Science, King Abdulaziz University, Jeddah, Saudi Arabia

[5] Advanced Manufacturing Lab, Department of Mechanical Engineering, National Institute of Technology Karanataka (NITK), Surathkal, P.O. Srinivasanagar, D.K., Mangalore 575 025, Karanataka, India

removal of materials from a block or injection of materials into a mold to make the product. For subtractive manufacturing in the classical sense, comprehensive process planning is required to calculate the machining steps necessary to create the physical designs. By comparison, AM is a tool-less technique that can help to reduce both equipment wear and setup times. Additionally, additive manufacturing allows for greater design freedom. In general, there seem to be no design constraints, as AM is a layer-by-layer approach. The layer thickness is usually on the order of a hundredth of a millimeter. Choosing a lesser layer thickness improves the approximation of the virtual and actual geometries. The layer thickness, on the other hand, is restricted by the parameters of the input material, such as the liquid build material's surface tension or the powder particle size if sintering is utilized. Additionally, because the shape of a component may be easily modified, AM enables more customizable and customized solutions. Furthermore, AM is employed for topology optimization, which has an effect on the process and supply chain. In the past decades, 3D printing was utilized only for creating prototypes of an object, and now it is being used for creating 3D objects in place of traditional manufacturing methods. The 3D printing setup cost is minimal which allows a higher degree of customization, as the first and last item cost is similar. Hence, it is an ideal technique for the kind production of products at affordable or cost-effective prices [3–5]. Now, designs, rather than physical objects, can be transported anywhere in the world as digital files and printed on any printer that meets the design specifications. The Internet eliminates the distance factor in information transfer, and 3D printing eliminates it for the material world. The simple written document is sent as a PDF file, and it is printed in 2D, and then the "STL" design file is sent to the other side instantly using the internet and finally printed in 3D form. Here, there is no necessity of building inventories of spare parts or new products while printing 3D objects in demanding conditions [6–9]. This manufacturing technique is capable to produce multi-types of wide-range 3D complex products without the problem of retooling, and the customization of printing is done without any additional costs. The quick apparent benefit of 3D printing is the capability of creating complex shapes that are not possible using traditional methods [10, 11]. Modeling AM processes presents its own set of difficulties. To begin, one must establish how the materials' addition will be modeled. Then there are unavoidable non-linearities inherent in the process, such as temperature dependency of thermal characteristics, fourth-order reliance of radiation heat losses, fluidity, and massive deformation models that must be taken into account. Initially, this technique allows designers to place a relevant material only where it is needed, and there is the possibility of utilizing natural resources (bone, wood, coral) to create stiffer and stronger lightweight structures. This computer-operated process requires a low-level expert operator, and it reduces human interaction while printing the objects. Furthermore, the direct part creation from the stored system model ensures that the printed part shows the replica of designer intent and eliminates the inaccuracies that exist in the traditional processes [12–15]. This AM technique has more advantages over traditional methods, such as lower consumption of energy, higher efficiency of using raw materials, less chemical usage, the possibility of producing environmentally friendly objects, and reduced scrap and material waste. There are different types of 3D printing techniques, namely, selective laser sintering (SLS), stereolithography (SLA), fused deposition modeling (FDM), inkjet bioprinting, direct ink writing (DIW), laser-induced forward transfer (LIFT), and PolyJet printing, etc. These techniques are especially preferred for the fabrication of polymer-based components using both thermoplastic and thermosetting polymer materials. The thermoplastic materials like polylactic acid (PLA), polycarbonate (PC), polyamide (PA), and acrylonitrile butadiene styrene (ABS), as well as epoxy resins (thermosetting materials), were processed using 3D printing techniques [16–19]. The epoxy resin is a commonly used polymer material in fiber-reinforced composites, and it is a reactive material that requires UV assisted or thermal curing to complete the process of polymerization. Hence, this material is suitable for thermal or UV-based 3D printing processes. These attracting factors of 3D printing are utilized for the manufacturing of complex parts in various industries, like architectural industries, biomedical fields, construction and building, aerospace, and small automotive component industries. However, there are some disadvantages associated with 3D printing techniques, such as limited material' usage, the requirement for post-processing, restricted printing size, lack of strength, reduction of fully functional behavior, and 3D printing reduces employment [20–23]. These issues can be reduced by combining reinforcement and matrix to achieve functional properties that are not possible using individual constituents. Figure 1 depicts the introduction of multifunctional properties from polymer to 3D printed polymer and then to 3D printed component. The functional properties such as thermal conductivity, electrical conductivity, actuating abilities, sensing, and self-healing are obtained either by incorporating additives or by customizing the component design [24–26].

The production of 3D complex geometric components is also possible using conventional techniques like casting and molding, and this process has happened through the material removal process, which causes the requirement of bulk raw materials and the utilization of more energy, dimensional inaccuracies, more production time, and material wastage occurring while removing excess material [27–29]. However, composites obtained from these processes are well understood and controlled, while difficulty occurs in the control of complex internal design structures. In current

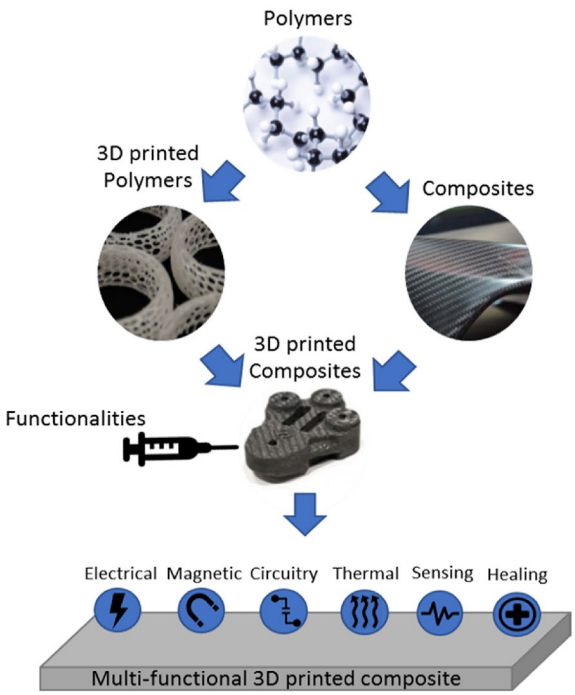

Fig. 1 Multifunctional concepts from polymers to 3D printed composites [26]. (Reused with the permission from Elsevier, License No. 5195350257776)

days, there is a continuous demand for products with multifunctionality and complexity, although many new materials have emerged, such as smart materials, nanomaterials, fast-drying concrete, and functional materials. These are used as feeding materials for the printing of real 3D application parts [30–32]. This 3D technology has the potential to alter production lines and can revolutionize industries. This technique is capable of increasing the production speed with a reduction in cost, and it influences the consumer demand for overproduction. This leads to greater input on the final products from the consumers, and they may request more specifications on the product [33–35]. At the same time, 3D printing facilities are located near to consumer and allow for more responsive and flexible manufacturing processes with higher controllability in quality parameters. Furthermore, there is less requirement for global transportation while using the 3D printing technique. This is due to the availability of manufacturing areas nearer to the final destinations. Furthermore, the distribution processes occur through fleet tracking technology, which saves both time and energy [36–39]. In the literature, there are numerous research works that deal with topology optimization, design methodologies, employed materials, and processing parameters. However, there are very few reviews of work done on the usage of 3D printing technology in polymer composites. Hence, this review outlines the description of various 3D printing technologies, the advancement of various types of polymer composites using 3D printing techniques, the characterization (mechanical, thermal) of 3D printed composites, and their applications in various sectors with future aspects.

2 3D printing technologies

There are various 3D printing technologies available for the manufacturing of components, and the selection of a technique depends on the type of material used for component printing. The 3D printing process begins with the virtual model creation of an object that to be printed. This virtual model is obtained using a three-dimensional scanner, CAD software, or through the photogrammetry technique (assembly of more object images obtained from several positions). After 3D model creation, it is converted to STL file format and stores the information through coordinate values. This 3D model file format can be universally recognized, and reading is possible for all types of 3D printers. The model is subjected to a slicing process followed by conversion to G-code file format. The slicing process involves 2D cross-section layer generation for the entire object. Finally, the printing head starts depositing melted material layer-by-layer and creates a 3D object as per the design fed at the beginning [40, 41]. Table 1 illustrates the brief introduction to 3D printing techniques.

2.1 Selective laser sintering (SLS)

The alternative names for selective laser sintering (SLS) are solid freeform fabrication (SFF), desktop manufacturing technique, layer manufacturing technique, and rapid prototyping technique. SLA was first invented at the University of Texas, and this process has been commercialized by EOS GmbH Electro-Optical System and DTM Corporation [48, 49]. The schematic representation of the SLS process is shown in Fig. 2a. SLS is a type of additive manufacturing process that involves a powder-based layer manufacturing process that is generally meant for rapid tooling and rapid prototyping. This process uses pulse mode or continuous mode laser beams (heat sources) for the purpose of scanning and joining powder materials as per pre-uploaded shapes and sizes of the layers. This scanned layer geometry corresponds to different cross-sections of the 3D CAD software model or STL file format of an object. After the completion of the primary layer scanning, the loose powder is deposited on it for the second layer, and this process is repeated until the creation of the 3D object. The SLS technique is also utilized for making design testing models, smaller volume functional parts, and investment casting patterns. This process is also popular in the manufacturing of sand casting molds, polymer

Table 1 Brief introduction to 3D printing techniques [42–47]

3D printing techniques	Compatible polymer materials	Description	Advantages	Disadvantages
SLA	Acrylonitrile butadiene styrene (ABS), polypropylene (PP), epoxy	UV-based scanning and curing	Fast production, high resolution, simple scalability	Printing size restrictions, higher cost
FDM	Polycarbonate (PC), ABS, nylon, PLA	Material extrusion through nozzle and deposition	Materials used are widely available and inexpensive, good strength	Slightly low process, anisotropy
DLP	Standard resin, transparent resin, and gray resin	Curing is done through a UV projector	Faster process, larger production, fully dense part printing	Lesser visibility of square pixels on the screen of an object
SLS	Polystyrenes (PS), polyamides (PA), thermoplastic elastomers (TPE), polyaryletherketones (PAEK)	Powdered material binding is done through a laser power source	Higher resolution, quick turnaround times, more strength, and stiffness of printed material	More expensive and required post-processing
MJF	Nylon, thermoplastic polymers	Fusing and heating to a solid layer on the nylon powder bed	Quick and accurate in printing prototypes of functional parts	Material options are a limited and initially expensive printers
PolyJet	ABS, nylon-12, PLA, PC, nylon-6	The printing head drops photopolymer and solidification done through UV light exposure	Creates smooth and detailed prototypes, easy printing of complex shapes	Larger parts printing is time-consuming and costly, not recommended for outdoor production

molds, sheet metal parts, EDM electrodes, PZT parts, and zirconia molds [50–52].

2.2 Stereolithography (SLA)

Stereolithography (SLA) is one of the most commonly used additive manufacturing techniques compared to other techniques. The schematic representation of the SLA process is shown in Fig. 2b. It involves a photo-curing process of liquid resin, which is stored in the reservoir, and a programmed laser head that scans over the surface of the liquid resin followed by photopolymerization. This resulted in the curing of the resin and converts it to solid phase from liquid phase through the chemical cross-linking processes. This SLA is capable of printing a wide range of consumer products, prototypes, and living tissues. There are two major issues in the SLA process, which are processing duration and the thermo-mechanical performance of printed parts [53–55]. There are two types of SLA techniques: scanning (SSL) and projection (PSL)-based stereolithography. Every layer printed in PSL is through single shots of the laser by producing light in predefined pattern, whereas SSL scans the surface of each layer for the creation of a pattern. The PSL technique is compatible for printing small parts with high resolution because of the restricted size pattern of laser light, while SSL is preferred for large-sized printing processes at a lower resolution cost. Both the processes require digital micromirror equipment for creating the laser light pattern. The SLA technique offers the highest resolution of 20 μm or even less as compared to other techniques. The reasons for the high resolution are time control and the accurate space of the incident laser photons [56–58].

2.3 Fused deposition modeling (FDM)

Fused deposition modeling (FDM) is a low-cost, widely used additive manufacturing technique for the purposes of systems modeling, fabrication, and production applications. The schematic representation of the FDM process is shown in Fig. 2c. This technique follows the melt extrusion process and produces a tissue scaffold followed by layer-by-layer deposition of thermoplastic polymers. It uses a movable nozzle to extrude a thermoplastic material with axis control and from which the 3D physical models have been built through layer-by-layer deposition [59, 60]. This FDM process does not require any solvent removal or loose polymer powder. Instead it gives more material flexibility while handling and processing. This technique requires consistent-sized and thermally stable polymer material that is passed through the roller and nozzle, and this handling is quite difficult in the FDM process. The printing part's quality is easily controllable by changing the process parameters, layer thickness, raster angle, raster width, air gap, and printing orientation.

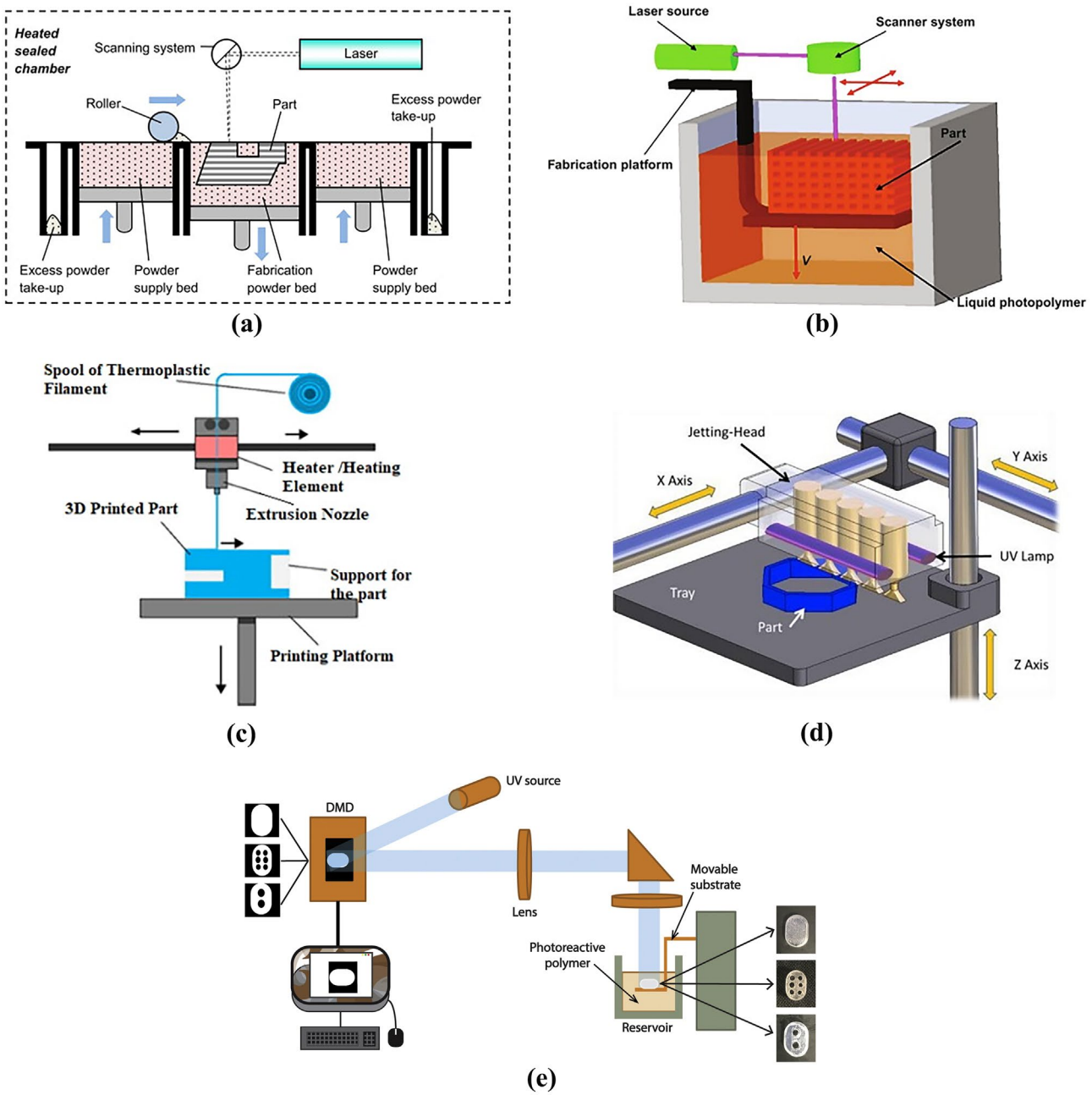

Fig. 2 Schematic representation of typical **a** SLS technique [76], **b** SLA technique [77], **c** FDM technique [78], **d** PolyJet 3D printing [79], **e** DLP technique [80]. (Reused with the permission from Elsevier, License No. 5195400198621, 5317690919052, 5195410413489, 5195351055869, 5195400867635)

Starting from the fabrication of lightweight tools to the final functional parts, FDM is preferred in the automobile sector. However, this process has some limitations, including limited material restrictions and anisotropic and weak properties of printed parts. Sometimes, it forms a weak bond between the printed layers. FDM can reduce tool manufacturing time by 85% while also producing complex jigs and fixtures [61, 62].

2.4 PolyJet 3D printing

The PolyJet 3D printing technique builds smooth-surfaced prototype models through the photopolymerization of resin materials. The schematic representation of the PolyJet 3D printing process is shown in Fig. 2d. This process enables simultaneous modeling material jetting for the creation

of 3D physical models. It is capable of printing complex geometric parts with photo-curable resin materials that are used in medical developments, automotive, electronics, consumer goods, etc. The PolyJet 3D printing head consists of a number of micro-jetting heads, which inject a resin layer of 16 μm thickness onto a build tray, corresponding to the cross-sectional profile of the model. After the jetting of the photopolymer droplet, it is immediately cured with a UV lamp, which is printed on the print carriage head. This repeating process of solidification and addition prints acrylic three-dimensional models with 0.016 mm of dimensional resolution. This PolyJet printing is capable of printing multiple materials simultaneously to obtain unique optical and mechanical properties. This process is fully controllable, and parameters can be changed as per customer requirements. The choice of raw materials is more for PolyJet printing and can be printed in a versatile manner [63–65].

2.5 Electron beam melting (EBM) technology

This electron beam melting (EBM) technology also works on the basis of the layer-by-layer deposition process and is similar to the selective laser melting process. In this EBM technique, the powder materials/particles are melted using electron beams in place of laser beams. During the process, the powder bed is maintained at a higher temperature, which is greater than 870 K, and after completing the build job, the bed is cooled overnight to reach room temperature. There are various controllable parameters in the EBM process, such as beam power, spacing of the beamline, scanning velocity of the beam, beam diameter, beam focus, plate temperature, and scan strategies. The control of all these parameters is slightly more difficult during the process as compared to the SLM technique, and hence, printing materials are limited in the EBM technique. This process exhibits some drawbacks, like a slow process, more expensive printed parts, and a restricted size of printed parts [66, 67].

2.6 Direct wire/3D plotting technique

This 3D printing works on the basis of viscous material extrusion from a high-pressure syringe for the creation of 3D-shaped materials. The syringe head moves along a three-dimensional axis, while the bed platform remains stationary, allowing the extruded material to deposit over the bed layer by layer. The curing of 3D printed parts is done by inserting two main reactive elements during the mixing in nozzles, or curing is also done either using UV light or heat. In a limited case, the finishing of the curing reaction has been done while delivering material to the plotting medium [68, 69]. The parameters like the speed of deposition and material viscosity relate to the final part's printed quality. The major advantage of this 3D plotting technology is its flexibility in material selection. The hydrogels, solutions, and pastes can be easily loaded into the plotting printer. But there is a requirement for temporary supporting material for the printed element because the printing of low-stiffness viscous material might collapse the complex structure of the printed material [70].

2.7 Other 3D printing techniques

The inkjet printing process has high printing resolution as compared to the direct retting and FDM processes. The photo-curable polymer materials are liquidized and deposited over different substrate materials (polyimide). The printing head propels the ink droplet through a piezoelectric or thermal drop-on-demand device, followed by a selective deposit on the substrate location. The surface droplets are then sintered or cured via a thermal or chemical process. The main challenge of inkjet printing is droplet deposition control, which is mainly affected by the merging of droplets, substrate surface energy, and droplet velocity. The other parameters like viscosity, nozzle diameter, and printing speed affect the quality of the printed parts [71, 72].

The newly emerged digital light processing (DLP) works on the basis of selective polymerization of the photopolymer surface through the projector light (Fig. 2e), while liquid deposition modeling (LDM) involves direct material layer deposition from volatile solvent solution [73, 74]. Fiber encapsulation additive manufacturing (FEAM) consists of direct encapsulation of fiber within the high viscous extruded polymer matrix material. As compared to the traditional 3D printing methods discussed above, these latest technologies have a wide material selection or a shorter processing duration. However, their usage is limited because of complexity and higher cost, although few researchers are adopting these processes for their work [75].

3 3D printing of polymer composites

Polymer materials possess a liquid state easily because of their lower melting point and are commonly preferred in 3D printing technology due to their lower cost, flexibility in processing, and lower weight. Even with these helpful factors, there are some difficulties in using polymer materials in 3D printing, such as large challenges in functionality, lower mechanical strength, and geometrical complexity while using them in wider applications. These challenges can be overcome by reinforcing different materials, and this also gives the desired functional and mechanical properties. The capabilities of polymer materials used in 3D printing can be observed using their molecular structures, and also it depends

on the processing of materials [81]. The usage of different types of polymer materials in 3D printing is discussed in the following sections.

3.1 Fiber-reinforced composites

The direct wire and FDM techniques are normally employed for the production of fiber-reinforced composites and also significantly enhance the properties of different polymer matrices. The process of direct writing involves the mixing of fibers and polymer paste, followed by the extrusion process. Common short fibers such as carbon and glass are preferred as reinforcements for the overall improvement of mechanical properties in 3D printed composites. The FDM process involves the mixing of fibers and polymer material pellets initially and then extruding them into filament. The secondary extrusion process is the main reason for the uniform distribution of fiber [82, 83]. The work highlights of different fiber-reinforced polymer composites are briefed in Table 2.

Mohammadizadeh et al. [94] studied the structural and mechanical behavior of 3D printed continuous fiber-reinforced composites where Kevlar, fiberglass (FG), and carbon fiber (CF) are used as reinforcements and nylon as a matrix material. The experimental results show that the composite with isotropic fiber orientation and fiber inclusions has good mechanical properties as compared to other specimens. Along with that, homogeneity in fiber orientation and more fiber packing density along the loading direction show optimum mechanical properties, which are confirmed by experimental tests. The increase in temperature above the optimum value leads to high creep deformation. The carbon fiber-reinforced composite specimen shows the highest packing density of fibers and exhibits higher resistance to failure. Also, it was noticed that the composite's lower fiber strength (Kevlar) and fiber packing density possessed lower resistance values to the failure. Akasheh and Aglan [95] conducted an investigation into the enhancement of notch sensitivity and fracture resistance of chopped carbon fiber and nylon composites that use the FDM printing process. The results of fracture behavior, fracture toughness, and mechanical properties reveal that the effective wrapping of fibers around the notches causes notch blunting and redirects the notch tip away from crack propagation, thereby improving the fracture resistance by lengthening the path of the crack. This improvement was limited to the saturation level. The more notch reinforcements above the critical limit, the more fracture resistance gain can be reduced because of notch targeted reinforcements. The deposition temperature optimization during printing of thermoplastic carbon fiber and matrix improves the adhesions and results in denser composites. The existence of fibers damaged inside the carbon bundles while printing leads to a reduction in the reinforcement effect in the printed composite. Invernizzi et al. [96] conducted a performance analysis of a UV-assisted 3D printed composite reinforced with glass and carbon fibers with diglycidyl ether as a matrix material. It ensures that there is an effective interaction between the reinforcing fibers and the matrix material. In particular, the carbon fiber-reinforced composite has a higher fraction of photo-curable resin, which is typically mandatory to ensure the appropriate processing. The results of DSC and DMA reveal the good thermal and mechanical stability of 3D printed parts. The interfacial adhesion between matrix and fiber is also improved by using the carbon fiber sizing treatment, which improves the mechanical properties of printed parts that are suitable for structural components. Dong et al. [97] evaluated the tensile properties of Kevlar/PLA composites that are fabricated using the FDM process. The fiber's orientation along the tensile direction shows the positive effect of tensile strength on the printed part. The printed composite structures with longer cell lengths possess lightweightness and optimum tensile properties, where these parameters are important for subjecting the printed components to engineering applications. Also, the increased number of fibers in the composite gives maximum tensile properties.

Balla et al. [98] conducted a study on treated soybean hull fibers and thermoplastic copolyester (TPC) composites, which are fabricated using the FFF process. The soybean hull fiber treatment affects the interlayer bonding, printing defects, and surface quality of the printed parts. The composite consists of dilute acid-treated fibers that reduce the porous size to 39 m from 81 m, elevating the composite relative density by 99%. The defects in these composites have been reduced and improved the elastic modulus value by 54 MPa, from 36 MPa. The composite at 50% strain rate exhibits higher stress and toughness values, which are 50% and 30% more than neat TPC composites, respectively. The surface characteristics of the printed parts were dependent on the material flow while printing and defects in the neat TPC material because of its more viscous nature than the composite with soybean hull fiber. Prajapati et al. [99] studied the effect of fiber volume fraction on the impact strength of HSHT glass fiber-reinforced onyx (chopped carbon fiber + nylon) matrix filament composite that is printed using the FDM process. It was observed that with the increase in fiber layer numbers, there was a requirement for more printing time. Hence, more fiber layers result in an increase in Izod impact strength to a larger extent. This 3D printed specimen's impact strength is significantly larger than most printed parts made from thermoplastic polymer. After reaching the specific limit of fiber layer addition, the impact strength increment rate was reduced. The fiber-reinforced composite specimen achieves the highest impact strength of 2448.34 J/m for 119 fiber layers and 1566.03 J/m of maximum impact strength for 29 fiber layers. This shows that the fiber volume percentage was increased to 101.46% due to fiber layer addition and increased the impact strength

Table 2 Work highlights of fiber-reinforced polymer composites

Reinforcements	Matrix	Printing technique	Work highlights	Ref.
Short carbon fibers	Onyx (carbon + nylon)	FFF	The generation of voids occurs when the filament flows from the nozzle and decreases in on-bed printing. The fiber's length has been reduced before and after the printing, which is attributed to the breakage of fibers when passing the melted materials through the converged nozzle zone	[84]
Ramie yarns	PLA	FDM	The elevation in matrix flowability causes an increment in forming pressure and impregnation duration. This resulted in a change in printing parameters, leading to microstructural changes. The maximum tensile strength was 86.4 MPa with less porosity and good adhesion between the parts	[85]
Bamboo fiber	PLA/polypropylene (PP)	FDM	The bamboo fibers were treated with NaOH solution before printing to increase their compatibility with the matrix material. The 5% PP reinforcement resulted in an improvement of tensile, impact, and flexural strengths by 13%, 23.5%, and 11.7%, respectively. The modification of BF improves the overall potential of 3D printed composites	[86]
Short carbon fibers	Polycarbonate (PC)	FFF	It was reported that the mechanical performance and surface characteristics were greatly affected by input process parameters like printing speed, orientation, layer thickness, and nozzle temperature. This means that the addition of more SCF fibers from 3 to 7.5%, more strength and modulus, but less ductility and toughness was observed	[87]
Continuous carbon fibers	Epoxy resin	FFF	The printed composite with 58 wt% of fiber content records the highest flexural strength and modulus values of 952.89 MPa and 74.05 GPa, respectively. To get the optimum mechanical properties, the author suggested some parameter values, such as 0.4 mm (thickness), 170 °C (curing temperature), 500 mm/min (printing speed), 1.2 mm (printing space), and a curing pressure of − 90 kPa	[88]
Carbon fiber	Nylon	FFF	Continuous carbon fiber/nylon composites have maximum stiffness and tensile strength values of 64 GPa and 986 MPa, whereas short fiber/nylon composites have a stiffness and strength value of 1.9 GPa and 33 MPa, respectively. The major disadvantages of printing continuous fibers are void creation and less control over fiber placement while printing complex shapes	[89]
Carbon fiber	Polylactide	FDM	The plastic impregnation into the bundles of fiber is easily possible when the liquefier temperature falls from 200 to 230 °C. The guaranteed bonding strength among layers and lines was observed with hatch spacing of nearly 0.6 mm and layer thickness of 0.4–0.6 mm. The 27% fiber content reinforcement gives maximum flexural modulus and strength values of 30 GPa and 335 MPa, respectively	[90]
Carbon fibers	Acrylic-based Peopoly resin	FDM	The thermoset composite with continuous fiber reinforcement has better mechanical properties and higher thermal stability, which is due to the existence of cross-linked structures in the polymers. The predicted modulus values fell between 2 and 5%, and the strength values were lower as compared to the predicted values	[91]
Flax yarns	PLA	FDM	The microstructure of printed flax/PLA biocomposites shows the uniform distribution of flax yarns, and twisted flax yarns have fiber-rich areas. The results of tensile strength and modulus values were 4.5 times higher than the natural fiber-based 3D printed composites results recorded in the literature	[92]
Carbon fibers	PLA	FDM	The annealing process before being subjected to tensile testing leads to an increment in crystallinity and has no significant effect on mechanical properties. The addition of short carbon fibers into the PLA matrix leads to an increment in elastic modulus value	[93]

by 15.85%. Li et al. [100] characterized the FDM-printed composite made of 1000 individual carbon fibers (reinforcement) bundles and PLA as a matrix material. The modified carbon fiber/PLA composite possesses a maximum glass transition temperature (T_g) of 66.8 °C, followed by 65.2 °C and 63.6 °C for carbon fiber/PLA and neat PLA composites, respectively. Also, the modified carbon fiber/PLA 3D printed composite achieves storage modulus and loss target values of 3.25 GPa and 1.32 GPa, respectively, and the other composite comparison is illustrated in Fig. 3. Carbon fiber preprocessing is the major requirement for subjecting the 3D printed component to potential applications. This is attributed to an improvement in interfacial adhesion between PLA resin and the carbon fiber. The experimental data reveals

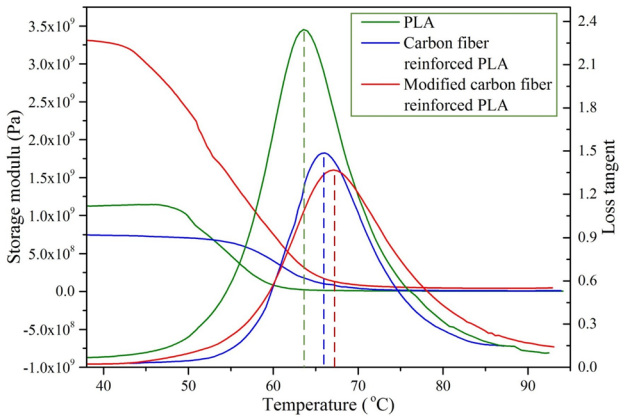

Fig. 3 Loss tangent and storage modulus of PLA, carbon/PLA, and modified carbon/PLA composites [100]. (Reused with the permission from Elsevier, License No. 5195360258657)

that the modification of carbon fiber improves the tensile and flexural strengths by 13.8% and 164%, respectively, as compared to unmodified carbon fiber composite samples.

Wang et al. [101] investigated the potential of FDM-printed short carbon fiber (CF) or glass fiber (GF)-reinforced PEEK polymer composites. The increase of fiber weight fraction from 5 to 15 wt% results in an increase in the melting point, crystallization, and thermal decomposition temperatures of the composites, where these values are higher than those of neat PEEK material, and it shows more thermal stability in the reinforcement of fibers with the PEEK matrix. The matrix/fiber interfacial bonding is better in the GF/PEEK composite than in the CF/PEEK composite, which is due to the presence of a more active group due to surface treatment. This better interfacial bonding restricts the molecular chain movements of PEEK material, which lowers the crystallinity and melting fluidity of the CF/PEEK composite. When the fiber weight fraction is increased to 15%, the tensile, flexural, impact, and ductility values of the composites decrease, but the composites remain stronger than neat PEEK material. The higher flow of melted composites creates scratches on the deposited surface and resulted in poor surface quality. Dickson et al. [102] fabricated glass, carbon, and Kevlar fiber-reinforced composites using the FDM process and nylon composites using the Mark One 3D printing system. The experimental results were compared with the existing literature values, which confirmed that the composite with carbon fibers yields higher values of mechanical strength and was 6.3 times stronger than without carbon-reinforced nylon polymer composites. The 18% glass fiber reinforcement gives maximum tensile strength efficiency, and up to 33% yielding gives a slight increase in tensile strength. Yavas et al. [103] evaluated the inter-laminar shear strength of FDM-printed short and continuous carbon fiber-reinforced polymer composites. The results reveal that the intrinsic ILSS value of a fully continuous carbon fiber-reinforced composite is 40.93 MPa, whereas a 3D printed composite with short carbon fibers and partially continuous fibers has an ILSS value of 24.42.4 MPa. This shows that the addition of short carbon fibers in place of 50% of continuous fiber reinforcement leads to a gradual decrease in ILSS value. This reduction might be as high as 45%. A 25% ILSS deviation was observed when the staking sequence of the fibers was changed. The analysis of both numerical and experimental results shows that the increase in short CFRP layer thickness causes improved toughness and fracture strength values, which prevents the cracking of the brittle matrix at lower stress levels and improves the short CFRP's plastic deformation. Sang et al. [104] investigated the mechanical, thermal, and rheological properties of treated (KH550) basalt fiber (KBF)/PLA and CF/PLA 3D printed composites. The results show that KBF/PLA composite exhibits acceptable tensile properties with superior flexural characteristics as compared to CF/PLA composites, which is due to the higher complex viscosity of CF/PLA composite that affects the adhesion of the interlayer. The higher KBF weight fraction and fiber length result in lower infill and defects in the composites, which was confirmed using CT scans and show good mechanical performance. Mosleh et al. [105] fabricated and analyzed the FDM-printed continuous carbon fiber/ABS polymer composites. Initially, the carbon fibers were subjected to pre-impregnation using the solution before printing with ABS material. The experimental results demonstrated that the tensile, ILSS, and flexural strength of continuous carbon fiber-reinforced composites have been improved as compared to neat samples. The combination of carbon and ABS composite is found to have a dramatic increase in ILSS value as compared to plane ABS material. All these improvements were due to lower printing speeds and initial pre-impregnation of carbon fibers, which provides suitable adhesion among adjacent layers and prevents the delamination of layers. Along with the improvement in material properties, the pre-impregnation also makes the printing of composites much easier than without pre-impregnation.

3.2 Nanocomposites

Nanocomposites exist as a multiphase solid material, where any one of the phases having one, two, or three dimensions with < 100 nm or a structure makes a different phase difference in nanoscale to make a structure. The common nanomaterials such as carbon nanotubes (CNTs), metal nanoparticles, graphite, and ceramic nanoparticles impose unique mechanical, thermal, and electrical properties to the reinforced composites. These nanoparticles are useful in the creation of multi-functional composites for high-performance applications [106]. A summary of different nanofiller-reinforced 3D printed composites are tabulated in Table 3.

Table 3 A brief summary of nanofiller-reinforced 3D printed composites

Polymers/filaments	Nanofillers	3D printing process	Observations	Ref.
Photocurable epoxy based SL resin	MWCNTs	SLA	The smaller amounts of MWCNTs added (0.025% w/v) result in enhanced tensile and flexural strengths by 5.7% and 26%, respectively. The agglomeration of nanoparticles creates stress concentration areas and decreases the potential of the nanocomposites	[107]
Methacrylate based (MA) resin	Graphene oxide (GO) nanoparticles	SLA	The addition of nanoparticles improves the overall physio-mechanical and thermal properties of the resultant functional nanocomposites. It was also observed that there was a strong interaction between the resin and the filler material	[108]
Polyethylene glycol diacrylate (PEGDA)	Silver nanoparticles ($AgNO_3$)	DLP	The embedding of $AgNO_3$ nanoparticles improves the overall material properties, and difficulties were observed during the printing process	[109]
PLA	Graphite nanoplatelets (GNPs)	FDM	The 2 wt% of modified GNPs loading in the PLA matrix results in improved tensile and flexural strengths by 43.6% and 28.5%, respectively. Also, the thermal stability of resultant nanocomposites was also enhanced, which led to an increment in degradation temperature of 60 °C and an increase in residual weight of 7% at the end	[110]
PLA	MWCNTs, GNPs	FDM	The shielding efficiency (SE) reaches up to 13.4 dB from 0.2 dB with the addition of both the fillers, which is 95% and 4% improvement in SE corresponding to the GNPs and MWCNT nanoparticles, respectively. The 12 wt% GNP loaded nanocomposites possess 263% higher thermal conductivity as compared to unfilled composites	[111]
PLA	ZnO nanofibers	Solvent cast 3D printing	PLA hydrolysis catalyzed by ZnO nanofibers reveals that printed nanocomposites possess lower thermal stability as compared to neat PLA material, which is due to PLA hydrolysis catalyzed by ZnO nanofibers. The presence of ZnO increases the crystallinity of the nanocomposites	[112]
PLA	Graphene	FDM	The electrical resistivity value is lower in the perpendicular direction to the layers than the volume resistivity in the layer direction. The addition of nanofillers improves thermo-mechanical properties with EMI shielding properties. Hence, this nanocomposite is suitable for lightweight EMI shielding material	[113]
Polycarbonate, ABS	Graphene	FDM	The addition of graphene (0.8 wt%) improves the tensile and impact strengths by 57% and 87%, respectively, while the reduction of surface roughness was found along the printing direction and an amount of 40% reduction as compared to neat PLA/ABS materials	[114]
ABS	Cellulose nanocrystals, silica	FDM	The hybrid fillers' insertion with ABS gives a better reinforcement effect as compared to individual reinforced fillers. The shrinking percentage and warpage degree were reduced due to the addition of hybrid fillers. The modification of hybrid fillers is also one of the reasons for the thermal property improvements in nanocomposites	[115]

Gnanasekaran et al. [116] evaluated the mechanical stability and printability of polybutylene terephthalate (PBT)-reinforced CNTs and graphene-filled FDM-printed composites. The results reveal that the mechanical and conductive properties of CNT/PBT show higher values and good performance as compared to graphene/PBT composites. The printing of multi-materials using a single process develops thermal stresses at the materials' interfaces because the coefficient of thermal expansion values is different for different materials. These difficulties were overcome by varying the printing bed temperatures. Sometimes, the higher specific Young's modulus value of graphite and CNT causes nozzle wear while printing the materials. There is no requirement for any alterations to process parameters while using CNTs and graphene as nanoparticles with PBT polymer because of the lower graphene (0.49 wt%) and CNT (0.31 vol.%) concentrations. Coppola et al. [117] fabricated nanoclay-filled PLA nanocomposites using the FDM technique. The addition of

nanoclay particles increases the crystallinity of the resultant nanocomposites, which is the reason for the existence of the crystalline phases. The DMA analysis results show an improvement in storage modulus value as compared to neat PLA composites. The cold crystallization temperature of nanoclay/PLA nanocomposite is lower in the range than the neat PLA material, which is due to the nucleating effect of nanoclay particles (acceleration of PLA crystallization). It is also reported that the elastic modulus value was enhanced by + 15 for the nanocomposite sample. Moreover, the nanoclay/PLA nanocomposite samples have sharper edges and better shape stability. Postiglione et al. [118] evaluated the conductive properties of multi-walled carbon nanotubes (MWCNTs)/PLA nanocomposites that are printed using the liquid deposition modeling (LDM) technique. The addition of more MWCNT content resulted in improvement of electrical properties in resultant nanocomposites. The electrical conductivity range of 10 to 100 S/m is obtained for higher MWCNT concentration of above 5 wt%, with a threshold concentration value of 0.67 wt%. Initially, the woven-like 3D structure was obtained through the deposition of two-layer materials on one top of the other with a printing speed of 0.1 mm/s and illustrated in Fig. 4a as an optical micrograph. The extrusion of filaments having MWCNTs/PLA nanocomposite resulted in a planar solid feature with an average width of 100 µm. The top and side views of ten-layer scaffold of 3D printed filaments are illustrated in Fig. 4b and c. The example of freeform printing with 3D microstructure solid filament with a diameter of 100 µm is capable to adopt a self-standing feature with a few mm of length, and it is illustrated in Fig. 4d**.** The application of this conductive nanocomposite in an electrical circuit is shown in Fig. 4e**.**

Chen et al. [119] printed and characterized the FDM-printed nanographene oxide (GO)-filled thermoplastic polyurethane/PLA nanocomposites. The nanocomposites were printed easily with complex shapes with good quality and proper dispersion of nano-GO particles in the polymer matrix which was observed in SEM and FTIR images. The loading of nano-GO particles significantly improves the mechanical properties of the resultant nanocomposites, which have tensile modulus and compression modulus values of 75.5% and 167%, respectively. The changes in printing orientations result in different mechanical responses due to weaker adhesion among layers during printing. The GO nanoparticle addition gives a better thermal stability by increasing the degradation temperature by 90 °C and better formation of crystalline structures. The smaller amounts of GO addition result in no toxicity to cell growth, and it is a benefit for cell proliferation. Wei et al. [120] analyzed the conductive properties of nanosilver material-coated carbon nanofibers (Ag@CNFs) that are printed using a direct 3D printing technique. The chosen nanocomposites can be printed in open air at ambient conditions with a lower percolation threshold (6 vol.%) and a higher electrical conductivity value of greater than 2.1 105 S/m without any post-treatment. Further, it was also found that the hybrid Ag@CNFs nanocomposites deliver a shape memory behavior through low-voltage triggered electrical response, and the response is quick; hence, it is preferred in the manufacturing of electroactive devices. The conductive nanocomposites are also popular in manufacturing different electrical components like sensors, lightweight scaffolds, low voltage smart grippers, and ambient conductive components. Viskadourakis et al. [121] studied the transport properties of graphene/PLA and graphite/PLA nanocomposites, which are fabricated using the FDM 3D printing technique. The 3D printed graphene/PLA nanocomposite possesses a higher order of magnitude of electrical conductivity than the PLA/graphite nanocomposites. The Seebeck coefficient value and power factor values are low for PLA/graphite nanocomposites, making them not acceptable comparatively for the thermoelectric application. Rosales et al. [122] investigated the electro-responsive behavior of carbon black nanoparticles filled with shape memory polymer (SMP) nanocomposites. The behavior reveals that the conductive CB/SMP nanocomposite specimen gave a response to the electrical current stimulus through the enhancement of toughness, which was four times more than without current applied while conducting a tensile test. The conductivity value was further enhanced by increasing the CB filler concentration in the SMP matrix material. Furthermore, the elongation value was enhanced to 44% from 9.45%. The SEM images reveal the uniform distribution of CB particles in the SMP material. Sanatgar et al. [123] studied the adhesive properties of nylon on polyamide, CB/PLA, and CNT/PLA nanocomposites printed using the FDM technique. It was observed that the different processing parameters had a significant effect on the adhesion of polymer materials to fabrics. As per the best-fitted model, there was a significant effect on the adhesive properties of nylon on polyamide fabric through the extruder temperature linear effect and quadratic effect on the printing speed. The adhesive force is not affected by platform temperature when the temperature range is below the glass transition temperatures of reinforced fabrics. This phenomenon was proven by the diffusion theory, which explains the adhesive nature of polymers through chainlike molecules. Figure 5 clearly illustrates the effect of processing parameters on the adhesion force of nylon on polyamide fabric. The 5% CB-loaded PLA nanocomposite has a more brittle nature with less break strength as compared to the 2% CNT-loaded nanocomposites. The loading of 5 wt% organic modified montmorillonite (OMMT) in the ABS matrix results in an improvement of 43% higher tensile strength in 3D printed ABS composites, while 28.9% of tensile strength enhancement was found in injection molded ABS composite

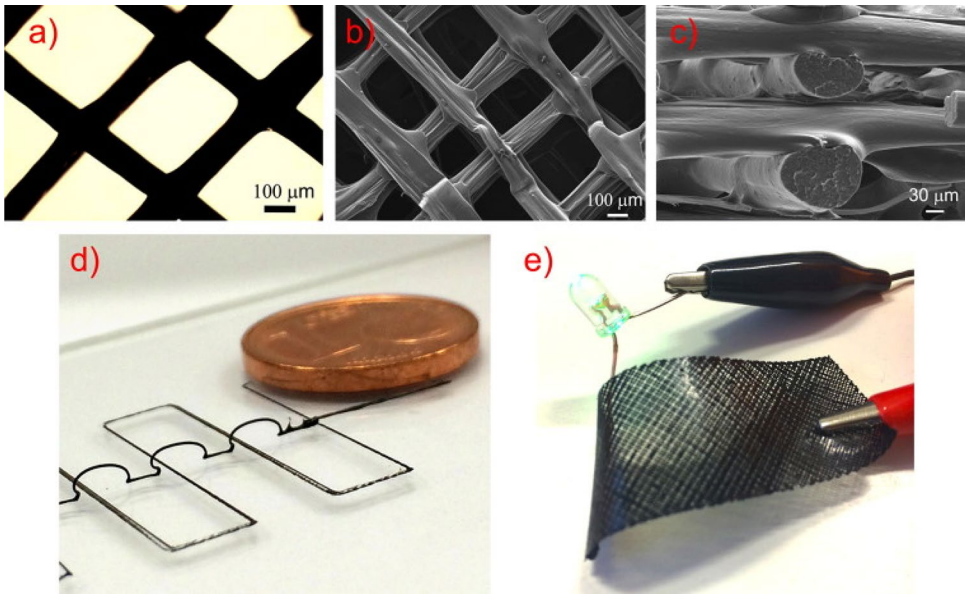

Fig. 4 **a** LDM printed 3D woven microstructure of two-layer filaments, SEM **b** top and **c** side view images of ten-layer scaffold structures, **d** LDM based filament 3D printed freeform structure, **e** application of PLA/MWCNT nanocomposite in electrical circuit [118]. (Reused with the permission from Elsevier, License No. 5195360542225)

samples. The addition of OMMT improves both mechanical and dynamic properties and reduced the TGA weight loss and the value of linear thermal expansion [124]. Guo et al. [125] evaluated the conductive and thermal properties of PLA and poly(butylene adipate-co-butylene terephthalate) (PBAT)-reinforced 3D printed nanocomposites filled with graphene nanoplatelets (GNPs). The GNP addition to PLA leads to improper dispersion because of poor affinity towards PLA material, and uniform and proper dispersion was observed in the PBAT matrix due to percolated network formation. The maximum electrical conductivity of 338 S/m and a thermal conductivity value of 3.15 W/m–K were obtained for 40 wt% GNP filler loading and achieved good mechanical performance due to strong interactions between the fillers and PBAT material.

3.3 Particle-reinforced composites

Concerning economic benefits, the particles are reinforced in the matrix material to improve composite properties. The particle reinforcements are easy with the polymers, either in the liquid form for the SLA or in the powder form for the SLS technique, also printable in the filament form through the FDM process [126]. The main key improvements due to particle additions were storage/tensile modulus (glass beads, copper, iron particles), wear resistance (aluminum, Al2O3), and dielectric permittivity (tungsten, ceramic particles) [127, 128]. The summary of different particle-reinforced polymer composites are tabulated in Table 4.

Liu et al. [139] evaluated the recovery characteristics of SiC and carbon particle-filled PLA composites printed using

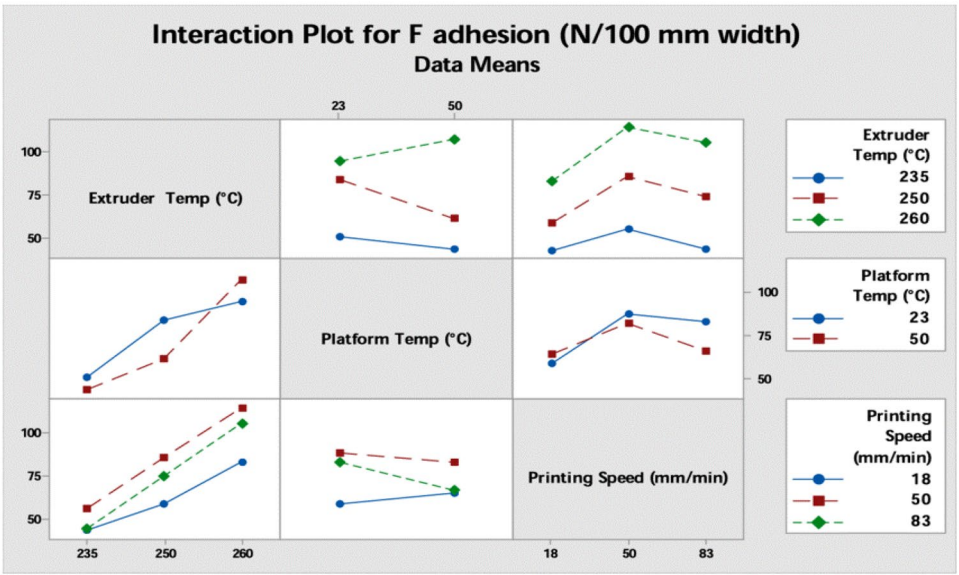

Fig. 5 Interaction plots for the adhesion force v/s different processing parameters of the 3D printer for nylon deposited on the polyamide fabric [123]. (Reused with the permission from Elsevier, License No. 5195360795891)

Table 4 Summary of particle-reinforced 3D printed composites

Reinforced filaments	Fillers	Printing process	Work outcomes	Ref.
ABS	Diamond micro-particles	DLP	Minor improvements in heat transfer rate were observed in ABS composite with up to 25% (w/v) diamond particle loading, but 30% (w/v) loading shows significant improvement based on diamond particle-aggregated interconnection network. The materials were printed for cooling coils and heat sinks for thermal applications	[129]
Polyurethane acrylate	Alumina	Magnetically assisted direct writing	The multi-material dispersion and component mixing units provide additional control over local composition in the printed materials. There was also control over magnetized particles' orientation in the 3D printed parts	[130]
Conductive ABS	Zinc oxide (ZnO)	FDM	The dynamic storage modulus value was improved due to the change in infill density from 50 to 100%. However, a gradual decrement was found in the damping factor and loss modulus values. The electrical conductivity and tensile properties were better in the inline pattern than in the rectilinear. These printed composites are suitable for thermoelectric applications	[131]
Polystyrene	Al_2O_3	SLS	The particles' addition to polystyrene (PS) improves the impact and tensile strength by 50% and 300%, respectively, as compared to unfilled PS material. The rough fractured surfaces were observed in treated particle-filled PS composites more than in unfilled and untreated PS composites. The treated particles absorb the laser and are well dispersed in the matrix material	[132]
PVA	Calcium silicate ($CaSiO_3$)	SLS	The compressive strength value was elevated to 15 wt% filler addition and reduced to 20 wt% $CaSiO_3$ content. The filler addition of less than 20 wt% improves the bioactivity of the printed scaffolds	[133]
HDPE, polypropylene (PP)	Silicon nitride (Si_3N_4)	FDM	The reinforcement of HDPE and PP materials with 10 vol.% of Si_3N_4 particles is not sufficient because of substantial critical strain decrement and an insignificant increment in elastic modulus value. The incorporation of these hard particles in higher volumes has no significant effect on filament properties. The filler particles improve the tribological behavior of 3D printed composites	[134]
PLA, polyethene terephthalate (PET)	Stainless steel and copper alloy powder	FFF and laser-based powder bed fusion process	The reinforcement of hybrid fillers develops interlocking structures, and their joint strength was improved by laser heating. The metal/polymer composite possesses good tensile and shear strength without any adhesives	[135]
ABS	Copper (Cu) particles	FDM	The maximum tensile strength and density values were obtained for the parameters of nozzle diameter, layer height, raster angle, and nozzle temperatures of 0.5 mm, 0.1 mm, 0/90, 240 °C, and 1 mm, 0.1 mm, 0/90, 240 °C, respectively	[136]
ABS	Zinc ferrite ($ZnFe_2O_4$)	FDM	The 14 wt% filler addition improves the density and tensile properties by 8% and 70%, respectively, as compared to neat ABS material. Similarly, the electrical and thermal conductivities were enhanced by 186% and 22%, respectively, for the same filler loading. This is attributed to the formation of a conductive network or chain between $ZnFe_2O_4$ and ABS materials	[137]

Table 4 (continued)

Reinforced filaments	Fillers	Printing process	Work outcomes	Ref.
Poly(ethylene glycol) diacrylate (PEGDA)	Silica (SiO_2)	SLA	A small amount of silica filler material (1 wt%) reinforcement improves the compression and tensile strengths of the PEGDA composite. The swelling rate depends on the thickness of the printed parts. The TGA test reveals the slight scattering of mass value with the different loading conditions. This also shows the improper distribution of silica particles. Especially when a higher percentage of fillers is present	[138]

the FDM technique. The 10 wt% of SiC and 50 wt% of C loading decrease the recovery time by 87% as compared to the neat PLA matrix. The 20% and 50% of SiC loading into PLA show a maximum recovery force of 12.9% and 76%, respectively. Quill et al. [140] evaluated the thermal and mechanical properties of FDM-printed boron nitride (BN)/ABS polymer composites. The author compared the conductivity values of injection molded and 3D printed parts. The 35 wt% BN loaded ABS composite possesses 1.45 W/m–K of in-plane conductivity printed through the injection molding process, while 0.93 W/m–K of conductivity value was obtained for the 3D printed composite for the same material and weight percentage, which is 5 times higher than neat ABS conductivity. The composites have anisotropic thermal conductivity, and their through-plane thermal conductivity value is lower by a factor of nearly 4 for 3D printing and 3 for injection molding. The addition of BN flakes increases the optimum flexural modulus value and decreases impact toughness and flexural strength to a greater extent. Tan and Low [141] evaluated the electrical properties of nickel and tin alloy-filled nylon-6 and HDPE composites printed using the FFF process. The conductivity value of nearly 3.1×104 S/m was obtained for the nylon-6 composite filled with 30 vol.% of metal loading. The nylon-6 matrix is hygroscopic, which reduces the thermal conductivity value when interacting with a humid environment. This could be avoided by composite drying for 48 h at a temperature of 60 °C. For the 35 vol.% of filler loading, the PE composite exhibits a conductivity value of 23,000 S/m. This PE matrix is non-hygroscopic, so there was no interaction effect on electrical conductivity with the environment.

Palmero et al. [142] demonstrated the printing suitability of stainless steel alloy and aluminum particle-filled ABS filaments using the FDM process. The filling factor of magnetic stainless steel particles in ABS composites has been accurately obtained by magnetization value comparison with initial powder magnetization. Also, there was no metallic particle degradation after processing, and it was confirmed through magnetic measurements. The author also studied the feasibility of using the smaller size and more uniform distribution of particles with the ABS materials. Hamzah et al. [143] characterized the copper ferrite ($CuFe_2O_4$)-reinforced ABS polymer composites printed using the FDM process. The composite is studied with 8, 11, and 14 wt% of filler reinforcement. It was found that 14 wt% of $CuFe_2O_4$ loading increases the tensile strength value by 135% as compared to

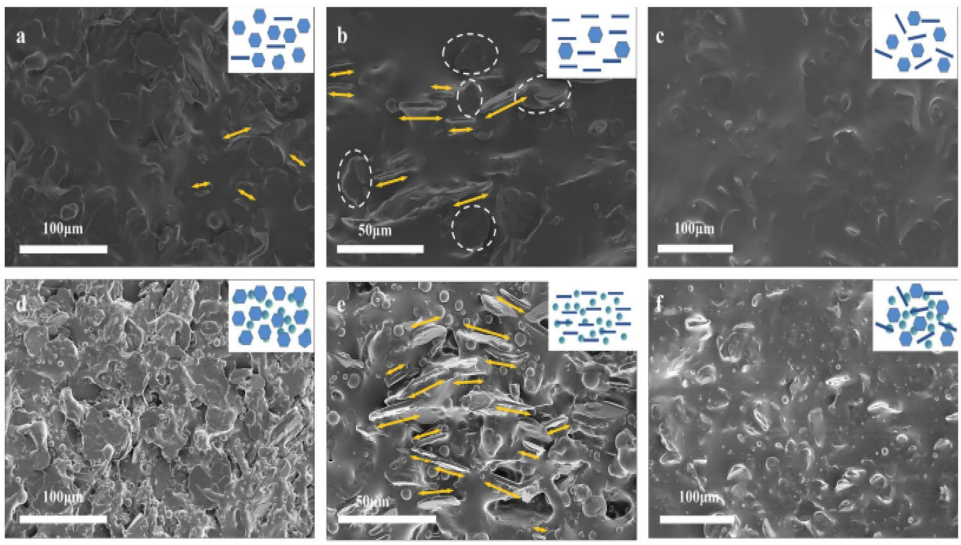

Fig. 6 SEM micrographs of **a** top view and **b** side view of 35 wt% BN reinforced composite. **c** Randomly oriented composites with 35 wt% BN particles. **d** Top view and **e** side view of oriented composites with 30 wt% Al_2O_3 and 35 wt%. **f** Random composites with 35 wt% BN and 30 wt% Al_2O_3. The orange arrows and white circles indicate vertically and horizontally alignment of BN particles [146]. (Reused with the permission from Elsevier, License No. 5195361066322)

neat ABS filament. Also, this specimen is 14% harder than the neat ABS material. The thermal conductivity value is elevated by 93% with a filler loading of 14 wt%. The improvement in mechanical properties was due to strong interlocking between the matrix and fillers at higher filler concentrations. The conductive nature was improved due to possible mutual contact of filler particles, which creates a conductive pathway and leads to good electrical conductivity. Yang et al. [144] developed FDM-printed particleboard wood flour (PWF)/PLA polymer composites filled with copper-zinc (mCu-Zn) alloy particles. The results reveal that the addition of mCu-Zn alloy particles to wood plastic composite improves overall mechanical and thermal properties and has good antibacterial performance. The addition of 2 wt% alloy particles increases the flexural strength by 47.1% and 18.9% as compared to neat PLA and PWF/PLA composites. A 1142.6% of the increment was found in surface gloss as compared to PWF/PLA wood polymer composites. Moreover, the inhibition rate against *Escherichia coli* was 90.43%. Hence, these antibacterial and novel high-loss characteristics of wood polymer composites have potential applications in classic art, furniture, toys, etc. Wu et al. [145] analyzed the gamma-ray shielding performance and mechanical properties of tungsten-filled poly-ether-ether-ketone (PEEK) composites printed using the FDM technique. The rate of gamma-ray shielding changes exponentially with varying tungsten particle percentage for the same specimen thickness. The printed shielding material has a short cycle, a denser structure, lower porosity, a simple process, and uniform dispersion of tungsten particles. These new shielded materials' mechanical properties were enhanced due to heat treatment. The 50, 60, and 70 wt% of PEEK/tungsten composite improved tensile and flexural strengths by 33.51%, 27.52%, 30.6%, and 33.28%, 34.81%, and 41.29%, respectively. Liu et al. [146] fabricated alumina and boron nitride (BN) particles filled with polydimethylsiloxane (PDMS) polymer composites using a 3D printing process. The SEM micrographs of the hybrid filler reinforcement in different views are illustrated in Fig. 6. The reinforced BN platelets act as a heat transfer rapid highway in the matrix, and it resulted in a thermal conductivity increment along the oriented direction. Further addition of spheres of Al_2O_3 improves the filler network and resulted in slurry viscosity growth. The hybrid filler reinforcements of BN (35 wt%) and Al_2O_3 (30 wt%) give 90.65% of higher degree orientation and 3.64 W/m–K of thermal conductivity. These oriented hybrid fillers also reduce the resistance at the thermal interface, and they show how the thermal conductivity of these fillers has changed.

Yang et al. [147] printed the boron nitride particles filled into polyamide 12 conductive composites using the SLS technique. The addition of BN particles to SLS parts shows a sharp improvement in thermal conductivity value. However, the presence of the void slightly lowers the conductivity value as compared to compression-molded parts. The printed parts were subjected to epoxy resin post-treatment, which improves the overall mechanical properties of the SLS printed parts. The tensile strength and Young's modulus values were improved by 19.3% and 123%, respectively, in post-treated SL parts. This epoxy resin treatment influences the mechanical properties but doesn't influence the thermal conductive network in the SL parts. Aw et al. [148] studied the effects of filler coating and printing parameters on ZnO-filled ABS composites printed using the FDM technique. The 11 wt% of ZnO addition gives the optimum tensile strength of the ZnO/ABS composite with coated fillers with 100% infill density along with the inline pattern. This improvement was due to the strong interfacial adhesion that exists between the coated filler and the matrix. The young's modulus, hardness, and strength values were enhanced by ZnO addition to the ABS matrix due to the high strength of the fillers and stiffening effect. The filler percentage reaching up to leads to agglomeration formation, which resulted in poor mechanical properties. The line pattern exhibits higher stability during the printing process, with higher quality because of less jerking during the process. However, this printing pattern doesn't affect the hardness of the printed composites. Dawoud et al. [149] analyzed the strain sensing behavior of FDM-printed carbon black-filled ABS polymer composites. During the tensile testing, the stress change was accompanied by conductivity changes based on the percolation effect and tunneling of filler effects. At lower strain levels, these mechanisms' effects are greater. At the higher strain level, the chances of breaking the percolation network are high and decrease the building of conductive tunnels. Finally, this reduced the conductivity of carbon black/ABS printed composites. Castles et al. [150] evaluated the dielectric behavior of a 3D printed barium titanate ($BaTiO_3$)/ABS polymer composite. The 70 wt% filler-loaded composite was studied for dielectric properties using a split post dielectric resonator (15 GHz) and shows the relative permittivity and loss tangent ranges of 2.6 to 8.7 and 0.005 to 0.027, respectively. These permittivity values can be reproduced during the entire process, and matching can be done with unprinted materials.

4 Characterization of 3D printed parts

Material characterization is the final process after the parts have been printed using different additive manufacturing techniques to check the feasibility of components for various potential applications. The different characterizations of 3D printed composites are discussed in the following sections.

4.1 Magnetic properties

The magnetic properties of additively manufactured polymer composites are obtained either by introducing magnetite

nanofillers into the polymer matrix or through the integration of an electromagnetic layer inside the multilayered composite. The performance and efficiency of the magnetic transformer were majorly affected by geometry. Using 3D printing in polymer composites enables the production of complex geometries, and it gives a contribution to the overall performance of the printed parts [151, 152]. There are various types of worthy magnetic materials for filler purposes, in that magnetic ceramics are more popular as compared to alloys and magnetic materials because of their potential advantages. The advantages are higher electrical resistivity, wear resistance, ease of synthesis, and corrosion resistance. Most of the research papers include iron oxide (a type of magnetic ceramic) as a filler material in various applications in different phases (maghemite, hematite, and magnetite) [153, 154]. Bollig et al. [155] studied the possibility of printing a transformer core using iron particles and PLA composite using the FDM technique. The 3D printed transformer core performance was enhanced with a good magnetic response using two factors, namely, utilization of the highest fill factors and increasing iron content. The factor of iron content increment causes complications during the extrusion process. The higher percentage of magnetically responsive particulates with lower susceptibility and coercivity leads to an increment in the performance of the printed core. It is also possible to optimize the performance by changing the turn ratio and diameter/radius of the transformer geometry. Khatri et al. [156] analyzed the magnetic response of stainless steel particles filled with ABS polymer composites fabricated using 3D printing technology. The pure ABS material has no significant magnetic response, and the addition of higher filler contents increases the ferromagnetism of the resultant composite. The composite sample with 40 vol.% stainless steel particles exhibits 15.6 mT of magnetic retentivity at 485 kA/m applied field. The filler addition of 0, 10, 20, 30, and 40 vol.% to the ABS gives a maximum field strength of 404, 375, 413, 423, and 485 k/Am, respectively. The results also reveal that the retentivity (BT) value doubles for every 10 vol.% of stainless steel particles added. These composite samples are not subjected to any post-treatment, and even without treatment, the composites exhibit similar properties as treated composites. The sample with doubled magnetic retentivity with higher filler content is a promising material for magnetic sensing applications. Zhang et al. [157] investigated the multifunctional properties of Fe_3O_4 particle-filled mesoporous bioactive glass (MBG) and polycaprolactone (PCL) polymer composites. The Fe_3O_4/MBG/PCL composite scaffolds show superparamagnetic behavior because of their lack of a hysteresis loop. The value of magnetization saturation for the Fe_3O_4/MBG/PCL scaffold increases with adding more Fe_3O_4 particles, and the magnetization value of MBG/PCL, Fe_3O_4 (5 wt%)/MBG/PCL, Fe_3O_4 (10 wt%)/MBG/PCL, and Fe_3O_4 (15 wt%)/MBG/PCL scaffolds is 0, 1.01, 2.02, and 2.90 emu/g, respectively. In the presence of an alternating magnetic field, the MBG/PCL scaffold has no significant increment in solution temperature, and this temperature was rapidly increased with the addition of filler contents. The 15 wt% of Fe_3O_4 particles loaded onto the MBG/PCL scaffold shows an increment in induced temperature from 20 to 43 °C at 180 G magnetic strength and 409 kHz of frequency within 2-min duration. Yue et al. [158] fabricated a magneto-responsive three-dimensional shape memory polymer composite using Fe_3O_4 and cellulose nanofibers' (CNFs) reinforcement with poly-hydroxybutyrate (PHB)/poly-(ε-caprolactone) (PCL) blends. The composite blend combination of 0.5 wt% CNFs, 10 wt% Fe_3O_4, and 80:20 ratio of PHB/PCL gives optimum magneto-responsive shape memory characteristics. The author prepared a snowflake model with dimensions of 33 mm × 36 mm × 1.2 mm with 100% infill density, 0° fill angle, and 200 °C printing temperature. Figure 7a–c illustrates the snowflake model instantaneous shape and temporary shape with the presence of the magnetic field. It is observed that the model achieves unfolding gradually with the temporary shape and regains its permanent shape within 35 s; this behavior shows that the 3D printed model has the favorable response of magnetic shape memory properties.

Schmitz et al. [159] assessed the effectiveness of electromagnetic interface shielding efficiency (EMI SE) in carbon black (CB)- and CNT-loaded ABS polymer composites printed using the FDM technique. The properties were also studied with hybrid filler reinforcements (HYB-CB + CNT). The EMI SE response of the FDM-printed composite is found to be affected by the printing direction and type of filler reinforcement in the specimens. The order of maximum EMI SE of the specimen is CNT/ABS > HYB/ABS > CB/ABS > neat ABS material independent of growing direction. The composite specimen fabricated in the perpendicular direction (PC) has better attenuation of electromagnetic radiation. For instance, the overall EMI SE of a CNT-based composite printed along PC was nearly − 16 dB, followed by − 10 and − 11 dB for horizontal concentric (HC) and horizontal alternate (H45) directions, respectively. whereas the HYB/ABS specimen shows EMI SE responses of − 12, − 8, and − 8 dB according to PC, HC, and H45 directions. The two plots in Fig. 8 differentiate the shielding effectiveness in terms of absorption and reflection. When the incident waves are propagated through the specimens, an appreciable shielding efficiency is obtained for the absorption commanding mechanism. This mechanism of attenuation is a function of both the magnetic and dielectric properties of individual elements in the composite.

Khamis et al. [160] conducted a study on the magnetic properties of recycled Fe_3O_4 (rFe_3O_4)-reinforced 3D printed polytetrafluoroethylene (PTFE) composites. The complex permittivity was enhanced with increasing rFe_3O_4 filler

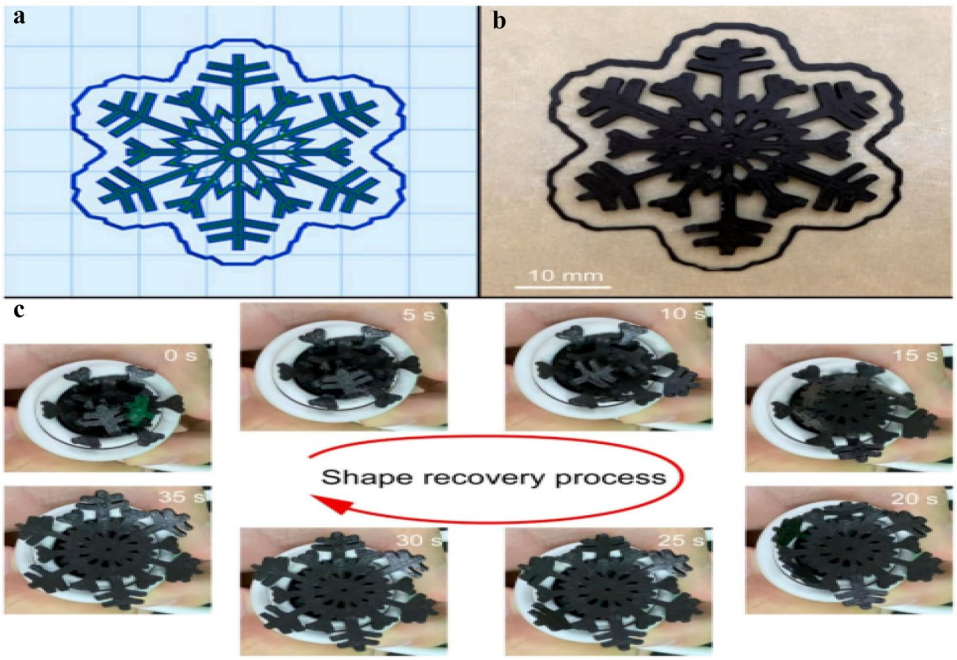

Fig. 7 **a** Printing path of the snowflake model in the slicing software. **b** Top view of the printed snowflake model. **c** The magneto-responsive shape recovery process of the snowflake model with the temporary shape with the presence of magnetic field [158]. (Reused with the permission from Elsevier, License No. 5195361309266)

content, which is attributed to the commencement of the polarization process through the interfacial polarization and enhanced conductivity and also due to charges exchanged among localized states. The higher rFe_3O_4 filler content in the PTFE composite reduces the existing space in the composite blend because of a larger specific area of fillers. Hence, this leads to difficulties in passing the magnetic field through the composite, thereby increasing the values of relative complex permeability. Hence, these composites are employed for applications related to tunable characteristics. At 10 GHz, the 25 wt% rFe_3O_4 filler-loaded composite had a maximum relative permeability value of 1.1. Palmero et al. [161] utilized MnA1C particles with a polyethylene (PE) matrix for the development of an earth-free permanent magnet composite, and this was printed using the Noztek Ltd. Extruder. This process involves the utilization of continuous filaments of a length exceeding 10 m. For quasi-spheroidal ferromagnetic MnAlC particles, a maximum of 86.5% of the filler factor was

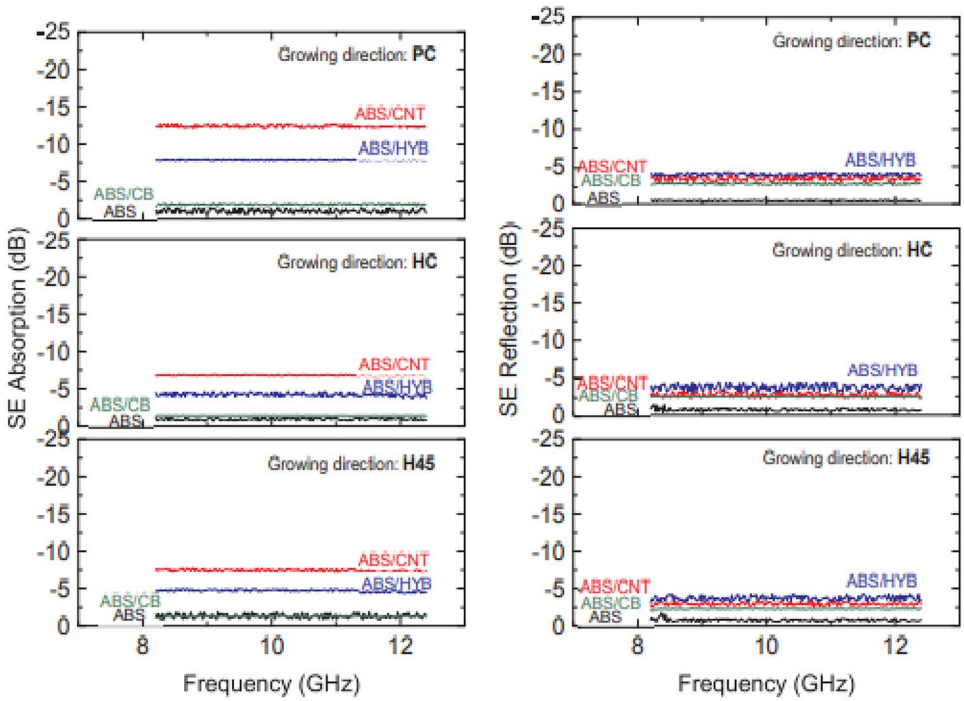

Fig. 8 Shielding by absorption (left stack plot) and by reflection portion (right stack plot) of ABS carbon-based composites in three different layer-by-layer growing directions: perpendicular (upper graph), horizontal concentric (middle graph), and horizontal alternate (bottom graph) [159]. (Reused with the permission from Elsevier, License No. 5195370004576)

used. The process parameters are 1.75 mm of nozzle output diameter, 20 cm/min of extrusion speed, and an extrusion temperature maintained at 120 °C. The fabricated magnetic composite shows no deterioration in the permanent magnetic properties of filler particles after filament extrusion and composite synthesis. The magnetization values directly vary with the contents of the magnetic particles in the composites.

4.2 Conductive properties

For decades, various carbon-based nanomaterials such as graphene (2D) and carbon nanotubes (1D) have been used as a second phase for conductive composite fabrication because of their attractive electrical properties. The introduction of these nanomaterials with different polymer matrices through 3D printing results in conductive nanocomposites with complex structures [162–164]. CNTs are the major potential candidates suitable for modification of filaments or 3D printable inks for the manufacturing of multifunctional structures. In the conductive composites, the determination of electrical performance is done through the percolation threshold, where the long-range conductive networks were formed with a minimum volume percentage of nanofillers [165–167]. When the filler percentage reaches beyond the threshold value, the formation of more conductive networks occurs and resulted in a significant improvement in conductivity values. This percolation threshold value is determined by filler type, size distribution, agglomeration, and dispersion. Hence, while choosing the functional filler ratio, both viscosity and percolation threshold have to be considered for the 3D printing process [168–170]. Chizari et al. [171] successfully developed lightweight composite structures with improved functional performance for electromagnetic interference shields. The highly conductive structures exhibited an electrical conductivity value that reaches maximum value up to nearly 5000 S/m, by filling the MWCNTs in the PLA matrix. The Fisnar dispensing robot (I&J2200-4) was utilized to print conductive ink, and the pressure was maintained between 2.1 and 4.2 MPa. The robot displacement rate was varied based on the presence of CNT contents, which is about 0.3 to 1.0 mm/s. The EMI test results show that the improvement was observed in EMI shielding effectiveness as compared to solid form CNT/PLA composites, which is nearly 70 dB g/cm^3. The final structural functional performance was possible to improve by varying structural parameters like printed layer number and inter-filament spacing. The detailed electrical conductivity value variation with filler contents and structures is shown in Fig. 9.

Sezer et al. [172] evaluated the electrical properties of MWCNT-filled ABS polymer composites fabricated using the FDM technique. The 1 wt% filler loading causes agglomeration, and the highest filler reinforcement (10 wt%) causes nanoparticle bunching. The conductivity value of the MWCNT/ABS composite shows critical behavior when the CNT loading reaches a percolation threshold value of 3 wt% filler loading for the raster angle of [0, 10]. The maximum electrical conductivity achieved was 232 e-2S/cm for the 10 wt% MWCNT loadings. The MFI value was dramatically reduced with filler loading, reaching 0.03 g/10 mm for 10% loading. This was due to the clogging of nanoparticles at the nozzle during the printing process. Rymansaib et al. [173] developed a conductive composite blend made of graphite and carbon nanofibers with thermoplastic polystyrene material. The authors developed electrodes suitable for experiments for conductivity studies using commercially available conductive polystyrene material. The prepared electrodes were subjected to a cyclic voltammetry process in the aqueous 1,1-ferrocenedimethanol solution and continued with differential voltammetry detection through anodic stripping for aq. Pb^{2+}. The graphite/CNF/polystyrene (10/10/80 wt%) composite possesses good conductivity values and a stable electrochemical interface with defined geometric surface areas. The 3D printed electrode forms a stable interface with the polystyrene shell and gives proper signals through the voltammetry response, which are also reusable after the polishing process. Hamzah et al. [174] studied the effect of printing orientation on the conductive properties of 3D printed carbon black/ABS polymer composites. The electrodes were prepared using these composites and studied in both the horizontal and vertical printed directions. The horizontal printing results in two types of electrodes, namely, horizontally printed smooth surface (HPSS) electrodes and horizontally printed rough surface (HPRS) electrodes. For the various redox couples, the vertically printed electrode shows improved current response as compared to HPRS and HPSS electrodes that are printed horizontally. There were no differences in capacitive responses; this indicates that all the electrodes possess identical conductive surface areas. The resistance to charge transfer and solution was reduced in vertically printed electrodes as compared to HPRS and HPSS. Hence, the electrochemical response was good in vertically printed composites, and it shows that the printing parameter is the main key factor in getting the optimum conductivity values. Ivanov et al. [175] reported the electrical properties of graphene nanoplatelets (GNPs) and MWCNT-filled PLA composites printed using the FDM technique. A slight synergic effect was found in the GNP and MWCNT hybrid filler reinforcement, which is 3% CNT/3% GNP and a 4.5% CNT/1.5% GNP PLA composite, showing high electrical conductivity as compared to individual filler reinforcement with a PLA matrix having the same filler percentage. This electrical conductivity improvement was due to GNPs and CNTs' interaction, which restricts the GNPs' agglomeration and forms a bridge with neighboring particles, which resulted in the effective path for conduction. The addition of 0.5 wt% graphene particles to the poly(trimethylene

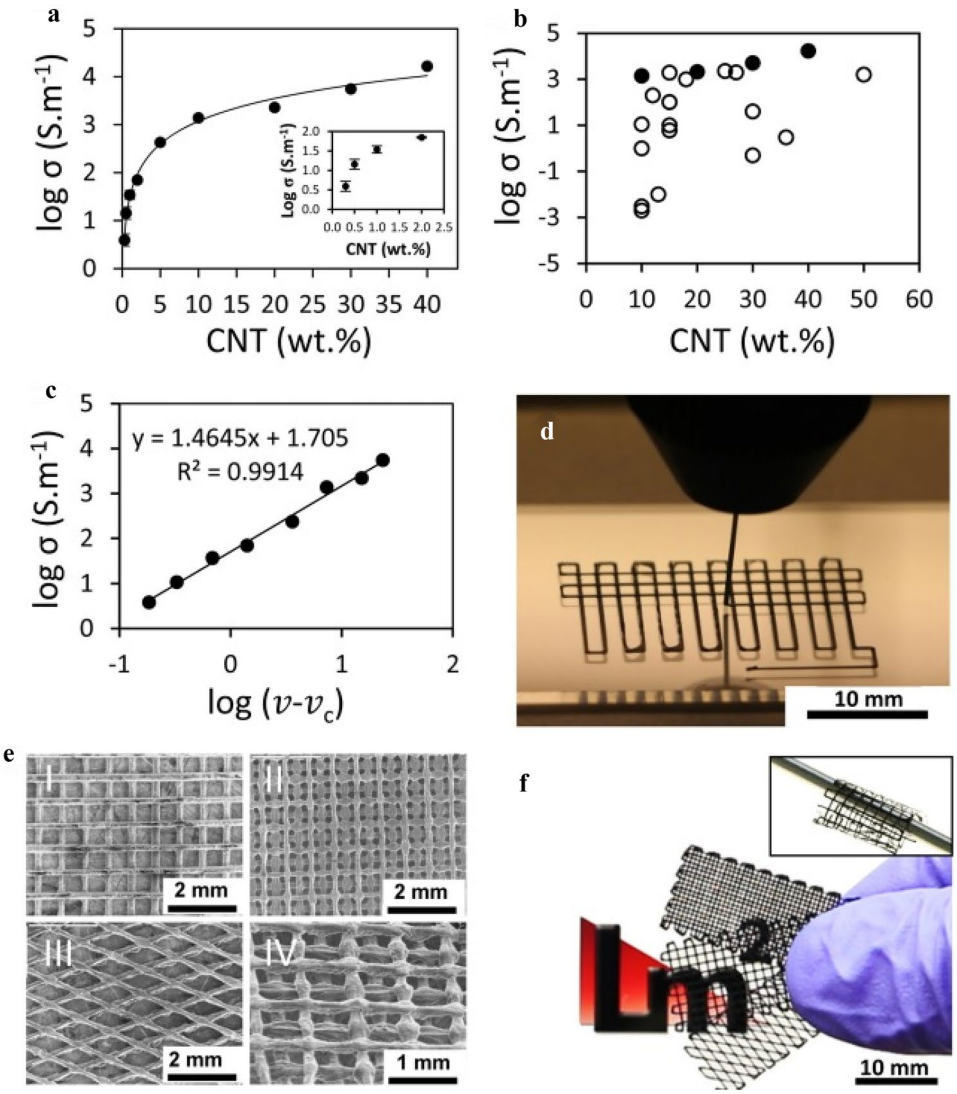

Fig. 9 **a** Plot of electrical conductivity variation with CNT concentration, **b** comparison of experimental conductivity results with literature values ((●) indicates experimental values, (○) indicates literature values), **c** plot of log σ against log (v-v_c), **d** 3D printed scaffolds, **e** top view of 3D printed scaffolds, and **f** the three structures with 4-layered printed scaffold [171]. (Reused with the permission from Elsevier, License No. 5195370408837)

carbonate) (PTMC) matrix resulted in an electrical conductivity value of nearly 1×10^{-3} S/m, whereas 3 wt% filler loading results in an improved conductivity value of 1×10^{-1} S/m [176]. Compton et al. [177] conducted a study on the electrical properties analysis of graphene-reinforced epoxy 3D printed composites. The measured average sheet resistance of composite samples along with the transverse direction to the printing is $6.7 \times 10\ 2$ Ω/sq and $1.06 \times 10\ 3$ Ω/sq, respectively. These measurements show that the printing process has a significant effect on the conductive network within the composites because of the graphene flake alignments in the printed composite. Postiglione et al. [118] evaluated the electrical conductivity values of MWCNT-filled PLA composites printed using the LDM technique. The electrical conductivity of PLA composite was influenced by the filler addition (0.5-10 wt%), which was validated through resistance measurements. The conductivity σ values were found to be substantially increased concerning PLA matrix upon the addition of 0.5 wt% MWCNT. Moreover, the progressive σ increment was observed with increasing filler concentration followed by percolation behavior, where the values fall in the range of 10–100 S/m for higher filler loading (5–10 wt%). These results demonstrate that the potentiality of LDM printed composite enables the assembling of internal electronic functionalities into 3D structures in a straightforward and versatile fashion. Yuan et al. [178] investigated the electrical conductivity behavior of carbon nanotube-filled thermoplastic polyamide 12 (PA12) and polyurethane (PU) composites printed using the SLS technique. The electrical conductivity value was found to increase when approaching the filler concentration of 0.5 wt% in laser sintered composite, which possesses the magnitude of conductivity values of over 10–5 S/cm at higher filler concentrations. The variation of DC conductivity value with the filler concentration in s-CNT-reinforced PU and PA12 composites is illustrated in Fig. 10a. It was also observed that higher electrical conductivity was found

in laser-sintered composites as compared to hot-compressed composites with the same filler concentration. Moreover, the s-CNT/PU composite possesses a higher conductivity value than the s-CNT/PA12 composite. Figure 10b depicts the variation of electrical measurement values in the *X–Y* and *X–Z* directions in cylindrical samples. It was found that the conductivity value is higher in the *X–Z* building direction than in the *X–Y* building direction. Similarly, these composites were studied with various AC frequency ranges, and it was discovered that a 0.5 wt% s-CNT-loaded PA12 composite has an increased electrical conductivity value ranging from 10^{-5} order to 10^{-2} S/cm in the frequency range of 104–107 Hz (Fig. 10c). The 0.5 wt% CNT-loaded PU composite, on the other hand, has frequency-independent electrical conductivity (over 10^{-4} S/cm) across the frequency range. The reinforcement of MWCNTs leads to the increased potential for electrical conductivity enhancement because of the higher aspect ratio and lower surface area. These particles' addition to epoxy forms conductive paths in the network when the filler concentration reaches above the critical volume fraction. The filler aspect ratio, dispersibility, and capability to conglomerate are the important factors for the conductivity study at the lower filler concentration. The treatment of these particles leads to aspect ratio reduction and elevates the percolation threshold value [179].

4.3 Self-healing properties

The self-healing unique composites have remarkable functionalities towards healing damage by restoring their original

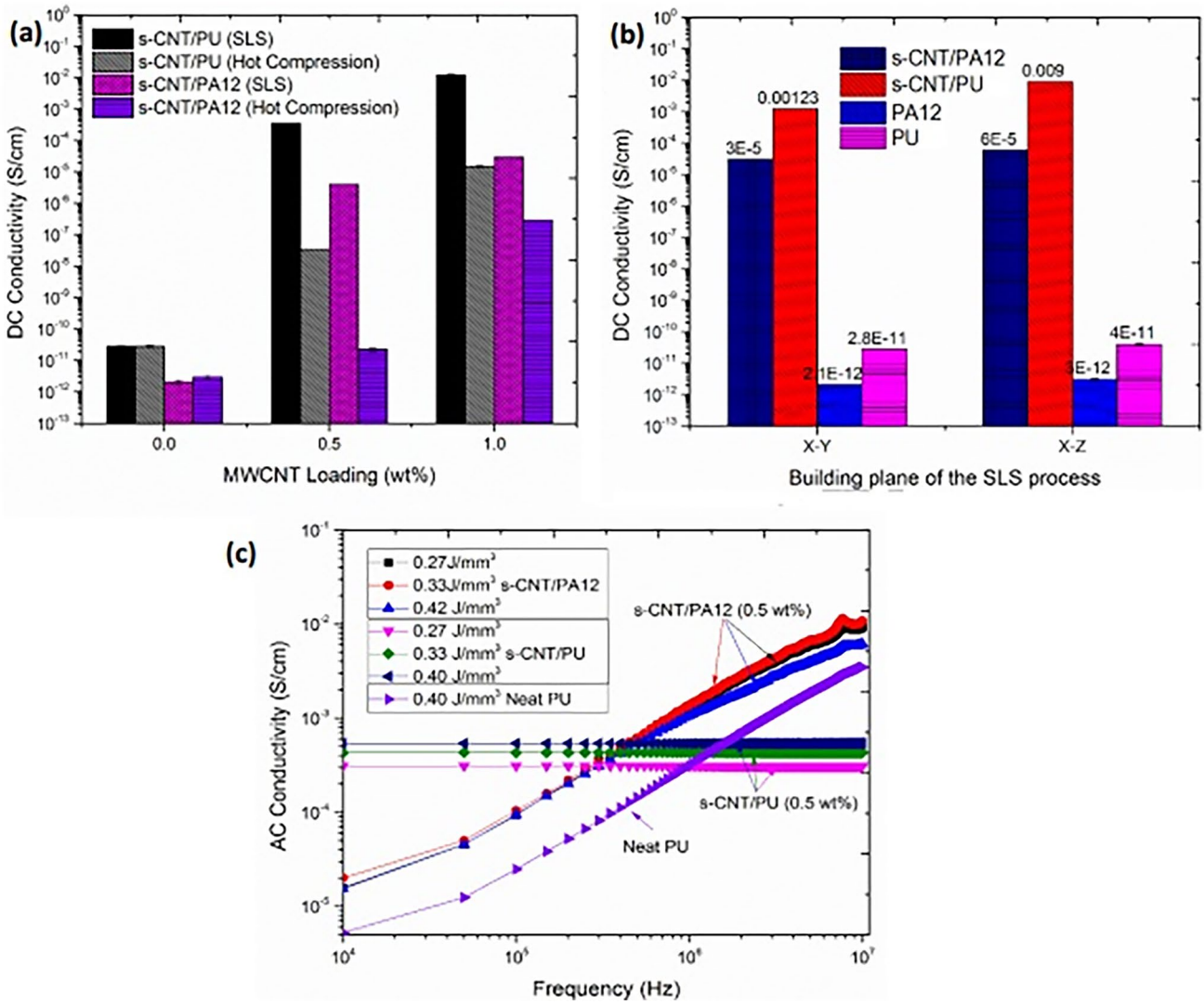

Fig. 10 **a** DC conductivity comparison in hot compressed and laser sintered composites, **b** effect of building directions (*X–Y* and *X–Z*) on DC conductivities of different composites, **c** variations of AC conductivities with different frequency range in s-CNT loaded composites [178]. (Reused with the permission from Elsevier, License No. 5195370603755)

performance fully or partially. Self-healing materials are mainly classified into two classes based on utilized heating mechanisms and adopted approaches; they are (i) autonomous and (ii) non-autonomous materials [180, 181]. Generally, self-healing composites are further categorized as intrinsic, vascular, and capsule-based conceptual approaches. It was quite difficult to upscale the material self-healing ability to the 3D structures, so there is a need to place selective self-healing functionality in a particular area that is prone to damage [182, 183]. The AM techniques are efficient tools for the introduction of accurate and selective self-healing (SH) functionality into particular areas of the composite structure. In the case of intrinsic SH structures, 3D printing has provided precise control over the distribution of SH functional parts, such as the development of self-healing polymers within or onto the structure [184, 185].

The SH components were manufactured with resin casting and FDM 3D printing by utilizing healing components that release upon damage to the microvascular network. The SH test was performed on the damaged composite samples, which demonstrates both mechanical recovery and aesthetical behavior. The uniaxial tensile test reveals that Epoxy-J and polydimethylsiloxane (PDMS) possess healing efficiencies of 82% and 79%, respectively. As the healing agents, these are preferred as a matrix material where they possess ideal chemical compatibility with low viscosity suitable for autonomic curing in the crack plane. The versatile nature of the manufacturing process allows the use of different materials with dual SH mechanisms through the integration of microvascular networks with a matrix that already has intrinsic molecular level self-healing functionality [186]. The presence of a self-healing mechanism in 3D printed structures has many advantages, such as being economical, versatile, requiring less production time, and allowing any imagined structure to be produced easily. The SH behavior in a 3D structure leads to strain release, which initiates cracks and causes damage to the material. However, these SH properties are capable of overcoming potential damage at the sub-surface level, which allows rapid healing of material cracks without affecting workability and leads to a significant reduction in vulnerability [187–189]. Wu et al. [190] developed a novel conductive self-healing polymer composite ink using 3D extrusion printing on PDMS substrates. Polyborosiloxane (PBS) is used as a matrix material, which possesses unique chemically activated mechanically adaptive properties that enable polymer composite extrusion in the liquefied state and is quickly restored to a solid-state when exposed to air. This was attributed to PBS's shear thinning behavior in both solid and liquefied states, with a 1% shear amplitude in the dynamic oscillation mode. Along with shear thinning behavior, the 5 vol.% electrochemical graphene addition leads to electrically self-healing ability in the printed composites. Sanders et al. [191] developed a self-healing composite consisting of anisole modified photocurable resin and PMMA-filled microcapsules using a direct SLA 3D printing technique. The addition of commercial SH capsules to the resins leads to a maximum recovery healing efficiency of 87% towards the critical load, analyzed through fracture toughness (mode 1). These promising results are optimum for bespoke structure applications with structural integrity. This technique of adding microcapsules results in functional incorporation, which is available for different commercial inks because of its flexibility and ease of adoption. The cellulose nanocrystals' (CNCs) reinforcement with polycaprolactone and polyurethane matrix results in improved interfacial compatibility and maintains the self-healing property through the 3D printing technique. The crack healing mechanism in the composite occurs in multiple stages. Initially, the SH process was triggered by the material heating at a temperature range higher than PCL's melting temperatures. At this stage, the molecular chains of PCL melt and flow towards the crack interface. After lowering the temperature, the molecular chains interlocked and recrystallized at the interface. This way, the crack interface was repaired through the diffusion of molecular chains. Also, the presence of hydrogen bonding among PCL, TPU, and CNCs promotes the self-healing process in the liquid phase of the material [192].

4.4 Mechanical properties

The fiber-reinforced polymer composites offer superior directional mechanical properties, and their usage with different 3D printing techniques improves the mechanical properties that lead to new innovative research work. The particular process parameters have been analyzed to improve the mechanical behavior by optimizing the group of properties or certain properties of a particular material [193–195]. Table 5 summarizes the mechanical observations in various 3D printed composites. The hydrous magnesium silicate-reinforced ABS composites printed using the FDM technique have maximum flexural and tensile strengths for the conditional parameters like lower layer thickness and lower printing speed as compared to other parameters for the samples. For the optimum conditions like 0.2-mm layer thickness and 30 mm/s of printing speed, the result is better adhesion with the previous layers, which causes an improvement in tensile and flexural strengths. The other sample process parameters like 0.25- and 0.3-mm layer thickness achieve a strength value which is marginally reduced as compared to 0.2-mm samples [196].

The major printing parameters like layer thickness affect both the tensile and bending properties of wood/PLA 3D printed composites. The maximum mechanical properties were achieved for a 0.05 mm thickness, followed by 0.1, 0.2, and 0.3 mm, respectively. The maximum bending strength and modulus values achieved were 128.3 MPa and 4887 MPa,

Table 5 Mechanical observations in various 3D printed composites

Composites	Fabrication technique	Working temperature range	Mechanical observations	Ref.
Spray dried hydroxyapatite (sdHA)/PLA	FDM	175–200 °C	The PLA and sdHA/PLA scaffolds exhibited stiffness values of 238.98 ± 19.05 MPa and 124.04 ± 25.21 MPa, respectively, for a strain range of 2–10%. The more stiffness of PLA scaffolds was due to different porosity. Overall, the sdHA reinforcing effect is less with PLA on mechanical properties	[197]
Nylon/glass (FG)/carbon (CF)/Kevlar	FDM	265–270 °C	The maximum amount of creep deformation was observed in nylon samples. The creep results follows the order of nylon > nylon/FG > nylon/Kevlar > nylon/CF. A similar trend was observed in creep recovery behavior	[198]
Carbon fiber/PA 12	FDM	240–260 °C	The 10 wt% CF reinforcement with PA12 enhances the tensile and flexural strengths by 102.2% and 251.1%, respectively. Without carbon reinforcement, the PA12 exhibits an impact strength of 22.5 kJ/m^2, whereas 2 wt% and 10 wt% show an impact value of 12.1 kJ/m^2 and 24.8 kJ/m^2, respectively. This reduction of impact properties was due to stress concentration generation at the fiber end	[199]
Glass fiber/PP/maleic anhydride polyolefin (POE-g-MA)	FDM and compression molding	175–200 °C	The composite with GF addition exhibit higher mechanical properties and modulus value with lower elongation at break and flexibility. The 10 and 20 wt% POE-g-MA addition improves elongation at break value and reduces modulus value. However, the increment of modulus value was observed at 30 wt% of POE-g-MA addition	[200]
ABS/graphene nanoplatelets	FDM	180–200 °C	The addition of filler particles improves the tensile modulus of ABS filament. It is also observed that the presence of GNPs causes a slight reduction of strain at break and ultimate tensile stress value in horizontal and vertical printed directions; moreover, the severe effect was found along the perpendicular direction	[201]
Polyetherimide (PEI)/PEEK	FDM	210–270 °C	The PEEK samples possess stronger fracture resistance during the bending test than PEI samples. The PEEK components produced using horizontal printing mode show maximum impact resistance of 113 kJ/m^2. The impact strength in PEI parts was slightly higher in lower nozzle temperature than higher nozzle temperature	[202]
Epoxy/acrylate	SLA	80–120 °C	The printed composite exhibit tensile and flexural strength of 36.28 MPa and 63.96 MPa, respectively. These samples show good toughness with an impact strength of 38.83 kJ/m^2 and higher elongation at a break value of 15.09%. This was attributed to the flexible nature of cured photopolymer and chain structures of photopolymer and ethyoxyl groups	[203]

Table 5 (continued)

Composites	Fabrication technique	Working temperature range	Mechanical observations	Ref.
Carbon fiber/bisphenol-F epoxy resin	Direct ink writing (DIW)	80–200 °C	The axially printed unidirectional CF parts (8 vol.%) show a 37% higher young's modulus value than random pressed part with the same fiber volume fraction. These improved observations were also found in compressive properties	[204]
Onyx/carbon	FDM	250–275 °C	The printed composite with concentric carbon fiber infill pattern shows better flexural strength than the isotropic CF infill pattern. The composite with 48.72% of CF shows a maximum flexural strength of 270.63 MPa. It was observed that the strength values depend on the concentration levels of carbon fibers	[205]
ABS/carbon fiber	FDM	200–240 °C	The printed sample with [0, 90] raster angle shows larger young's modulus, tensile and yield strength than the specimen printed with [−45, +45] raster angle. The optimum tensile properties were obtained for 25 mm/s of infill speed; further increment in infill speed leads to lower interaction and inter-bonding among contiguous rasters	[206]
Wood flour (WF)/PLA	FDM	171–175 °C	In the context of 0–1.5% strain range, the tensile stress was elevated with WF addition, and above 1.5% strain range gives lower value strength than the neat PLA. The tensile strength of the specimen is approximately 66% of compressive strength, which means the tensile strength is lower than compressive strength	[207]

respectively, for a 0.05 mm specimen. Similarly, the 0.3-mm layer thickness sample has 84.3 MPa and 3580 MPa of bending strength and modulus values, respectively. The layer thickness increment causes bigger gaps, which resulted in porosity in the printed samples. This specimen porosity causes a reduction in mechanical properties [208]. The FDM-printed continuous carbon fiber-reinforced thermosetting epoxy composite possesses better mechanical properties than similar thermoplastic reinforced composites. The continuous carbon fibers with thermosetting epoxy composite reach maximum tensile strength and modulus values of 792.8 MPa and 161.4 MPa, respectively, while flexural strength and modulus values are 202 MPa and 143.9 MPa, respectively. The tensile specimen's failure mechanism reveals that the failure occurs initially through the matrix cracking in the specimens, followed by layer separation, fiber breaking, and debonding with increasing applied load. These fractured cross-sections are similar to the conventionally manufactured composite specimen failure mechanism [209]. The wood particles added to PLA composites possess a lighter density with increasing wood particle content. The FFF-printed PLA filaments improve the tensile strength from 55 to 57 MPa with 10% wood particle addition, whereas 50% wood particle addition reduces the tensile strength value to 30 MPa. The elastic modulus value of the PLA filaments was elevated from 3.27 to 3.94 GPa due to 20% wood particle addition, and it was decreased to 3 GPa when the composite sample was loaded with 50% wood particle addition. This is attributed to lower levels of filler loading providing a reinforcing effect, whereas a higher level of loading causes difficulties in particle encapsulation in the filaments, which leads to limited load transfer and poor bonding between the particles and the filament [210]. When filled with graphene nanoplatelets (GNPs), the PLA composite shows the best performance towards tensile and flexural stress when printed using the FFF technique. The upright-oriented printed specimen has 1.5 and 1.7 times more tensile and flexural stress, respectively, than the neat PLA and PLA 3D850 sample. Similarly, the graphene/PLA composite possesses 1.2 times more inter-laminar shear strength than the neat PLA and PLA 3D850 samples. The GNP addition reduces the impact strength by 1.2 to 1.3 times in comparison to neat samples. The reduction of impact strength was due

to the brittle behavior of the graphene/PLA composite both in flat and on-edge orientations. The GNPs strongly adhered to the interlayers of PLA filaments, and hence, the overall performance was enhanced without altering the dimensional accuracy [211]. Melenka et al. [212] evaluated the elastic properties of carbon, glass fiber, and Kevlar fiber-reinforced 3D printed composites and predicted these values using the average stiffness (VAS) method. The experimental elastic values achieved were 1767.2, 6920, and 9001.2 MPa, respectively, for 4.04, 8.08, and 10.1% of fiber volume fractions. But the predicted modulus values are 4155.7, 7380, and 8992.1 MPa, respectively, for carbon, glass, and Kevlar fibers. The difference between experimental and predicted values is found to be 57.5, 6.2, and 0.1%, respectively, for continuous fibers. This developed model allows the designers to predict the elastic properties of continuous fiber-reinforced 3D components as functional components. The 5% and 10% TiO_2 reinforcement in ABS filaments shows improvement in tensile and flexural strengths as compared to 1% and unfilled ABS composites, while TiO_2 percentage variation has no significant effect on Young's modulus and stress values. In these studies, the nanoparticle's size variation also plays a dominant role in determining tensile and flexural strengths [213]. The tensile and flexural strengths of GF/PEEK and CF/PEEK increased with increasing platform temperature and nozzle temperature, respectively, whereas impact performance was not affected by any kind of temperature. The optimum parameters of 440 °C nozzle temperature and 280 °C platform temperature lead to maximum mechanical properties in 3D printed CF/PEEK and GF/PEEK composites. The highest nozzle temperature caused better formability and melting fluidity of the printed filaments. The diffusion and infiltration among deposited materials were improved due to the higher platform temperature that produces maximum energy. All of these beneficial things improve the adhesion between interlayers with void reduction, so the overall mechanical performance of the printed composites was improved. However, the increased layer thickness and printing speed cause a reduction in the mechanical properties of the printed PEEK composites [214]. The raster angles during printing affect the mechanical properties of the 3D printed parts. It was observed that the 6 wt% GNP addition to the PA12 matrix improves the elastic modulus values by 50.6%, 48.3%, 40.5%, and 43.4% for 0°, 45°, 90°, and compression-molded specimens, respectively. The 0° raster angle specimen exhibits the largest increment in modulus values, and it indicates that the GNPs behave as efficient reinforcements in 3D printed parts. The GNPs are preferentially oriented along the stretching direction and form the conductive paths easily with the dissipation of energy during tensile testing. This resulted in retardation of crack growth during failure, and hence, modulus values are elevated. A slight decrement in tensile strength was observed with GNPs' incorporation, and this might be due to a compromise between stress concentrations due to GNPs' addition with larger size and GNPs' reinforcing effect [215]. The addition of short carbon fibers to the PLA matrix improves the tensile modulus in the printing direction, the tensile modulus in the transverse direction, and the shear modulus values by 2.2, 1.25, and 1.16 times higher than neat PLA material [216]. For both glass and carbon fiber, it was observed that the stress values elevated linearly with a strain before breaking at 6.2% and 5.2% strain, respectively, for glass and carbon fibers, which indicates the brittle nature of printed composites. The carbon/nylon composite possesses maximum tensile strength and young's modulus values of 600 MPa and 12.99 GPa, respectively, whereas glass/nylon possesses 450 MPa and 7.2 GPa, respectively. Glass fibers exhibit more elongation before failure than carbon fibers due to their greater flexibility. The drop in stress–strain slope is shown in Fig. 11a. The fracture modes of 3D printed carbon and glass fiber composites are illustrated in Fig. 11b, c. The failure mechanism during the tensile test is illustrated in Fig. 11d, e. The extensive fiber breakage reveals that the failure mode of tensioned 3D printed glass and carbon reinforced thermoplastic composites is fiber dominant, indicating that there was an effective load transfer from matrix to fiber (Fig. 11f, g). The fiber pull-out was attributed to improper nylon matrix coating on the surface of the fiber during filament printing. The flexural strength and flexural modulus values were higher for carbon reinforcement than glass fiber due to more stiffness [217].

Liu et al. [218] evaluated the mechanical properties of PLA-reinforced composites with wood, copper, carbon fiber, aluminum, and ceramic as additive materials. The neat PLA, PLA/wood, and PLA/carbon show better printing formability than copper, aluminum, and ceramic-based composites. The mechanical properties were enhanced due to the addition of aluminum, copper, and ceramic materials as compared to neat PLA, while the addition of chopped carbon fibers and wood reduced the mechanical properties. The parameters like $+45°/-45°$ raster angles with on-edge orientation show a maximum mechanical strength in the majority of the cases. Because of weak interlayer bonding, the upright-oriented samples possess lower mechanical strength and modulus values. The carbon fiber and wood-based PLA have higher porosity, poor adhesion, and compaction between printed layers as compared to neat PLA, which resulted in lower mechanical strength. The carbon fiber reinforcement with ABS, polyethylene terephthalate (PETG), and amphora increases the value of modulus of elasticity in all the printing directions, while the 0° oriented PETG sample possesses a 313.2% improvement in PETG printed samples. This also shows an increment in tensile strength of 48.2%. This increment was attributed to carbon fiber's alignment along loading direction with 0° orientation in printed composites [219]. The reinforcement of 10 vol.% carbon fiber to the polypropylene

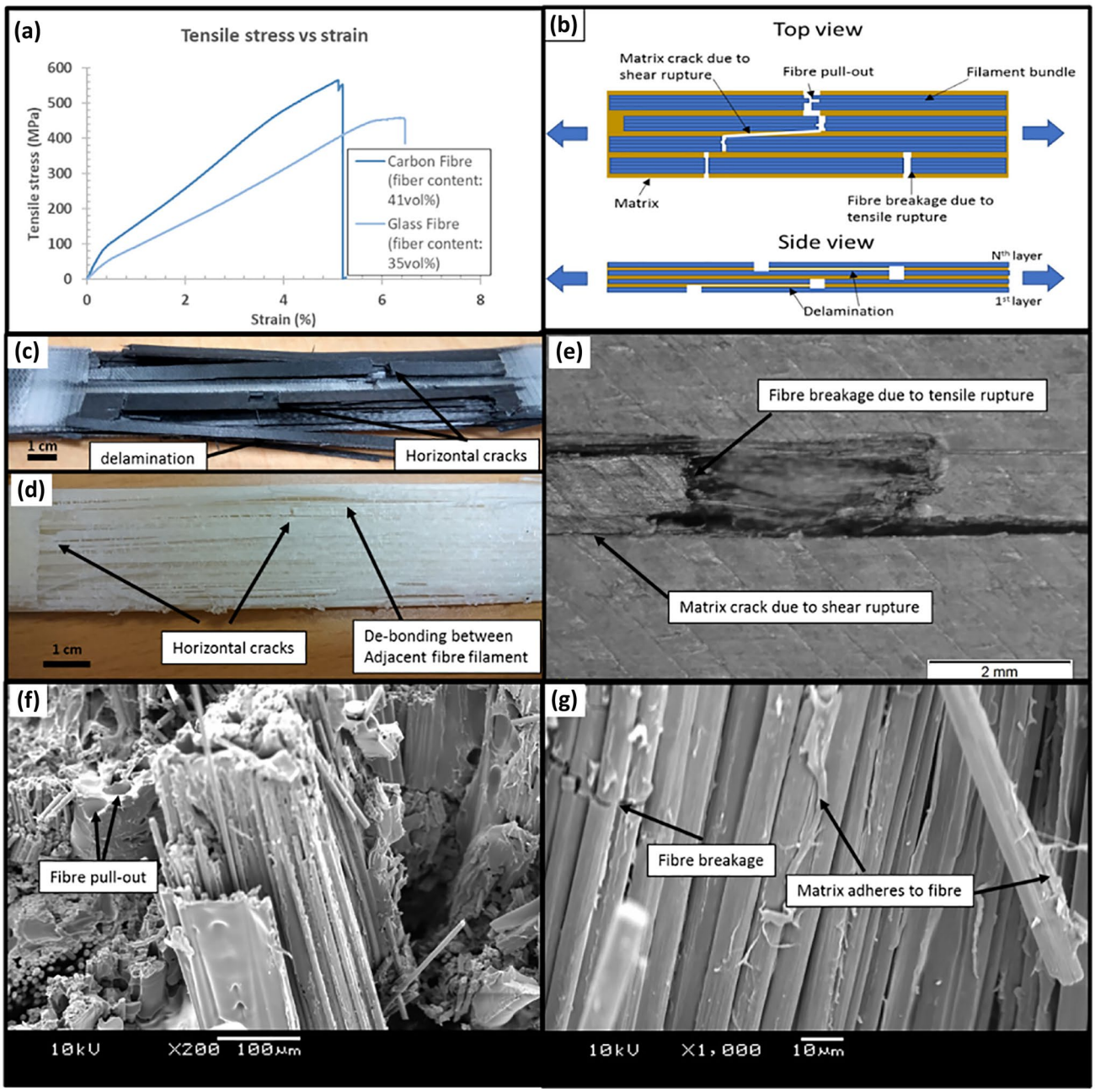

Fig. 11 **a** Stress–strain curves for glass and carbon fiber-reinforced nylon composite, **b** tensile specimen fracture mechanism illustration, **c** fracture mode of carbon fiber-reinforced tensile specimen, **d** fracture mode of glass fiber-reinforced tensile specimen, **e** illustration of matrix crack due to tensile rupture, **f** fibers pull out in fractured surface, **g** SEM image of matrix-fiber adhesion and fiber breakage [217]. (Reused with the permission from Elsevier, License No. 5195370798948)

leads to an increment in filament yield stress of more than 100% and the young's modulus value of more than 400% and decreases the strain yield value by 50% as compared to neat PP filament. This was attributed to the anisotropic behavior of fibers oriented in the flow direction, which improves the stress transfer between matrix and fiber, which causes good compatibility and restricts the polymer chain movement. The CF10/PP composite shows more brittle behavior in fractured surfaces than neat PP filament and exhibits plastic deformation in smaller zones, which results in 2–4 times lower impact energies than neat PP [220]. The stress–strain behavior of MWCNT-filled FDM-printed thermoplastic polyurethane (TPU) for different weight percentages during loading and unloading is illustrated in Fig. 12. The MWCNT addition improves the overall strength of the FDM-printed TPU composite. It is observed that 5 wt% MWCNT-loaded

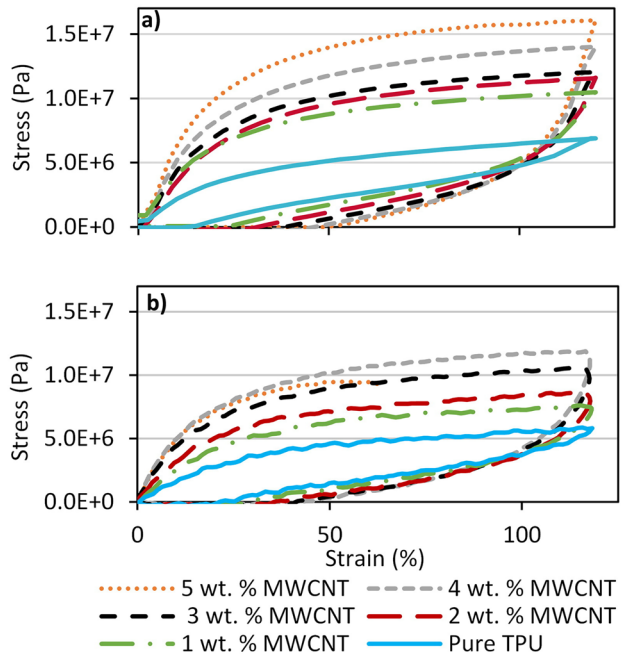

Fig. 12 Stress/strain response during loading and unloading of **a** extruded filament, **b** FDM-printed MWCNT/TPU nanocomposite with different weight percentage [221]. (Reused with the permission from Elsevier, License No. 5195370963593)

nanocomposite couldn't be strained up to 100%, instead of that it falls nearly 60% strain. This lower strain failure was attributed to weaker adhesion and a decrement in the tackiness of the overall nanocomposites. Also, more defects were observed in 5 wt% loaded MWCNT composites [221]. The optimum reinforcement of 6 wt% CNTs in ABS filament results in significant improvement of tensile strength and modulus value accompanied by reduction of elongation at break value [222].

4.5 Thermal properties

The 3D printing offers flexibility in design and fabrication while manufacturing heat exchangers with lightweight characteristics and more thermal exchange efficiency using polymer/metal composites. The novel combination of two processes was utilized for the fabrication: fiber encapsulation additive manufacturing (FEAM) and FDM [223]. The heat exchanger component design consists of continuous conductive natural metallic fibers that pass through the walls of polymer channels, which behave as a thermal link among two-fluid flows. These specific designs and assemblies overcome the drawbacks in heat exchangers associated with polymers and heat exchangers made of metals; also these designs improve heat transfer efficiency in the printed parts [224, 225]. The thermogravimetric analysis of silver nanowires (Ag NWs)/PLA composite between room temperature and 550 °C is illustrated in Fig. 13a, and their residue SEM image is shown in Fig. 13b. The initial weight loss was observed in the TGA curve at 100° C due to moisture loss in PLA. The effect of Ag NWs on thermal degradation behavior was illustrated through the DTGA curve in Fig. 13a. It was observed that the degradation temperature was almost unchanged with Ag NW addition. This was due to less chemical interaction among PLA and Ag NWs. The bare Ag NWs are unstable over 300 °C temperature, and the majority of Ag NWs remain intact inside nanocomposites. The DSC curves for neat PLA and Ag NWs/PLA are shown in Fig. 13c. The melting temperature, cold crystallization, and glass transition temperatures were recorded at 168 °C, 98 °C, and 62 °C, respectively. These temperatures are almost unchanged due to nanowire addition, and it is indicated in dashed lines [226]. The percolation threshold value of thermal diffusivity falls between 20 and 30% discrete carbon fiber additions with PEEK filament. The 20% discrete CF filling in PEEK leads to a modest increment in thermal diffusivity of approximately 20–25% as compared to unfilled PEEK. The 30% filler reinforcement improves the thermal diffusivity value by three times as compared to neat PEEK, and it has good agreement with the rule of mixture. The thermal conductivity of 3D printed CF/PEEK composite possesses 25–30% lower values than casted composites due to imperfections and additional porosity [227].

The maximum degradation temperature (Tmax) for neat polyamide-12 (PA12) is 454.89 °C, whereas the addition of 10 wt% carbon black (CB) to PA12 elevates the T_{max} value to 468.61 °C. This was attributed to the presence of higher thermal stability in CB particles, and it enhances the overall thermal stability of the printed composites. A smaller amount of CB (1.5, 3 wt%) improves the thermal stability due to the reduction of peak heat release rate. This enhancement was attributed to carbon layer formation that inhibits the combustion process. These CB particles have no significant effect on the semi-crystalline nature of PA-12 filament, hence no significant changes in melting and glass transition temperatures [228]. The addition of micro-diamond particles into ABS filament with 37.5% and 60% concentration resulted in improved thermal conductivity value of 0.37 W/m–K and 0.94 W/m–K as compared to near ABS filament (0.17 W/m–K). Similarly, the thermal diffusivity values were also improved to 0.27 ± 0.01 mm^2/s and 0.46 ± 0.01 mm^2/s for 37.5% and 60% diamond particle concentration as compared to neat ABS filament (0.13–0.18 mm^2/s). The DSC thermograph reveals that the D-ABS (37.5%) composite filament shows a glass transition temperature (T_g) at 108 °C for styrene, followed by acrylonitrile melting at 138 °C endothermic peak. It was noted that the transition peaks are less distinct and broader in the DSC curves; also the contribution of the micro-diamond particle is less in Tm and T_g peaks. The response from D-ABS (60%) composite filament shows that the styrene T_g peak

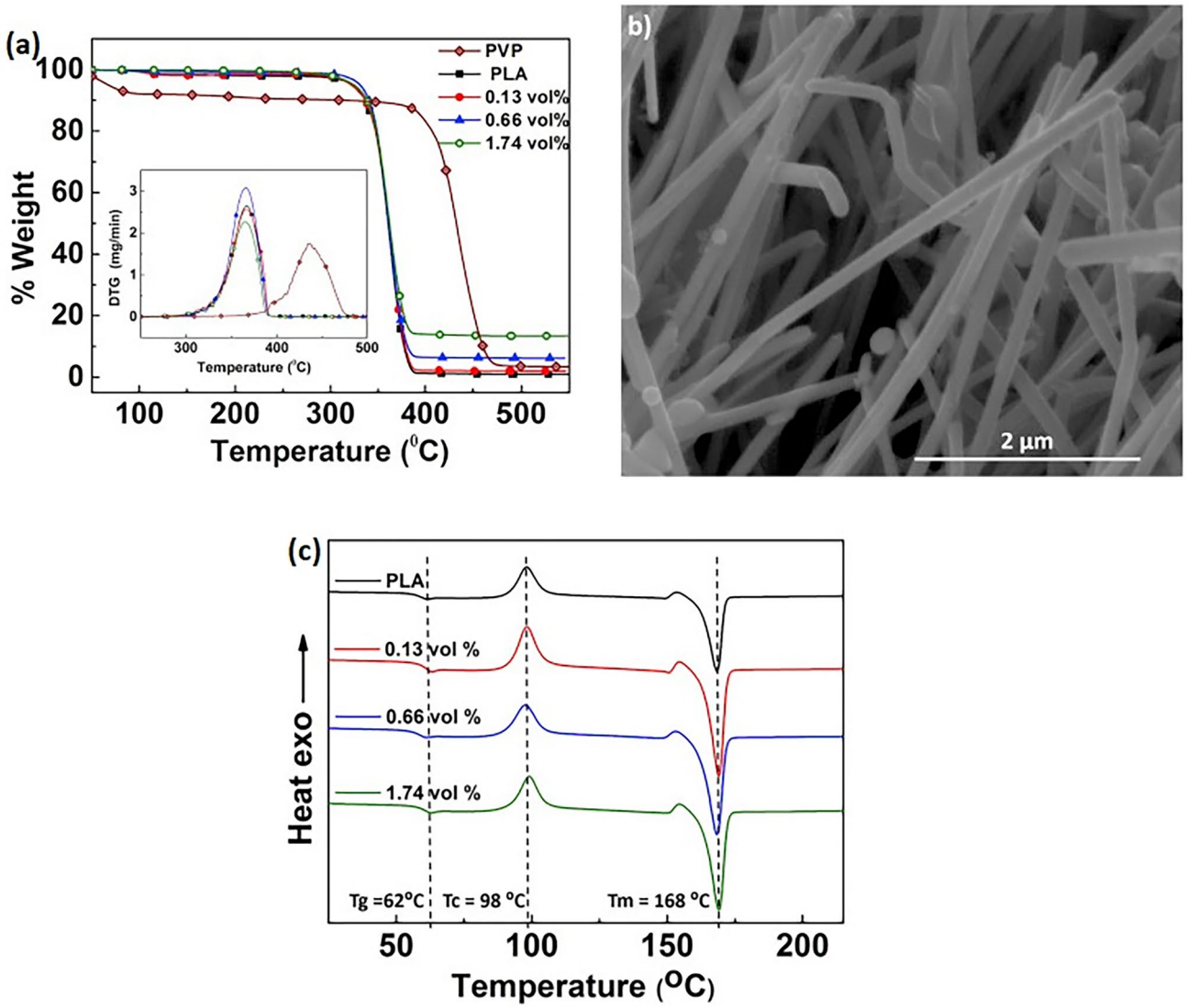

Fig. 13 **a** Thermal gravimetric analysis of PLA and Ag NWs/PLA nanocomposites, **b** SEM micrograph of TGA residue, **c** second heating DSC graph for PLA and nanocomposite [226]. (Reused with the permission from Elsevier, License No. 5195371141137)

was shifted to 114 °C higher temperature, followed by acrylonitrile melt at 146 °C. This is attributed to strong physical interlocking between diamond particles and polymer matrix at higher filler loading, which resulted in restricted molecular chain mobility [229]. The boron nitride (hBN) materials are commonly employed for nanocomposites ink that can enhance the mechanical performance, biocompatibility, and thermal conductivity in printed scaffolds. The 3D BioPlotter printer was utilized for the printing process with variations of printing speed (5–20 mm/s) and printing pressure (0.5–3 bar). These hBN-included scaffolds are popular in bioelectronics applications where thermal conductivity is of greater importance. The nanocomposite ink was printed at room temperature through the extrusion process for complex architecture designs by minimizing the post-printing process [230]. The lower concentration of copper particles (10 vol.%) in ABS has no significant effect on thermal conductivity, but the addition of 30 vol.% copper particles over matrix glass transition temperature increases the thermal conductivity value of copper/ABS composites. The reason was the mobility increment of copper particles in the molten matrix beyond its glass transition temperature. Also, the addition of up to 10 vol.% fillers is not capable to overcome the thermal resistance of the ABS matrix. A further addition to 20 vol.% was found to begin the formation of conductive chains and lead to smaller improvement in conductivity values. On the other hand, the addition of iron particles has a lower effect on the thermal conductivity of ABS filaments than copper particles. In this case, only above 30 vol.% of iron particles reinforcement leads to the initial formation of conductivity chains. The heat flow and heat capacity

values are higher for unfilled ABS filament than iron filler ABS composite [231]. The heat resistance capacity of CNT-filled epoxy/carbon fiber is better below the T_g value and worse above the T_g value as compared to CNTs adhered CF/epoxy composites, and these T_g values are 133 °C and 130 °C, respectively, for CNT-CF/epoxy and CNT-epoxy/CF composites. It is also evident that the treated fibers enhance the T_g value in resultant composites [232]. The TGA and DSC test reveal that thermal stability is higher for PLA with nylon glass fiber, carbon, and PET-G polymer composite blend than the neat PLA. The PLA filament with 30% nylon glass fiber composite has the highest degradation temperature because of silicon compound presence. The order of thermal degradation is PLA/30% nylon glass > PLA/10% CF > PLA + PET-G > PLA. The PLA possesses a different characteristic that it degrades easily under continuous heating conditions. A considerable increment in melting temperature was employed for PLA/10% CF than the PLA filament due to the increment in the amorphous nature of the resultant composite. The effect of carbon fibers reinforcement on the thermal stability of PLA polymer blends is less than the nylon glass reinforcements. The PLA/30% nylon glass, PLA/10% CF, PLA + PET-G, and PLA composite blend records a glass transition temperature of 50.6 °C, 60.3 °C, 74.0 °C, and 58.5 °C; similarly, the degradation temperatures were found to be 442.3 °C, 346.2 °C, 351.1 °C, and 329.0 °C [233, 234].

5 Applications

5.1 Electronics and electrical devices

The usage of 3D printing techniques certainly provides appropriate and precise geometrical electronic prototypes with minimized development time. The insertion of electrically conductive fillers in 3D printed polymer composites can act as electronic equipment that can be used in many ways [235]. 3D printed nylon-6-based polymer composites are studied with electrical characteristics with variations of filling volume and non-homogeneous relative permittivity as a dielectric material for the manufacturing of RF/microwave circuits or 3D structures [236]. Jakus et al. [237] developed a 3D printed graphene/PLA conductive composite for functional electronic applications because of its flexibility and ability to be mechanically robust in retaining electrical conductivity greater than 800 S/m. These conductive composites are printable in different ambient conditions through extrusion-oriented 3D printing to create a graphene structure with 100 m smaller dimensions containing two layers to hundreds of layers with thicker objects. Leigh et al. [238] fabricated a 3D printed CB/PCL composite for piezoresistive and capacitive sensors using the BFB3000 3D printer. The production of these functional sensor components is simple, quick production and can be printed with a low-cost 3D printer. The printed CB/PCL was subjected to resistivity tests, and it confirmed the existence of piezoresistive behavior in the composite blends. The piezoresistive sensor range is capable of sensing mechanical flexing when it is hidden inside the printed object or on the existing object, where the capacitive sensor is embedded inside the "smart" vessel as a custom interface device that also senses the liquid present inside the 3D printed object in quantity. The 3D printed piezoresistive sensor, capacitive sensor, and sensor pads are shown in Fig. 14. The response from the sensors can be easily detected with simple electronics and simple potential dividers without the need for amplification.

Farahani et al. [239] designed strain sensors using SWCNTs and epoxy composites through the UV-assisted direct-wire (UV-DW) technique. The UV-DW technique flexibility allows the sensors and housing elements to be manufactured in single monolithic structures. The electrical conductivity analysis of printed composite reveals that the printed sensors are more sensitive to smaller mechanical disturbances, even with smaller loadings of SWCNTs than the traditional metallic loadings. Using a highly volatile solvent, the CNTs are uniformly dispersed in the PLA through direct deposition and are followed by the formation of 3D microstructures after solvent evaporation. These 3D flexible conductive parts printed using these materials were utilized for simple electrical circuits in commercial LEDs, increasing their potential in the field of electronics. Some of the other efforts were found in the literature regarding the use of metal wires with polymer matrices for the printing process for the manufacturing of electronic devices. This process is almost similar to continuous fiber-reinforced composite processing. Molten styrene and copper wire copolymers are extruded as a demonstration of 3D printed composites for open membrane switches. This activated switch membrane was deformed under pressure contact and resulted in physical contact of copper wires together with the adjacent polymers [240, 241]. Kim et al. [242] studied the influence of FDM 3D printing on dielectric nanocomposites made of MWCNTs, $BaTiO_3$, and poly(vinylidene) fluoride (PVDF) extensively for energy storage and harvesting and sensor applications because of their unique dipole polarization characteristics. To improve the dielectric properties, the CNTs are utilized with a homogeneous dispersion of $BaTiO_3$ nanoparticles, which leads to an ultra-high polarization density and behaves as a local microcapacitor within the matrix. It was observed that the 3D printing technique maintains the uniformity in nanoparticle dispersion with enhanced dielectric property and reduces the voids, cracks, and agglomerations in the printed composites. Paper electronic development requires the low cost and versatile manufacturing of materials and processes. The direct-write laser patterning was employed for the development of

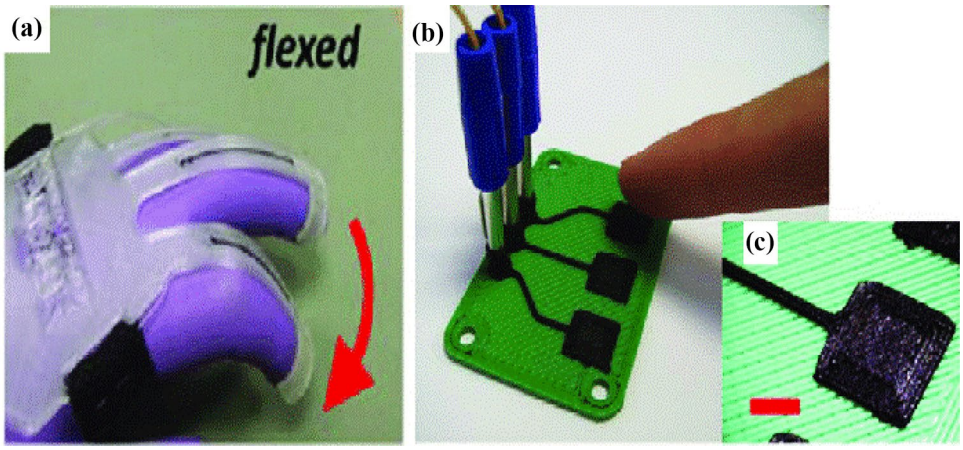

Fig. 14 3D printed CB/PCL composites for **a** piezoresistive sensor, **b** capacitive sensor, **c** macro-image of 5-mm scale bar printed sensor pad [238]. (Reused with the permission from Elsevier, License No. 5195371370822)

a molybdenum carbide/graphene composite (MCG) directly on the paper substrate. Further, this MCG structure was soaked into gelatin-mediated inks containing molybdenum ions. The resultant composites are electrochemically active and mechanically stable for potential applications such as supercapacitors, gas sensors, energy harvesters, and electrochemical ion detectors [243]. A solid-state supercapacitor was constructed using a 3D printed polyaniline/graphene oxide composite that exhibits 1329 mF cm^{-2} of areal specific capacitance. The fabrication of a planar supercapacitor is difficult using traditional techniques, so it is preferred to use time-saving, low-cost, and flexible 3D printing techniques [244].

5.2 Biomedical applications

The continuous development of magnetic resonance imaging (MRI) and computed tomography (CT) techniques helps to get 3D images of organs and tissues with accurate, informative, and higher resolution. Using the gathered data and images, the patient's specified organs and tissues are printed with précised microstructures using 3D printing techniques [245, 246]. Many polymer materials are available for this biomedical application, such as naturally synthesized materials (collagen, gelatin, chitosan, alginate, etc.) and/or synthetic polymer molecules (PVA, PLGA, PEG, etc.). These materials should possess good structural properties, biocompatibility, printability, and mechanical properties when used in biomedical applications. It is also to ensure that the transplanted 3D printed scaffolds function properly with living organs and interact well with endogamous tissues [247, 248]. The 3D printed antibacterial scaffolds composed of PLA with silver, copper, and bronze particles show better mechanical, thermal, and biological properties for bone scaffold application. The bronze incorporation into PLA shows an improvement in elastic modulus values of up to 27% and 10% for 90° and 0° configured samples, respectively. The 3D printed scaffold surface was treated with acetic acid, which creates a porous network at the nanoscale on the scaffold surface. This acid treatment and the presence of metallic/alloy particles in PLA increase the antibacterial properties by nearly 20–25% and bioactivity by 18–100% [249]. The 3D printed PLA and modified PLA/hydroxyapatite (PLA-HAp) scaffolds are stronger through the analysis of compressive strength and hence suggested for bone tissue applications. Additionally, the post-fabrication modification with HAp after printing leads to better proliferation and cell attachment with improved mechanical properties. The 90°-oriented 3D PLA-HAp scaffold exhibits improved stability and mechanical strength of up to 47.16%. The HAp nanoparticles' interaction on the surface of the PLA scaffold was influenced by cell attachments, which facilitate cellular activity and absorb protein [250]. Similarly, pristine graphene-filled poly(-caprolactone) (PCL) composites are used in bone tissue engineering applications. These polymers are reinforced with electroactive particles, which modulate the printed scaffolds via cell differentiation and proliferation. The addition of pristine graphene nanoparticles with lower concentrations shows enhanced proliferation and viability without cytotoxicity. These nanoparticles also act as an intermediate for controlling the water-in-air contact angle more effectively than the neat PCL materials. Further, the biological behavior and cell attachment were improved by treating the scaffolds with a 5 M NaOH solution. All these parameters count towards the usage as a promising substrate for bone tissue applications [251]. The synthesis of PLA delivers PLA stereocomplex (SC), where these SC polymers possess higher mechanical performance, hydrolysis resistance, and melting temperature than neat PLA. This process of stereocomplexation strengthens and stabilizes the PLA-based nanoparticles or hydrogels for biomedical applications and also improves the PLA's barrier properties with prolonged drug release by PLA-based materials. The combination of PLA SC and graphene 3D printed composites possesses better thermo-mechanical properties suitable for biomedical applications such as drug delivery,

scaffolds, biological imaging, and cancer therapy [252]. The 3D printed nanocomposite scaffold made of polylactic-co-glycolic acid (PLGA) and TiO_2 nanoparticles with a ratio of 10:1 is employed for bone tissue engineering applications. The addition of TiO_2 nanoparticles raises the compressive modulus, thermal decomposition onset, and glass transition temperature of the resulting composites above that of neat PLGA. Additionally, these nanoparticles improve the surface wettability, and it was found to reduce contact angles from 90.5° ± 3.2° to 79.8° ± 2.4°, which is favorable to cellular activity and attachment. Moreover, the PLGA/TiO_2 nanocomposites improve osteoblast proliferation, calcium secretion, and possess higher ALP activity. Figure 15A illustrates the cells attached to scaffold images obtained through the laser microscope, and these attachments with cell penetration depths in different focus planes are illustrated in Fig. 15B, C [253]. The desktop FDM technique was utilized to print a 3D porous PLA/nano-hydroxyapatite (PLA/PHA) scaffold with enhanced osteoconductivity and osteogenesis for bone regeneration applications. The fabricated porous PLA/nHA nanocomposite scaffolds are capable of loading and releasing levofloxacin and vancomycin, which was confirmed through a vitro antibacterial experiment. The cytocompatibility was evaluated with MG-63 cells in the printed scaffold through cellular morphology and proliferation analysis. Hence, all these evaluations show the potential of the printed scaffold for regeneration and repair of larger bone defects [254].

The MWCNT-reinforced (0.25, 0.75, and 3 wt%) poly(-caprolactone) (PCL) nanocomposites were created using a 3D printing technique, and these printed scaffolds were tested biologically for bone tissue regeneration applications. The printed scaffolds within a range of 366 mm–397 mm pore sizes are produced, and these are capable of sustaining prior stage human adipose-derived proliferation and mesenchymal stem cell attachment. Figure 16 illustrates the live (green color) and dead (red color) cells in the seeded scaffold after day 1 (Fig. 16a–d) and 21 days (Fig. 16e–h). After 24 h of cell seeding, only a few cells are dead, and most of them are alive on the scaffolds. In that, more numbers were observed in neat PCL scaffolds due to poor surface characteristics than in the MWCNT-filled scaffolds. After the completion of 21 days, the majority of the cells are alive and are attached to the scaffold with more cells bridging among layers and higher cell density. We also observed fewer dead cells in the 0.25 wt% MWCNT-loaded scaffold. Overall, the 3 wt% MWCNT-loaded PCL scaffolds are promising candidates for bone tissue regeneration [255]. The nano-hydroxyapatite (HA)-filled PEEK 3D printed scaffold was tested in vitro for 28 days using stimulated body fluid immersion tests, and apatite formation on the sample surfaces that contained HA and doped HA particles was observed. There were not many significant differences observed in the crystallinity and mechanical behavior of printed composites due to filler addition. Hence, the production of bioactive HA/PEEK composite is potentially suitable for craniofacial bone repair applications [256]. The FDM-printed carbon fiber-reinforced PEEK composites are potentially stable for dental and orthopedic applications. The CF/PEEK composite shows good biocompatibility, higher cell densities, and mechanical strength without any surface modifications. Hence, it is a potential biomaterial for tissue engineering and bone grafting applications [257].

5.3 Aerospace applications

3D printing techniques in the aerospace industry have become more popular in recent years due to the production of complex geometrical parts that are time-consuming and costly in traditional manufacturing processes [258]. In recent years, turbine blades and engine exhaust aerospace components have been manufactured using 3D printed metal materials because

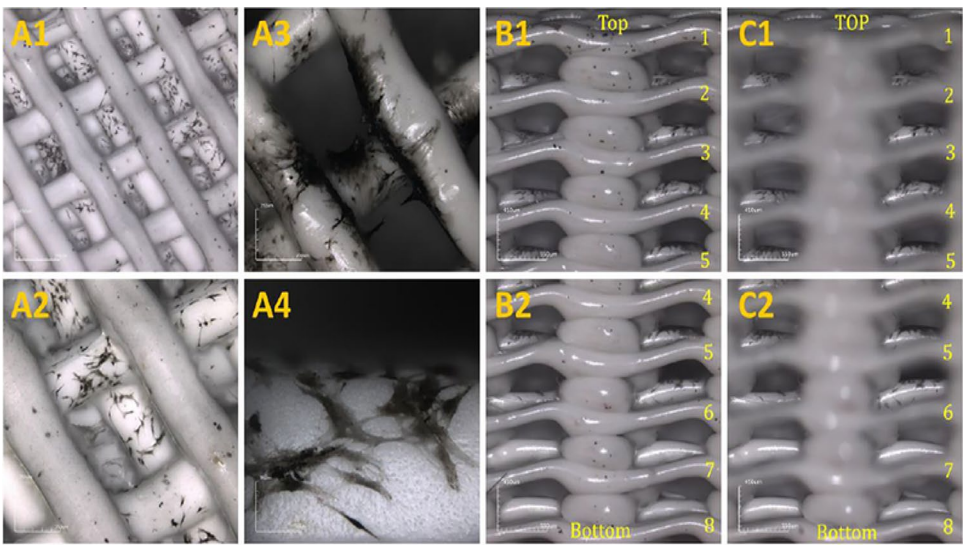

Fig. 15 Osteoblasts cultured on PLGA/TiO_2 composite scaffold panels with different magnifications obtained through laser microscope (**A**). The depth of cell penetration in different focal planes (**B** and **C**) [253]. (Reused with the permission from Elsevier, License No. 5195380074414)

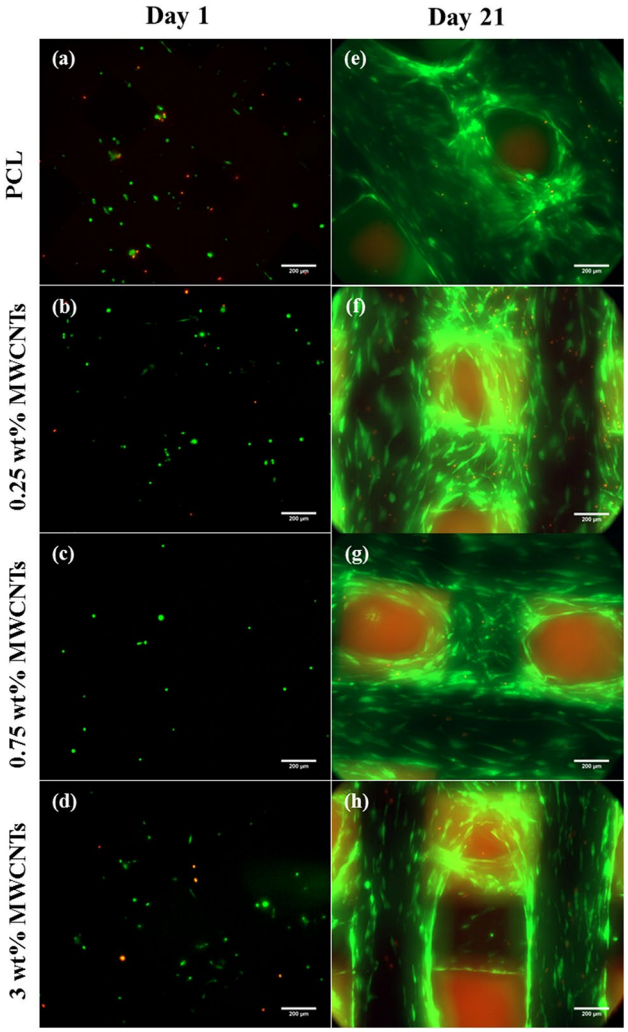

Fig. 16 Live and dead cell assay at days 1 and 21 for all combinations of scaffold panels (live cells, green color; dead cells, red color) [255]. (Reused with the permission from Elsevier, License No. 5195380256857)

of their higher strength and flame retardant properties. Now, researchers are working hard to replace 3D printed metals with 3D printed polymer composites in order to improve fuel efficiency [259, 260]. It is possible to create thermal barriers or thermal pathways in the printed parts through control over print orientation and geometry. The insertion of silver and graphite particles/flakes into ABS and carbon fiber reinforcements imposes heat blocking and heat spreading effects on the 3D printed parts. By the careful design of the structure, these composites can act as protective elements for sensitive electronics from heat sources. These heating effects are found in space cube satellites, as their system heat dissipation is restricted to radiative heat transfer. Hence, the addition of these anisotropic materials protects the electronics from thermal loads [261]. The preliminary 3D printing test was conducted on a model with a vertical column and with unique features of decreased angles from bottom 50° to top 20°, with higher printing complexity. In this particular case, both glass and carbon fiber-reinforced composite formulations possessed excellent reproducibility towards the target model with 10 mm/s printing speed and 30 min UV exposure, and 20° and 30° angles were demonstrated with different formulations. All these things give a clear idea of the good processability while printing the composites using the UV-3D printing technique. For this technique, the CF and GF reinforced composite formulations were used as ink to fabricate aerospace structural components like propellers and airfoils, as shown in Fig. 17. The printing parameters employed for component development are 5 mm/s printing speed, 45 min, and 30 min UV exposure time for propeller and airfoil production, respectively [96, 262].

6 Limitations

The application of 3D printing in polymer composites is limited because of restrictions on selecting printable materials. The preferred material is limited to thermoplastic polymers with a suitable range of melting viscosity and lower glass transition temperature. Some photopolymers and powdered materials are also used as printing materials [77, 263, 264]. Hence, these limited materials are unable to meet the complete requirements of the industries, so material diversity should be enhanced [265, 266]. The reinforcement effect is less in the 3D printed composites as compared to traditionally fabricated composites in terms of mechanical strength, and it reduces the functional performance of the printed composites. The lower mechanical strength was due to the void's presence in the printed composites. After printing, the composites are subjected to a post-treatment process such as consolidation or infiltration, which leads to an increment in processing time and cost [267–269]. The addition of reinforcements leads to porosity, which is attributed to poor interfacial adhesion between the matrix and reinforcements. Furthermore, getting consistency and repeatability in printed parts is difficult in printed parts that might lead to ununiformed properties in the printed composites [270, 271]. The higher volume production of printed materials is more difficult and time-consuming than traditional manufacturing techniques. 3D printing techniques like SLM or SLS possess higher resolution, so they require more processing energy and high-cost materials [272, 273]. The 3D printing capability in producing 3D complex geometries for biomedical applications causes more cost, especially in scaffold printing in bone tissue engineering applications. One is the selection of printing materials, and the other one is selection of printing techniques [274–276]. The void formation is common in contour crafting or FDM techniques, which results in layer delamination and inferior mechanical properties. The filament thickness increment decreases porosity but results in deteriorated cohesion in printed composites, and it increases the moisture intake

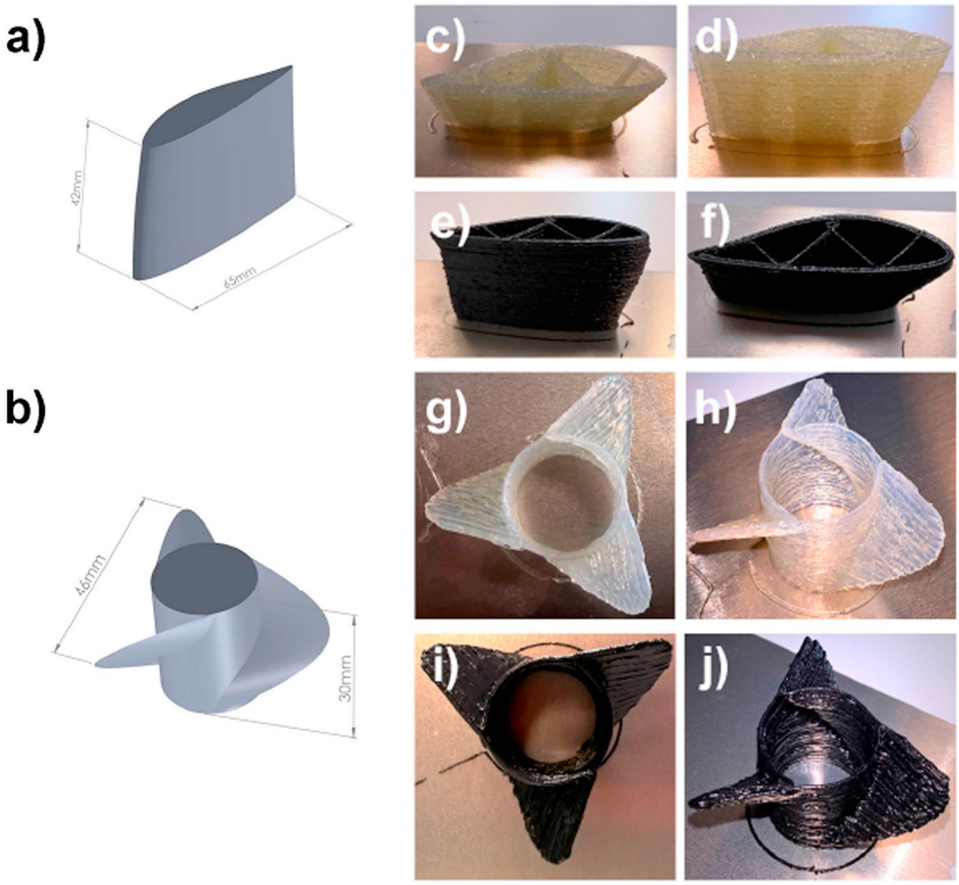

Fig. 17 (**a**) Airfoil projection, (**b**) propeller projection, UV 3D printed reproduction of airfoil (**c**–**f**), propeller (**g**–**j**), the 3D polymer composite models developed using GFR (**c**, **d**, **g**, **h**) and CFR (**e**, **f**, **i**, **j**) [262]. (Reused with the permission from Elsevier, License No. 5195380449551)

percentage and reduces the tensile strength [277–280]. The usage of the laser source in different 3D printing techniques causes control over the sintering process, but anisotropy was found because of intensity variations in the depth of printed materials. The process and printing parameters like orientation, extrusion pressure, laser power, printing speed, and printing direction greatly influence the mechanical, thermal, and electrical properties of the printed composites [281–284]. The CAD software tool is the main requirement for designing the parts for 3D printing. Because of some drawbacks in the 3D printing techniques, the printed composite exhibits some defects that are not expected in the design section [285–287]. The CAD system employs the tessellation concept to model approximations in boundaries and solid geometry. However, the CAD transfer into 3D printed parts offers some defects and inaccuracies, especially on curved surfaces [288–290]. The clear appearance of layer-by-layer formation in the printed parts is the main limitation while subjecting too many applications. This appearance is not an important thing when the printed parts are hidden in final applications, for example, in tissue engineering applications [291–293]. A flat and plane surface is preferred over a layer-by-layer printed appearance in specific applications such as aerospace, building, and toys, or chemical post-treatments or sintering can be able to reduce this appearance, but this raises the cost and processing duration [294–296]. The layer-by-layer appearance of printed filaments is more in contour crafting, inkjet, and FDM 3D printing techniques than in stereolithography or powder bed printing techniques. The limitation of printing layers is severe for layer-by-layer appearance in the 3D printing techniques [297–299].

7 Future aspects

The integration of multiple nozzles or the use of swarm intelligence might completely transform the 3D printing process. The multiple nozzles can be mounted on the existing single-nozzle printers to print certain areas of the building component in the shortest time. Inappropriate parameter selection can result in poor print quality and, in some cases, catastrophic failure. The layering effect, which generates uneven surfaces with voids between the layers, is the main constraint of the 3D printing method. As a result, tool path optimization must take into account with build time, layer printing time gaps, and surface finish as output factors. Alternatively, the post-processing needs to be done for the 3D printed part to increase the overall surface quality. Future heat sink research should concentrate on ideas based

on conjugate heat transfer numerical models that take into account material properties and topology, as well as printing process optimization to reduce porosity and structural optimization. Future trends may include developing materials having printable and tailorable functional features, such as coefficient of thermal expansion and thermal conductivity for smart constructions, or determining the optimal composition of materials that is still printable while keeping acceptable material properties. Additionally, printing structures and heat channels that can transmit heat from a source of heat to a specified place or to the environment are possible. Moving beyond the current printing-on-arrival system, in which robot printers navigate to desired printing spots and begin printing, our future research should focus on the research on printing-while-moving strategies that fully exploit the advantages of mobile robot printers and further expand the printing scale.

8 Conclusions

Complex structure printability, freedom of design, minimum waste, and mass customization are the benefits of using 3D printing techniques. This review focused on the description of various 3D printing techniques, an overview of different types of reinforced polymer composites (fibers, nanomaterials, and particle reinforcements), the characterization of 3D printed parts, the applications in various sectors, and limitations on future aspects. Energy usage in additive manufacturing techniques is determined by a number of characteristics that vary by process. Certain parameters are consistent throughout all AM processes. For example, increasing the resolution in any AM technique lengthens the manufacturing process, resulting in increased energy usage. 3D printing is a promising technique that has the potential to revolutionize conventional building, and construction processes in terms of perceptible benefits such as low cost, high-efficiency automatic construction, design freedom, and labor requirements and risks associated with construction are less. However, 3D printing technology continues to encounter difficulties with mechanical strength, reinforcements, curing, and durability, as well as with correlated qualities such as buildability, extrudability, and flowability. Extrusion-based 3D printing techniques such as LDM and FDM are commonly preferred because of their simplicity, speed of processing, and low cost. The FDM technique utilizes thermoplastic filaments, and now it uses pellets also through extrusion for a diverse range of polymers. The types of filaments and properties determine the processability and properties of printed parts. The LDM technique has many advantages over FDM in terms of compatibility and ambient working temperature range with a broad spectrum of molecules. The selective laser sintering technique uses polymer particles as reinforcements and works based on the powder bed fusion process. These particulates melt and soften upon heating through the sintering process and solidify upon cooling. The sintering window was primarily determined by polymer transition points like crystallization, melting, and glass transition temperatures. The powder size distribution, rheological viscosity, and surface tension affect the printing stability and laser power interactions. The reinforcement of smaller particles within a range of less than 20–80 m resulted in higher printing resolutions, and less than 20 m smaller particles cause aggregates due to van der Waals force and also possibly form airborne clouds that affect printing resolution. Materials in the form of powder, wire, filaments, paste, inks, and sheets can be used as printing elements. Polymers are preferred as common materials for the development of fast prototypes. Polymers such as polylactic acid (PLA), polycarbonate (PC), polyamide (PA), acrylonitrile–butadiene–styrene (ABS), and thermosetting powders like polystyrene, photopolymer resins, and polyamides are usually used in 3D printing. The polymer reinforcement with nanomaterials and fibers improves the mechanical properties of the printed composites with improved functional performance. The addition of carbon nanotubes (CNTs) and, preferably, MWCNTs offers superior mechanical, electrical, and thermal properties for the multifunctional 3D printed composites. This usage of suitable material types, interfacial adhesions, interactions, particle dispersion, and concentrations was also included in this review. The hybridization of particles caused agglomeration, and it might reduce the overall functionality of the resultant composites. The parts consolidation and assembly effort with functionality incorporation offer cost and mass savings. The parts with the appropriate strong value proportion are created through selective deposition with functionality adoption within the 3D structures. The magnetic, sensing, electrical, and thermal functionalities have been adopted in prototype structures like cube satellites and sensing gloves with high technology readiness levels' (TRLs) demonstration. However, the self-healing functionalities and embedded circuitry maturity are limited in a research laboratory. Hence, the development of reliable novel materials with related fabrication techniques is needed for industrial adoption with the above-mentioned functionalities. Materials and process were the two major pillars of 3D printing techniques. Addressing these two points carries equal measures while facing the current challenges, and progression will take place in the development of multifunctional 3D printed composites. The major hurdle in the printing process was inherent porosity, which affects the functional performance of the final products. This can be overcome by increasing the concentration of functional filler materials. However, this comes at a cost of limited printability due to the increase in viscosity that leads to clogging at the nozzle. The current limitations are quoted in this review. The potential efforts and research work are needed to overcome these challenges to explore 3D printed polymer composite parts in higher-value manufacturing areas like defense, automotive, aerospace, and aviation industries.

Author contribution All authors contributed equally.

Funding This project was funded by King Mongkut's University of Technology North Bangkok (KMUTNB), Grant No. KMUTNB-PHD-65–02.

Availability of data and material Not applicable.

Code availability Not applicable.

Declarations

Ethics approval The authors hereby state that the present work is in compliance with the ethical standards.

Consent to participate Not applicable.

Consent for publication All authors have read and agreed to publish the manuscript.

Conflict of interest The authors declare no competing interests.

References

1. Schubert C, Van Langeveld MC, Donoso LA (2014) Innovations in 3D printing: a 3D overview from optics to organs. Br J Ophthalmol 98:159–161. https://doi.org/10.1136/bjophthalmol-2013-304446
2. Jiménez M, Romero L, Domínguez IA, Espinosa MDM, Dominguez M (2019) Additive manufacturing technologies: an overview about 3D printing methods and future prospects. Complexity. https://doi.org/10.1155/2019/9656938
3. Dawood A, Marti BM, Sauret-Jackson V, Darwood A (2015) 3D printing in dentistry. Br Dent J 219:521–529. https://doi.org/10.1038/sj.bdj.2015.914
4. Gopinathan J, Noh I (2018) Recent trends in bioinks for 3D printing. Biomater Res 22–11. https://doi.org/10.1186/s40824-018-0122-1
5. Oropallo W, Piegl LA (2016) Ten challenges in 3D printing. Eng Comput 32:135–148. https://doi.org/10.1007/s00366-015-0407-0
6. Chia HN, Wu BM (2015) Recent advances in 3D printing of biomaterials. J Biol Eng 9:1–14. https://doi.org/10.1186/s13036-015-0001-4
7. Lee JY, An J, Chua CK (2017) Fundamentals and applications of 3D printing for novel materials. Appl Mater Today 7:120–133. https://doi.org/10.1016/j.apmt.2017.02.004
8. Shahrubudin N, Lee TC, Ramlan R (2019) An overview on 3D printing technology: technological, materials, and applications. Procedia Manuf 35:1286–1296. https://doi.org/10.1016/j.promfg.2019.06.089
9. MacDonald E, Wicker R (2016) Multiprocess 3D printing for increasing component functionality. Science 80:353. https://doi.org/10.1126/science.aaf2093
10. Chen Z, Li Z, Li J, Liu C, Lao C, Fu Y, He Y (2019) 3D printing of ceramics: a review. J Eur Ceram Soc 39:661–687. https://doi.org/10.1016/j.jeurceramsoc.2018.11.013
11. Gross BC, Erkal JL, Lockwood SY, Chen C, Spence DM (2014) Evaluation of 3D printing and its potential impact on biotechnology and the chemical sciences. Anal Chem 86:3240–3253. https://doi.org/10.1021/ac403397r
12. Liu Z, Zhang M, Bhandari B, Wang Y (2017) 3D printing: printing precision and application in food sector. Trends Food Sci Technol 69:83–94. https://doi.org/10.1016/j.tifs.2017.08.018
13. Ambrosi A, Pumera M (2016) 3D-printing technologies for electrochemical applications. Chem Soc Rev 45:2740–2755. https://doi.org/10.1039/c5cs00714c
14. Ford S, Minshall T (2019) Invited review article: where and how 3D printing is used in teaching and education. Addit Manuf 25:131–150. https://doi.org/10.1016/j.addma.2018.10.028
15. Yan Q, Dong H, Su J, Han J, Song B, Wei Q, Shi Y (2018) A review of 3D printing technology for medical applications. Engineering 4:729–742. https://doi.org/10.1016/j.eng.2018.07.021
16. Bose S, Vahabzadeh S, Bandyopadhyay A (2013) Bone tissue engineering using 3D printing. Mater Today 16:496–504. https://doi.org/10.1016/j.mattod.2013.11.017
17. Bourell D, Kruth JP, Leu M, Levy G, Rosen D, Beese AM, Clare A (2017) Materials for additive manufacturing. CIRP Ann - Manuf Technol 66:659–681. https://doi.org/10.1016/j.cirp.2017.05.009
18. Tengsuthiwat J, Sanjay MR, Siengchin S, Pruncu CI (2020) 3D-MID technology for surface modification of polymer-based composites: a comprehensive review. Polymers 12:1408. https://doi.org/10.3390/polym12061408
19. Aimar A, Palermo A, Innocenti B (2019) The role of 3D printing in medical applications: a state of the art. J Healthc Eng 2019(5340616):10
20. Chimene D, Lennox KK, Kaunas RR, Gaharwar AK (2016) Advanced bioinks for 3D printing: a materials science perspective. Ann Biomed Eng 44:2090–2102. https://doi.org/10.1007/s10439-016-1638-y
21. Compton BG, Lewis JA (2014) 3D-printing of lightweight cellular composites. Adv Mater 26:5930–5935. https://doi.org/10.1002/adma.201401804
22. Giannopoulos AA, Mitsouras D, Yoo SJ, Liu PP, Chatzizisis YS, Rybicki FJ (2016) Applications of 3D printing in cardiovascular diseases. Nat Rev Cardiol 13:701–718. https://doi.org/10.1038/nrcardio.2016.170
23. Tack P, Victor J, Gemmel P, Annemans L (2016) 3D-printing techniques in a medical setting: a systematic literature review. Biomed Eng Online 15:1–21. https://doi.org/10.1186/s12938-016-0236-4
24. Valot L, Martinez J, Mehdi A, Subra G (2019) Chemical insights into bioinks for 3D printing. Chem Soc Rev 48:4049–4086. https://doi.org/10.1039/c7cs00718c
25. Tümer EH, Erbil HY (2021) Extrusion-based 3d printing applications of pla composites: A review. Coatings 11:1–42. https://doi.org/10.3390/coatings11040390
26. Bekas DG, Hou Y, Liu Y, Panesar A (2019) 3D printing to enable multifunctionality in polymer-based composites: a review. Compos Part B Eng 179:107540. https://doi.org/10.1016/j.compositesb.2019.107540
27. Ngo TD, Kashani A, Imbalzano G, Nguyen KT, Hui D (2018) Additive manufacturing (3D printing): a review of materials, methods, applications and challenges. Compos Part B Eng 143:172–196. https://doi.org/10.1016/j.compositesb.2018.02.012
28. Skylar-Scott MA, Mueller J, Visser CW, Lewis JA (2019) Voxelated soft matter via multimaterial multinozzle 3D printing. Nature 575:330–335. https://doi.org/10.1038/s41586-019-1736-8
29. Guvendiren M, Molde J, Soares RMD, Kohn J (2016) Designing biomaterials for 3D printing. ACS Biomater Sci Eng 2:1679–1693. https://doi.org/10.1021/acsbiomaterials.6b00121
30. Khoo ZX, Teoh JEM, Liu Y, Chua CK, Yang S, An J, Yeong WY (2015) 3D printing of smart materials: a review on recent progresses in 4D printing. Virtual Phys Prototyp 10:103–122. https://doi.org/10.1080/17452759.2015.1097054

31. Gebler M, Schoot Uiterkamp AJM, Visser C (2014) A global sustainability perspective on 3D printing technologies. Energy Policy 74:158–167. https://doi.org/10.1016/j.enpol.2014.08.033
32. AbouHashem Y, Dayal M, Savanah S, Štrkalj G (2015) The application of 3D printing in anatomy education. Med Educ Online 20:1–4. https://doi.org/10.3402/meo.v20.29847
33. Martin JH, Yahata BD, Hundley JM, Mayer JA, Schaedler TA, Pollock TM (2017) 3D printing of high-strength aluminium alloys. Nature 549:365–369. https://doi.org/10.1038/nature23894
34. Yuk H, Lu B, Lin S, Qu K, Xu J, Luo J, Zhao X (2020) 3D printing of conducting polymers. Nat Commun 11:4–11. https://doi.org/10.1038/s41467-020-15316-7
35. Sun J, Zhou W, Huang D, Fuh JY, Hong GS (2015) An overview of 3D printing technologies for food fabrication. Food Bioprocess Technol 8:1605–1615. https://doi.org/10.1007/s11947-015-1528-6
36. Hamilton CA, Alici G, in het Panhuis M (2018) 3D printing vegemite and marmite: redefining breadboards. J Food Eng 220:83–88. https://doi.org/10.1016/j.jfoodeng.2017.01.008
37. Lei D, Yang Y, Liu Z, Chen S, Song B, Shen A, You Z (2019) A general strategy of 3D printing thermosets for diverse applications. Mater Horizons 6:394–404. https://doi.org/10.1039/c8mh00937f
38. Seyednejad H, Gawlitta D, Kuiper RV, de Bruin A, van Nostrum CF, Vermonden T, Hennink WE (2012) In vivo biocompatibility and biodegradation of 3D-printed porous scaffolds based on a hydroxyl-functionalized poly(ε-caprolactone). Biomaterials 33:4309–4318. https://doi.org/10.1016/j.biomaterials.2012.03.002
39. Horn TJ, Harrysson OLA (2012) Overview of current additive manufacturing technologies and selected applications. Sci Prog 95:255–282. https://doi.org/10.3184/003685012X13420984463047
40. Wegst UGK, Bai H, Saiz E (2015) Bioinspired structural materials. Nat Mater 14:23–36. https://doi.org/10.1038/nmat4089
41. Zhu C, Han TYJ, Duoss EB, Golobic AM, Kuntz JD, Spadaccini CM, Worsley MA (2015) Highly compressible 3D periodic graphene aerogel microlattices. Nat Commun 6:1–8. https://doi.org/10.1038/ncomms7962
42. Schniederjans DG (2017) Adoption of 3D-printing technologies in manufacturing: a survey analysis. Int J Prod Econ 183:287–298. https://doi.org/10.1016/j.ijpe.2016.11.008
43. Godoi FC, Prakash S, Bhandari BR (2016) 3d printing technologies applied for food design: status and prospects. J Food Eng 179:44–54. https://doi.org/10.1016/j.jfoodeng.2016.01.025
44. Zhou LY, Fu J, He Y (2020) A review of 3D printing technologies for soft polymer materials. Adv Funct Mater 30:1–38. https://doi.org/10.1002/adfm.202000187
45. Karakurt I, Lin L (2020) 3D printing technologies: techniques, materials, and post-processing. Curr Opin Chem Eng 28:134–143. https://doi.org/10.1016/j.coche.2020.04.001
46. Nyberg EL, Farris AL, Hung BP, Dias M, Garcia JR, Dorafshar AH, Grayson WL (2017) 3D-printing technologies for craniofacial rehabilitation, reconstruction, and regeneration. Ann Biomed Eng 45:45–57. https://doi.org/10.1007/s10439-016-1668-5
47. Wang Y, Xu Z, Wu D, Bai J (2020) Current status and prospects of polymer powder 3D printing technologies. Materials (Basel). https://doi.org/10.3390/ma13102406
48. Kumar S (2003) Selective laser sintering: a qualitative and objective approach. Jom 55:43–47. https://doi.org/10.1007/s11837-003-0175-y
49. Fina F, Goyanes A, Gaisford S, Basit AW (2017) Selective laser sintering (SLS) 3D printing of medicines. Int J Pharm 529:285–293. https://doi.org/10.1016/j.ijpharm.2017.06.082
50. Praveenkumara J, HN VS, Madhu P, Gowda Y, Rangappa SM, Khan MR, Khan I, Siengchin S (2021) A comprehensive review on the effect of synthetic filler materials on fiber-reinforced hybrid polymer composites. J Text Inst 1(9). https://doi.org/10.1080/00405000.2021.1920151
51. Charoo NA, Barakh Ali SF, Mohamed EM, Kuttolamadom MA, Ozkan T, Khan MA, Rahman Z (2020) Selective laser sintering 3D printing–an overview of the technology and pharmaceutical applications. Drug Dev Ind Pharm 46:869–877. https://doi.org/10.1080/03639045.2020.1764027
52. Mokrane A, Boutaous M, Xin S (2018) Process of selective laser sintering of polymer powders: modeling, simulation, and validation. Comptes Rendus - Mec 346:1087–1103. https://doi.org/10.1016/j.crme.2018.08.002
53. Martinez PR, Goyanes A, Basit AW, Gaisford S (2017) Fabrication of drug-loaded hydrogels with stereolithographic 3D printing. Int J Pharm 532:313–317. https://doi.org/10.1016/j.ijpharm.2017.09.003
54. Mukhtarkhanov M, Perveen A, Talamona D (2020) Application of stereolithography based 3D printing technology in investment casting. Micromachines. https://doi.org/10.3390/mi11100946
55. Hull C (2012) On stereolithography Virtual Phys Prototyp 7:177. https://doi.org/10.1080/17452759.2012.723409
56. Manapat JZ, Chen Q, Ye P, Advincula RC (2017) 3D printing of polymer nanocomposites via stereolithography. Macromol Mater Eng 302:1–13. https://doi.org/10.1002/mame.201600553
57. Ge Q, Li Z, Wang Z, Kowsari K, Zhang W, He X, Zhou J, Fang NX (2020) Projection micro stereolithography based 3D printing and its applications. Int J Extrem Manuf 2:0–13
58. Lee MP, Cooper GJT, Hinkley T, Gibson GM, Padgett MJ, Cronin L (2015) Development of a 3D printer using scanning projection stereolithography. Sci Rep. https://doi.org/10.1038/srep09875
59. Mazzanti V, Malagutti L, Mollica F (2019) FDM 3D printing of polymers containing natural fillers: a review of their mechanical properties. Polymers (Basel). https://doi.org/10.3390/polym11071094
60. Wasti S, Adhikari S (2020) Use of biomaterials for 3D printing by fused deposition modeling technique: a review. Front Chem 8:1–14. https://doi.org/10.3389/fchem.2020.00315
61. Melocchi A, Uboldi M, Maroni A, Foppoli A, Palugan L, Zema L, Gazzaniga A (2020) 3D printing by fused deposition modeling of single- and multi-compartment hollow systems for oral delivery – a review. Int J Pharm 579:119155. https://doi.org/10.1016/j.ijpharm.2020.119155
62. Nguyen VH, Huynh TN, Nguyen TP, Tran TT (2020) Single and multi-objective optimisation of processing parameters for fused deposition modelling in 3D printing technology. Int J Automot Mech Eng 17:7542–7551. https://doi.org/10.15282/IJAME.17.1.2020.03.0558
63. Das SC, Ranganathan R, Murugan N (2018) Effect of build orientation on the strength and cost of PolyJet 3D printed parts. Rapid Prototyp J 24:832–839. https://doi.org/10.1108/RPJ-08-2016-0137
64. Tee YL, Peng C, Pille P, Leary M, Tran P (2020) PolyJet 3D printing of composite materials: experimental and modelling approach. Jom 72:1105–1117. https://doi.org/10.1007/s11837-020-04014-w
65. Meisel NA, Elliott AM, Williams CB (2015) A procedure for creating actuated joints via embedding shape memory alloys in PolyJet 3D printing. J Intell Mater Syst Struct 26:1498–1512. https://doi.org/10.1177/1045389X14544144
66. Gokuldoss PK, Kolla S, Eckert J (2017) Additive manufacturing processes: selective laser melting, electron beam melting and binder jetting-selection guidelines. Materials (Basel). https://doi.org/10.3390/ma10060672
67. Baumers M, Tuck C, Wildman R, Ashcroft I, Hague R (2017) Shape complexity and process energy consumption in electron beam melting: a case of something for nothing in additive manufacturing? J Ind Ecol 21:S157–S167. https://doi.org/10.1111/jiec.12397

68. Billiet T, Vandenhaute M, Schelfhout J, Van Vlierberghe S, Dubruel P (2012) A review of trends and limitations in hydrogel-rapid prototyping for tissue engineering. Biomaterials 33:6020–6041. https://doi.org/10.1016/j.biomaterials.2012.04.050
69. Luo Y, Lode A, Wu C, Chang J, Gelinsky M (2015) Alginate/nanohydroxyapatite scaffolds with designed core/shell structures fabricated by 3D plotting and in situ mineralization for bone tissue engineering. ACS Appl Mater Interfaces 7:6541–6549. https://doi.org/10.1021/am508469h
70. Murphy SV, Atala A (2014) 3D bioprinting of tissues and organs. Nat Biotechnol 32:773–785. https://doi.org/10.1038/nbt.2958
71. Vaithilingam J, Simonelli M, Saleh E, Senin N, Wildman RD, Hague RJ, Tuck CJ (2017) Combined inkjet printing and infrared sintering of silver nanoparticles using a swathe-by-swathe and layer-by-layer approach for 3-dimensional structures. ACS Appl Mater Interfaces 9:6560–6570. https://doi.org/10.1021/acsami.6b14787
72. Saleh E, Zhang F, He Y, Vaithilingam J, Fernandez JL, Wildman R, Tuck C (2017) 3D inkjet printing of electronics using UV conversion. Adv Mater Technol 2:1–8. https://doi.org/10.1002/admt.201700134
73. Cooperstein I, Layani M, Magdassi S (2015) 3D printing of porous structures by UV-curable O/W emulsion for fabrication of conductive objects. J Mater Chem C 3:2040–2044. https://doi.org/10.1039/c4tc02215g
74. Rosenthal M, Henneberger C, Gutkes A, Bues CT (2018) Liquid deposition modeling: a promising approach for 3D printing of wood. Eur J Wood Prod 76:797–799. https://doi.org/10.1007/s00107-017-1274-8
75. Saari M, Cox B, Richer E, Krueger PS, Cohen AL (2015) Fiber encapsulation additive manufacturing: an enabling technology for 3D printing of electromechanical devices and robotic components. 3D Print Addit Manuf 2:32–39. https://doi.org/10.1089/3dp.2015.0003
76. Leong KF, Liu D, Chua CK (2014) Tissue engineering applications of additive manufacturing. In: Hashmi S, Batalha GF, Van Tyne CJ, Yilbas B. (eds) Comprehensive Materials Processing, Elsevier, 251-264, ISBN 9780080965338. https://doi.org/10.1016/B978-0-08-096532-1.01010-4
77. Jagadeesh P, Ningappa VSH, Puttegowda M, Girijappa YGT, Rangappa SM, Khan MR, Khan I, Siengchin S (2021) Pongamia pinnata shell powder filled sisal/kevlar hybrid composites: physicomechanical and morphological characteristics. Polym Compos 42:4434–4447. https://doi.org/10.1002/pc.26160
78. Jaisingh Sheoran A, Kumar H (2020) Fused Deposition modeling process parameters optimization and effect on mechanical properties and part quality: Review and reflection on present research. Mater Today Proc 21:1659–1672. https://doi.org/10.1016/j.matpr.2019.11.296
79. Gay P, Blanco D, Pelayo F, Noriega A, Fernández P (2015) Analysis of factors influencing the mechanical properties of flat PolyJet manufactured parts. Procedia Eng 132:70–77. https://doi.org/10.1016/j.proeng.2015.12.481
80. Kadry H, Wadnap S, Xu C, Ahsan F (2019) Digital light processing (DLP)3D-printing technology and photoreactive polymers in fabrication of modified-release tablets. Eur J Pharm Sci 135:60–67. https://doi.org/10.1016/j.ejps.2019.05.008
81. Arefin AME, Khatri NR, Kulkarni N, Egan PF (2021) Polymer 3D printing review: materials, process, and design strategies for medical applications. Polymers (Basel) 13:1–24. https://doi.org/10.3390/polym13091499
82. Guo N, Leu MC (2013) Additive manufacturing: technology, applications and research needs. Front Mech Eng 8:215–243. https://doi.org/10.1007/s11465-013-0248-8
83. Love LJ, Kunc V, Rios O, Duty CE, Elliott AM, Post BK, Blue CA (2014) The importance of carbon fiber to polymer additive manufacturing. J Mater Res 29:1893–1898. https://doi.org/10.1557/jmr.2014.212
84. Yang D, Zhang H, Wu J, McCarthy ED (2021) Fibre flow and void formation in 3D printing of short-fibre reinforced thermoplastic composites: an experimental benchmark exercise. Addit Manuf 37:101686. https://doi.org/10.1016/j.addma.2020.101686
85. Cheng P, Wang K, Chen X, Wang J, Peng Y, Ahzi S, Chen C (2021) Interfacial and mechanical properties of continuous ramie fiber reinforced biocomposites fabricated by in-situ impregnated 3D printing. Ind Crops Prod 170:113760. https://doi.org/10.1016/j.indcrop.2021.113760
86. Long H, Wu Z, Dong Q, Shen Y, Zhou W, Luo Y, Dong X (2019) Mechanical and thermal properties of bamboo fiber reinforced polypropylene/polylactic acid composites for 3D printing. Polym Eng Sci 59:E247–E260. https://doi.org/10.1002/pen.25043
87. Gupta A, Hasanov S, Fidan I (2019) Processing and characterization of 3d-printed polymer matrix composites reinforced with discontinuous fibers. In: Solid Freeform Fabrication 2019: Proceedings of the 30th Annual International Solid Freeform Fabrication Symposium - An Additive Manufacturing Conference, SFF 2019. pp 1054–1066
88. Ming Y, Zhang S, Han W, Wang B, Duan Y, Xiao H (2020) Investigation on process parameters of 3D printed continuous carbon fiber-reinforced thermosetting epoxy composites. Addit Manuf 33:101184. https://doi.org/10.1016/j.addma.2020.101184
89. Blok LG, Longana ML, Yu H, Woods BKS (2018) An investigation into 3D printing of fibre reinforced thermoplastic composites. Addit Manuf 22:176–186. https://doi.org/10.1016/j.addma.2018.04.039
90. Tian X, Liu T, Yang C, Wang Q, Li D (2016) Interface and performance of 3D printed continuous carbon fiber reinforced PLA composites. Compos Part A Appl Sci Manuf 88:198–205. https://doi.org/10.1016/j.compositesa.2016.05.032
91. Rahman MA, Islam MZ, Gibbon L, Ulven CA, La Scala JJ (2021) 3D printing of continuous carbon fiber reinforced thermoset composites using UV curable resin. Polym Compos 42:5859–5868. https://doi.org/10.1002/pc.26266
92. Le Duigou A, Barbé A, Guillou E, Castro M (2019) 3D printing of continuous flax fibre reinforced biocomposites for structural applications. Mater Des 180:107884. https://doi.org/10.1016/j.matdes.2019.107884
93. Ivey M, Melenka GW, Carey JP, Ayranci C (2017) Characterizing short-fiber-reinforced composites produced using additive manufacturing. Adv Manuf Polym Compos Sci 3:81–91. https://doi.org/10.1080/20550340.2017.1341125
94. Mohammadizadeh M, Imeri A, Fidan I, Elkelany M (2019) 3D printed fiber reinforced polymer composites - structural analysis. Compos Part B Eng 175:107112. https://doi.org/10.1016/j.compositesb.2019.107112
95. Akasheh F, Aglan H (2019) Fracture toughness enhancement of carbon fiber–reinforced polymer composites utilizing additive manufacturing fabrication. J Elastomers Plast 51:698–711. https://doi.org/10.1177/0095244318817867
96. Invernizzi M, Natale G, Levi M, Turri S, Griffini G (2016) UV-assisted 3D printing of glass and carbon fiber-reinforced dual-cure polymer composites. Materials (Basel). https://doi.org/10.3390/MA9070583
97. Dong K, Liu L, Huang X, Xiao X (2020) 3D printing of continuous fiber reinforced diamond cellular structural composites and tensile properties. Compos Struct 250:112610. https://doi.org/10.1016/j.compstruct.2020.112610
98. Balla VK, Tadimeti JGD, Kate KH, Satyavolu J (2020) 3D printing of modified soybean hull fiber/polymer composites. Mater Chem Phys 254:123452. https://doi.org/10.1016/j.matchemphys.2020.123452

99. Prajapati AR, Dave HK, Raval HK (2021) Effect of fiber volume fraction on the impact strength of fiber reinforced polymer composites made by FDM process. Mater Today Proc 44:2102–2106. https://doi.org/10.1016/j.matpr.2020.12.262
100. Li N, Li Y, Liu S (2016) Rapid prototyping of continuous carbon fiber reinforced polylactic acid composites by 3D printing. J Mater Process Technol 238:218–225. https://doi.org/10.1016/j.jmatprotec.2016.07.025
101. Wang P, Zou B, Ding S, Huang C, Shi Z, Ma Y, Yao P (2020) Preparation of short CF/GF reinforced PEEK composite filaments and their comprehensive properties evaluation for FDM-3D printing. Compos Part B Eng 198:108175. https://doi.org/10.1016/j.compositesb.2020.108175
102. Dickson AN, Barry JN, McDonnell KA, Dowling DP (2017) Fabrication of continuous carbon, glass and Kevlar fibre reinforced polymer composites using additive manufacturing. Addit Manuf 16:146–152. https://doi.org/10.1016/j.addma.2017.06.004
103. Yavas D, Zhang Z, Liu Q, Wu D (2021) Interlaminar shear behavior of continuous and short carbon fiber reinforced polymer composites fabricated by additive manufacturing. Compos Part B Eng 204:108460. https://doi.org/10.1016/j.compositesb.2020.108460
104. Sang L, Han S, Li Z, Yang X, Hou W (2019) Development of short basalt fiber reinforced polylactide composites and their feasible evaluation for 3D printing applications. Compos Part B Eng 164:629–639. https://doi.org/10.1016/j.compositesb.2019.01.085
105. Mosleh N, Rezadoust AM, Dariushi S (2021) Determining process-window for manufacturing of continuous carbon fiber-reinforced composite using 3D-printing. Mater Manuf Process 36:409–418. https://doi.org/10.1080/10426914.2020.1843664
106. Torrado Perez AR, Roberson DA, Wicker RB (2014) Fracture surface analysis of 3D-printed tensile specimens of novel ABS-based materials. J Fail Anal Prev 14:343–353. https://doi.org/10.1007/s11668-014-9803-9
107. Hector Sandoval J, Wicker RB (2006) Functionalizing stereolithography resins: effects of dispersed multi-walled carbon nanotubes on physical properties. Rapid Prototyp J 12:292–303. https://doi.org/10.1108/13552540610707059
108. Palaganas JO, Palaganas NB, Ramos LJI, David CPC (2019) 3D printing of covalent functionalized graphene oxide nanocomposite via stereolithography. ACS Appl Mater Interfaces 11:46034–46043. https://doi.org/10.1021/acsami.9b12071
109. Fantino E, Chiappone A, Calignano F, Fontana M, Pirri F, Roppolo I (2016) In situ thermal generation of silver nanoparticles in 3D printed polymeric structures. Materials (Basel) 9:21–23. https://doi.org/10.3390/ma9070589
110. Wang Y, Lei M, Wei Q, Wang Y, Zhang J, Guo Y, Saroia J (2020) 3D printing biocompatible l-Arg/GNPs/PLA nanocomposites with enhanced mechanical property and thermal stability. J Mater Sci 55:5064–5078. https://doi.org/10.1007/s10853-020-04353-8
111. Spinelli G, Lamberti P, Tucci V, Kotsilkova R, Ivanov E, Menseidov D, Kuzhir P (2019) Nanocarbon/poly(lactic) acid for 3D printing: Effect of fillers content on electromagnetic and thermal properties. Materials (Basel). https://doi.org/10.3390/ma12152369
112. Nonato RC, Mei LHI, Bonse BC, Chinaglia EF, Morales AR (2019) Nanocomposites of PLA containing ZnO nanofibers made by solvent cast 3D printing: production and characterization. Eur Polym J 114:271–278. https://doi.org/10.1016/j.eurpolymj.2019.02.026
113. Prashantha K, Roger F (2017) Multifunctional properties of 3D printed poly(lactic acid)/graphene nanocomposites by fused deposition modeling. J Macromol Sci Part A Pure Appl Chem 54:24–29. https://doi.org/10.1080/10601325.2017.1250311
114. Tambrallimath V, Keshavamurthy R, Bavan SD, Patil AY, Khan Y, Badruddin IA, Kamangar S (2021) Mechanical properties of pc-abs-based graphene-reinforced polymer nanocomposites fabricated by fdm process. Polymers (Basel). https://doi.org/10.3390/polym13172951
115. Huang B, He H, Meng S, Jia Y (2019) Optimizing 3D printing performance of acrylonitrile-butadiene-styrene composites with cellulose nanocrystals/silica nanohybrids. Polym Int 68:1351–1360. https://doi.org/10.1002/pi.5824
116. Gnanasekaran K, Heijmans T, van Bennekom S, Woldhuis H, Wijnia S, De With G, Friedrich H (2017) 3D printing of CNT- and graphene-based conductive polymer nanocomposites by fused deposition modeling. Appl Mater Today 9:21–28. https://doi.org/10.1016/j.apmt.2017.04.003
117. Coppola B, Cappetti N, Di Maio L, Scarfato P, Incarnato L (2017) Layered silicate reinforced polylactic acid filaments for 3D printing of polymer nanocomposites. IEEE 3rd International Forum on Research and Technologies for Society and Industry 3–6. https://doi.org/10.1109/RTSI.2017.8065892
118. Postiglione G, Natale G, Griffini G, Levi M, Turri S (2015) Conductive 3D microstructures by direct 3D printing of polymer/carbon nanotube nanocomposites via liquid deposition modeling. Compos Part A Appl Sci Manuf 76:110–114. https://doi.org/10.1016/j.compositesa.2015.05.014
119. Chen Q, Mangadlao JD, Wallat J, De Leon A, Pokorski JK, Advincula RC (2017) 3D printing biocompatible polyurethane/poly(lactic acid)/graphene oxide nanocomposites: anisotropic properties. ACS Appl Mater Interfaces 9:4015–4023. https://doi.org/10.1021/acsami.6b11793
120. Wei H, Cauchy X, Navas IO, Abderrafai Y, Chizari K, Sundararaj U, Therriault D (2019) Direct 3D printing of hybrid nanofiber-based nanocomposites for highly conductive and shape memory applications. ACS Appl Mater Interfaces 11:24523–24532. https://doi.org/10.1021/acsami.9b04245
121. Viskadourakis Z, Perrakis G, Symeou E, Giapintzakis J, Kenanakis G (2019) Transport properties of 3D printed polymer nanocomposites for potential thermoelectric applications. Appl Phys A Mater Sci Process. https://doi.org/10.1007/s00339-019-2469-0
122. Garcia Rosales CA, Garcia Duarte MF, Kim H, Chavez L, Hodges D, Mandal P, Tseng TLB (2018) 3D printing of shape memory polymer (SMP)/carbon black (CB) nanocomposites with electro-responsive toughness enhancement. Mater Res Express 5:065704. https://doi.org/10.1088/2053-1591/aacd53
123. Sanatgar RH, Campagne C, Nierstrasz V (2017) Investigation of the adhesion properties of direct 3D printing of polymers and nanocomposites on textiles: effect of FDM printing process parameters. Appl Surf Sci 403:551–563. https://doi.org/10.1016/j.apsusc.2017.01.112
124. Weng Z, Wang J, Senthil T, Wu L (2016) Mechanical and thermal properties of ABS/montmorillonite nanocomposites for fused deposition modeling 3D printing. Mater Des 102:276–283. https://doi.org/10.1016/j.matdes.2016.04.045
125. Guo Y, Zuo X, Xue Y, Tang J, Gouzman M, Fang Y, Rafailovich MH (2020) Engineering thermally and electrically conductive biodegradable polymer nanocomposites. Compos Part B Eng 189:107905. https://doi.org/10.1016/j.compositesb.2020.107905
126. Isakov DV, Lei Q, Castles F, Stevens CJ, Grovenor CRM, Grant PS (2016) 3D printed anisotropic dielectric composite with meta-material features. Mater Des 93:423–430. https://doi.org/10.1016/j.matdes.2015.12.176
127. Shemelya CM, Rivera A, Perez AT, Rocha C, Liang MIN, Yu X, Roberson DA (2015) Mechanical, electromagnetic, and X-ray shielding characterization of a 3D printable tungsten–polycarbonate polymer matrix composite for space-based applications. J Electron Mater 44:2598–2607. https://doi.org/10.1007/s11664-015-3687-7
128. Chung H, Das S (2006) Processing and properties of glass bead particulate-filled functionally graded nylon-11 composites produced by selective laser sintering. Mater Sci Eng A 437:226–234. https://doi.org/10.1016/j.msea.2006.07.112
129. Kalsoom U, Peristyy A, Nesterenko PN, Paull B (2016) A 3D printable diamond polymer composite: a novel material for

fabrication of low cost thermally conducting devices. RSC Adv 6:38140–38147. https://doi.org/10.1039/c6ra05261d
130. Kokkinis D, Schaffner M, Studart AR (2015) Multimaterial magnetically assisted 3D printing of composite materials. Nat Commun. https://doi.org/10.1038/ncomms9643
131. Aw YY, Yeoh CK, Idris MA, Teh PL, Elyne WN, Hamzah KA, Sazali SA (2018) Effect of printing parameters on tensile, dynamic mechanical, and thermoelectric properties of FDM 3D printed CABS/ZnO composites. Materials (Basel). https://doi.org/10.3390/ma11040466
132. Zheng H, Zhang J, Lu S, Wang G, Xu Z (2006) Effect of core-shell composite particles on the sintering behavior and properties of nano-Al2O3/polystyrene composite prepared by SLS. Mater Lett 60:1219–1223. https://doi.org/10.1016/j.matlet.2005.11.003
133. Shuai CJ, Mao ZZ, Han ZK, Peng SP (2014) Preparation of complex porous scaffolds via selective laser sintering of poly(vinyl alcohol)/calcium silicate. J Bioact Compat Polym 29:110–120. https://doi.org/10.1177/0883911514522570
134. Zgalat-Lozynskyy OB, Matviichuk OO, Tolochyn OI, Ievdokymova OV, Zgalat-Lozynska NO, Zakiev VI (2021) Polymer materials reinforced with silicon nitride particles for 3D printing. Powder Metall Met Ceram 59:515–527. https://doi.org/10.1007/s11106-021-00189-2
135. Chueh YH, Wei C, Zhang X, Li L (2020) Integrated laser-based powder bed fusion and fused filament fabrication for three-dimensional printing of hybrid metal/polymer objects. Addit Manuf 31:100928. https://doi.org/10.1016/j.addma.2019.100928
136. Nabipour M, Akhoundi B (2021) An experimental study of FDM parameters effects on tensile strength, density, and production time of ABS/Cu composites. J Elastomers Plast 53:146–164. https://doi.org/10.1177/0095244320916838
137. Aqzna SS, Yeoh CK, Idris MS, Teh PL, bin Hamzah KA, Aw YY, Atiqah TN (2018) Effect of different filler content of ABS–zinc ferrite composites on mechanical, electrical and thermal conductivity by using 3D printing. J Vinyl Addit Technol 24:E217–E229. https://doi.org/10.1002/vnl.21640
138. Dizon JRC, Chen Q, Valino AD, Advincula RC (2019) Thermomechanical and swelling properties of three-dimensional-printed poly (ethylene glycol) diacrylate/silica nanocomposites. MRS Commun 9:209–217. https://doi.org/10.1557/mrc.2018.188
139. Liu W, Wu N, Pochiraju K (2018) Shape recovery characteristics of SiC/C/PLA composite filaments and 3D printed parts. Compos Part A Appl Sci Manuf 108:1–11. https://doi.org/10.1016/j.compositesa.2018.02.017
140. Quill TJ, Smith MK, Zhou T, Baioumy MGS, Berenguer JP, Cola BA, Bougher TL (2018) Thermal and mechanical properties of 3D printed boron nitride – ABS composites. Appl Compos Mater 25:1205–1217. https://doi.org/10.1007/s10443-017-9661-1
141. Tan JC, Low HY (2018) Embedded electrical tracks in 3D printed objects by fused filament fabrication of highly conductive composites. Addit Manuf 23:294–302. https://doi.org/10.1016/j.addma.2018.06.009
142. Palmero EM, Casaleiz D, de Vicente J, López-Vidal S, Ramiro E, Bollero A (2019) Composites based on metallic particles and tuned filling factor for 3D-printing by fused deposition modeling. Compos Part A Appl Sci Manuf 124:105497. https://doi.org/10.1016/j.compositesa.2019.105497
143. Hamzah KA, Yeoh CK, Noor MM, Teh PL, Aw YY, Sazali SA, Wan Ibrahim WMA (2022) Mechanical properties and thermal and electrical conductivity of 3D printed ABS-copper ferrite composites via 3D printing technique. J Thermoplast Compos Mater 35:3–16. https://doi.org/10.1177/0892705719869405
144. Yang F, Zeng J, Long H, Xiao J, Luo Y, Gu J, Dong X (2020) Micrometer copper-zinc alloy particles-reinforced wood plastic composites with high gloss and antibacterial properties for 3d printing. Polymers (Basel). https://doi.org/10.3390/polym12030621
145. Wu Y, Cao Y, Wu Y, Li D (2020) Mechanical properties and gamma-ray shielding performance of 3D-printed. Materials 13:4475. https://doi.org/10.3390/ma13204475
146. Liu M, Chiang SW, Chu X, Li J, Gan L, He Y, Du H (2020) Polymer composites with enhanced thermal conductivity via oriented boron nitride and alumina hybrid fillers assisted by 3-D printing. Ceram Int 46:20810–20818. https://doi.org/10.1016/j.ceramint.2020.05.096
147. Yang L, Wang L, Chen Y (2020) Solid-state shear milling method to prepare PA12/boron nitride thermal conductive composite powders and their selective laser sintering 3D-printing. J Appl Polym Sci 137:1–13. https://doi.org/10.1002/app.48766
148. Aw YY, Yeoh CK, Idris MA, Teh PL, Elyne WN, Hamzah KA, Sazali SA (2018) Influence of filler precoating and printing parameter on mechanical properties of 3D printed acrylonitrile butadiene styrene/zinc oxide composite. Polym Plast Technol Eng 58:1–13. https://doi.org/10.1080/03602559.2018.1455861
149. Dawoud M, Taha I, Ebeid SJ (2018) Strain sensing behaviour of 3D printed carbon black filled ABS. J Manuf Process 35:337–342. https://doi.org/10.1016/j.jmapro.2018.08.012
150. Castles F, Isakov D, Lui A, Lei Q, Dancer CEJ, Wang Y, Grant PS (2016) Microwave dielectric characterisation of 3D-printed BaTiO3/ABS polymer composites. Sci Rep 6:1–8. https://doi.org/10.1038/srep22714
151. Leigh SJ, Purssell CP, Bowen J, Hutchins DA, Covington JA, Billson DR (2011) A miniature flow sensor fabricated by microstereolithography employing a magnetite/acrylic nanocomposite resin. Sensors Actuators A Phys 168:66–71. https://doi.org/10.1016/j.sna.2011.03.058
152. Jabr RA (2005) Application of geometric programming to transformer design. IEEE Trans Magn 41:4261–4269. https://doi.org/10.1109/TMAG.2005.856921
153. Shokrollahi H, Janghorban K (2007) Influence of additives on the magnetic properties, microstructure and densification of Mn-Zn soft ferrites. Mater Sci Eng B Solid-State Mater Adv Technol 141:91–107. https://doi.org/10.1016/j.mseb.2007.06.005
154. Grau-Crespo R, Al-Baitai AY, Saadoune I, De Leeuw NH (2010) Vacancy ordering and electronic structure of γ-Fe2O 3 (maghemite): a theoretical investigation. J Phys Condens Matter. https://doi.org/10.1088/0953-8984/22/25/255401
155. Bollig LM, Hilpisch PJ, Mowry GS, Nelson-Cheeseman BB (2017) 3D printed magnetic polymer composite transformers. J Magn Magn Mater 442:97–101. https://doi.org/10.1016/j.jmmm.2017.06.070
156. Khatri B, Lappe K, Noetzel D, Pursche K, Hanemann T (2018) A 3D-printable polymer-metal soft-magnetic functional composite-development and characterization. Materials (Basel). https://doi.org/10.3390/ma11020189
157. Zhang J, Zhao S, Zhu M, Zhu Y, Zhang Y, Liu Z, Zhang C (2014) 3D-printed magnetic Fe3O4/MBG/PCL composite scaffolds with multifunctionality of bone regeneration, local anticancer drug delivery and hyperthermia. J Mater Chem B 2:7583–7595. https://doi.org/10.1039/c4tb01063a
158. Yue C, Li M, Liu Y, Fang Y, Song Y, Xu M, Li J (2021) Three-dimensional printing of cellulose nanofibers reinforced PHB/PCL/Fe3O4 magneto-responsive shape memory polymer composites with excellent mechanical properties. Addit Manuf 46:102146. https://doi.org/10.1016/j.addma.2021.102146
159. Schmitz DP, Ecco LG, Dul S, Pereira ECL, Soares BG, Barra GMO, Pegoretti A (2018) Electromagnetic interference shielding effectiveness of ABS carbon-based composites manufactured via fused deposition modelling. Mater Today Commun 15:70–80. https://doi.org/10.1016/j.mtcomm.2018.02.034
160. Khamis AM, Abbas Z, Azis RAS, Mensah EE, Alhaji IA (2021) Effects of recycled fe2o3 nanofiller on the structural, thermal,

mechanical, dielectric, and magnetic properties of ptfe matrix. Polymers (Basel). https://doi.org/10.3390/polym13142332
161. Palmero EM, Rial J, de Vicente J, Camarero J, Skårman B, Vidarsson H, Bollero A (2018) Development of permanent magnet MnAlC/polymer composites and flexible filament for bonding and 3D-printing technologies. Sci Technol Adv Mater 19:465–473. https://doi.org/10.1080/14686996.2018.1471321
162. Ligon SC, Liska R, Stampfl J, Gurr M, Mülhaupt R (2017) Polymers for 3D printing and customized additive manufacturing. Chem Rev 117:10212–10290. https://doi.org/10.1021/acs.chemrev.7b00074
163. Jariwala D, Sangwan VK, Lauhon LJ, Marks TJ, Hersam MC (2013) Carbon nanomaterials for electronics, optoelectronics, photovoltaics, and sensing. Chem Soc Rev 42:2824–2860. https://doi.org/10.1039/c2cs35335k
164. Ghoshal S (2017) Polymer/carbon nanotubes (CNT) nanocomposites processing using additive manufacturing (three-dimensional printing) technique: an overview. Fibers. https://doi.org/10.3390/fib5040040
165. Last BJ, Thouless DJ (1971) Percolation theory and electrical conductivity. Phys Rev Lett 27:1719–1721. https://doi.org/10.1103/PhysRevLett.27.1719
166. De Leon AC, Chen Q, Palaganas NB, Palaganas JO, Manapat ARC (2016) High performance polymer nanocomposites for additive manufacturing applications. React Funct Polym 103:141–155. https://doi.org/10.1016/j.reactfunctpolym.2016.04.010
167. Wei X, Li D, Jiang W, Gu Z, Wang X, Zhang Z, Sun Z (2015) 3D printable graphene composite. Sci Rep 5:1–7. https://doi.org/10.1038/srep11181
168. Asp LE, Greenhalgh ES (2014) Structural power composites. Compos Sci Technol 101:41–61. https://doi.org/10.1016/j.compscitech.2014.06.020
169. Leng J, Lan X, Liu Y, Du S (2011) Shape-memory polymers and their composites: stimulus methods and applications. Prog Mater Sci 56:1077–1135. https://doi.org/10.1016/j.pmatsci.2011.03.001
170. He M, Zhao Y, Wang B, Xi Q, Zhou J, Liang Z (2015) 3D printing fabrication of amorphous thermoelectric materials with ultralow thermal conductivity. Small 11:5889–5894. https://doi.org/10.1002/smll.201502153
171. Chizari K, Arjmand M, Liu Z, Sundararaj U, Therriault D (2017) Three-dimensional printing of highly conductive polymer nanocomposites for EMI shielding applications. Mater Today Commun 11:112–118. https://doi.org/10.1016/j.mtcomm.2017.02.006
172. Sezer HK, Eren O (2019) FDM 3D printing of MWCNT reinforced ABS nano-composite parts with enhanced mechanical and electrical properties. J Manuf Process 37:339–347. https://doi.org/10.1016/j.jmapro.2018.12.004
173. Rymansaib Z, Iravani P, Emslie E, Medvidović-Kosanović M, Sak-Bosnar M, Verdejo R, Marken F (2016) All-polystyrene 3D-printed electrochemical device with embedded carbon nanofiber-graphite-polystyrene composite conductor. Electroanalysis 28:1517–1523. https://doi.org/10.1002/elan.201600017
174. Bin Hamzah HH, Keattch O, Covill D, Patel BA (2018) The effects of printing orientation on the electrochemical behaviour of 3D printed acrylonitrile butadiene styrene (ABS)/carbon black electrodes. Sci Rep 8:1–8. https://doi.org/10.1038/s41598-018-27188-5
175. Ivanov E, Kotsilkova R, Xia H, Chen Y, Donato RK, Donato K, Angelov V (2019) PLA/Graphene/MWCNT composites with improved electrical and thermal properties suitable for FDM 3D printing applications. Appl Sci. https://doi.org/10.3390/app9061209
176. Sayyar S, Bjorninen M, Haimi S, Miettinen S, Gilmore K, Grijpma D, Wallace G (2016) UV cross-linkable graphene/poly(trimethylene carbonate) composites for 3D printing of electrically conductive scaffolds. ACS Appl Mater Interfaces 8:31916–31925. https://doi.org/10.1021/acsami.6b09962
177. Compton BG, Hmeidat NS, Pack RC, Heres MF, Sangoro JR (2018) Electrical and mechanical properties of 3D-printed graphene-reinforced epoxy. Jom 70:292–297. https://doi.org/10.1007/s11837-017-2707-x
178. Yuan S, Zheng Y, Chua CK, Yan Q, Zhou K (2018) Electrical and thermal conductivities of MWCNT/polymer composites fabricated by selective laser sintering. Compos Part A Appl Sci Manuf 105:203–213. https://doi.org/10.1016/j.compositesa.2017.11.007
179. Gojny FH, Wichmann MHG, Fiedler B, Kinloch IA, Bauhofer W, Windle AH, Schulte K (2006) Evaluation and identification of electrical and thermal conduction mechanisms in carbon nanotube/epoxy composites. Polymer (Guildf) 47:2036–2045. https://doi.org/10.1016/j.polymer.2006.01.029
180. Chowdhury RA, Hosur MV, Nuruddin M, Tcherbi-Narteh A, Kumar A, Boddu V, Jeelani S (2015) Self-healing epoxy composites: preparation, characterization and healing performance. J Mater Res Technol 4:33–43. https://doi.org/10.1016/j.jmrt.2014.10.016
181. Kim SY, Jones AR, Sottos NR, White SR (2017) Manufacturing of unidirectional glass/epoxy prepreg with microencapsulated liquid healing agents. Compos Sci Technol 153:190–197. https://doi.org/10.1016/j.compscitech.2017.10.017
182. Moll JL, Jin H, Mangun CL, White SR, Sottos NR (2013) Self-sealing of mechanical damage in a fully cured structural composite. Compos Sci Technol 79:15–20. https://doi.org/10.1016/j.compscitech.2013.02.006
183. Bekas DG, Baltzis D, Paipetis AS (2017) Nano-reinforced polymeric healing agents for vascular self-repairing composites. Mater Des 116:538–544. https://doi.org/10.1016/j.matdes.2016.12.049
184. Pang JWC, Bond IP (2005) A hollow fibre reinforced polymer composite encompassing self-healing and enhanced damage visibility. Compos Sci Technol 65:1791–1799. https://doi.org/10.1016/j.compscitech.2005.03.008
185. Kostopoulos V, Kotrotsos A, Tsantzalis S, Tsokanas P, Loutas T, Bosman AW (2016) Toughening and healing of continuous fibre reinforced composites by supramolecular polymers. Compos Sci Technol 128:84–93. https://doi.org/10.1016/j.compscitech.2016.03.021
186. Postiglione G, Alberini M, Leigh S, Levi M, Turri S (2017) Effect of 3D-printed microvascular network design on the self-healing behavior of cross-linked polymers. ACS Appl Mater Interfaces 9:14371–14378. https://doi.org/10.1021/acsami.7b01830
187. Aïssa B, Therriault D, Haddad E, Jamroz W (2012) Self-healing materials systems: overview of major approaches and recent developed technologies. Adv Mater Sci Eng. https://doi.org/10.1155/2012/854203
188. Nadgorny M, Xiao Z, Connal LA (2017) 2D and 3D-printing of self-healing gels: design and extrusion of self-rolling objects. Mol Syst Des Eng 2:283–292. https://doi.org/10.1039/c7me00023e
189. Almutairi MD, Aria AI, Thakur VK, Khan MA (2020) Self-healing mechanisms for 3D-printed polymeric structures: from lab to reality. Polymers (Basel) 12:1–27. https://doi.org/10.3390/polym12071534
190. Wu T, Gray E, Chen B (2018) A self-healing, adaptive and conductive polymer composite ink for 3D printing of gas sensors. J Mater Chem C 6:6200–6207. https://doi.org/10.1039/c8tc01092g
191. Sanders P, Young AJ, Qin Y, Fancey KS, Reithofer MR, Guillet-Nicolas R, Chin JM (2019) Stereolithographic 3D printing of extrinsically self-healing composites. Sci Rep 9:1–6. https://doi.org/10.1038/s41598-018-36828-9
192. Bi H, Ren Z, Ye G, Sun H, Guo R, Jia X, Xu M (2020) Fabrication of cellulose nanocrystal reinforced thermoplastic polyurethane/polycaprolactone blends for three-dimension printing self-healing

nanocomposites. Cellulose 27:8011–8026. https://doi.org/10.1007/s10570-020-03328-x
193. Sanei SHR, Popescu D (2020) 3d-printed carbon fiber reinforced polymer composites: a systematic review. J Compos Sci. https://doi.org/10.3390/jcs4030098
194. Brenken B, Barocio E, Favaloro A, Kunc V, Pipes RB (2018) Fused filament fabrication of fiber-reinforced polymers: a review. Addit Manuf 21:1–16. https://doi.org/10.1016/j.addma.2018.01.002
195. Zhang J, Wang J, Dong S, Yu X, Han B (2019) A review of the current progress and application of 3D printed concrete. Compos Part A Appl Sci Manuf 125:105533. https://doi.org/10.1016/j.compositesa.2019.105533
196. Christiyan KGJ, Chandrasekhar U, Venkateswarlu K (2016) A study on the influence of process parameters on the mechanical properties of 3D printed ABS composite. IOP Conf Ser Mater Sci Eng. https://doi.org/10.1088/1757-899X/114/1/012109
197. Esposito Corcione C, Gervaso F, Scalera F, Padmanabhan SK, Madaghiele M, Montagna F, Maffezzoli A (2019) Highly loaded hydroxyapatite microsphere/ PLA porous scaffolds obtained by fused deposition modelling. Ceram Int 45:2803–2810. https://doi.org/10.1016/j.ceramint.2018.07.297
198. Mohammadizadeh M, Fidan I, Allen M, Imeri A (2018) Creep behavior analysis of additively manufactured fiber-reinforced components. Int J Adv Manuf Technol 99:1225–1234. https://doi.org/10.1007/s00170-018-2539-z
199. Liao G, Li Z, Cheng Y, Xu D, Zhu D, Jiang S, Zhu Y (2018) Properties of oriented carbon fiber/polyamide 12 composite parts fabricated by fused deposition modeling. Mater Des 139:283–292. https://doi.org/10.1016/j.matdes.2017.11.027
200. Sodeifian G, Ghaseminejad S, Yousefi AA (2019) Preparation of polypropylene/short glass fiber composite as fused deposition modeling (FDM) filament. Results Phys 12:205–222. https://doi.org/10.1016/j.rinp.2018.11.065
201. Dul S, Fambri L, Pegoretti A (2016) Fused deposition modelling with ABS-graphene nanocomposites. Compos Part A Appl Sci Manuf 85:181–191. https://doi.org/10.1016/j.compositesa.2016.03.013
202. Ding S, Zou B, Wang P, Ding H (2019) Effects of nozzle temperature and building orientation on mechanical properties and microstructure of PEEK and PEI printed by 3D-FDM. Polym Test 78:105948. https://doi.org/10.1016/j.polymertesting.2019.105948
203. Yu R, Yang X, Zhang Y, Zhao X, Wu X, Zhao T, Huang W (2017) Three-dimensional printing of shape memory composites with epoxy-acrylate hybrid photopolymer. ACS Appl Mater Interfaces 9:1820–1829. https://doi.org/10.1021/acsami.6b13531
204. Lewicki JP, Rodriguez JN, Zhu C, Worsley MA, Wu AS, Kanarska Y, King MJ (2017) 3D-printing of meso-structurally ordered carbon fiber/polymer composites with unprecedented orthotropic physical properties. Sci Rep 7:1–14. https://doi.org/10.1038/srep43401
205. Yu T, Zhang Z, Song S, Bai Y, Wu D (2019) Tensile and flexural behaviors of additively manufactured continuous carbon fiber-reinforced polymer composites. Compos Struct 225:111147. https://doi.org/10.1016/j.compstruct.2019.111147
206. Ning F, Cong W, Hu Y, Wang H (2017) Additive manufacturing of carbon fiber-reinforced plastic composites using fused deposition modeling: Effects of process parameters on tensile properties. J Compos Mater 51:451–462. https://doi.org/10.1177/0021998316646169
207. Tao Y, Wang H, Li Z, Li P, Shi SQ (2017) Development and application of wood flour-filled polylactic acid composite filament for 3d printing. Materials (Basel) 10:1–6. https://doi.org/10.3390/ma10040339
208. Ayrilmis N, Kariz M, Kwon JH, Kitek Kuzman M (2019) Effect of printing layer thickness on water absorption and mechanical properties of 3D-printed wood/PLA composite materials. Int J Adv Manuf Technol 102:2195–2200. https://doi.org/10.1007/s00170-019-03299-9
209. Hao W, Liu Y, Zhou H, Chen H, Fang D (2018) Preparation and characterization of 3D printed continuous carbon fiber reinforced thermosetting composites. Polym Test 65:29–34. https://doi.org/10.1016/j.polymertesting.2017.11.004
210. Kariz M, Sernek M, Obućina M, Kuzman MK (2018) Effect of wood content in FDM filament on properties of 3D printed parts. Mater Today Commun 14:135–140. https://doi.org/10.1016/j.mtcomm.2017.12.016
211. Caminero MÁ, Chacón JM, García-Plaza E, Núñez PJ, Reverte JM, Becar JP (2019) Additive manufacturing of PLA-based composites using fused filament fabrication: effect of graphene nanoplatelet reinforcement on mechanical properties, dimensional accuracy and texture. Polymers (Basel). https://doi.org/10.3390/polym11050799
212. Melenka GW, Cheung BKO, Schofield JS, Dawson MR, Carey JP (2016) Evaluation and prediction of the tensile properties of continuous fiber-reinforced 3D printed structures. Compos Struct 153:866–875. https://doi.org/10.1016/j.compstruct.2016.07.018
213. Skorski MR, Esenther JM, Ahmed Z, Miller AE, Hartings MR (2016) The chemical, mechanical, and physical properties of 3D printed materials composed of TiO2-ABS nanocomposites. Sci Technol Adv Mater 17:89–97. https://doi.org/10.1080/14686996.2016.1152879
214. Wang P, Zou B, Ding S, Lei LI, Huang C (2021) Effects of FDM-3D printing parameters on mechanical properties and microstructure of CF/PEEK and GF/PEEK. Chinese J Aeronaut 34:236–246. https://doi.org/10.1016/j.cja.2020.05.040
215. Zhu D, Ren Y, Liao G, Jiang S, Liu F, Guo J, Xu G (2017) Thermal and mechanical properties of polyamide 12/graphene nanoplatelets nanocomposites and parts fabricated by fused deposition modeling. J Appl Polym Sci 134:1–13. https://doi.org/10.1002/app.45332
216. Ferreira RTL, Amatte IC, Dutra TA, Bürger D (2017) Experimental characterization and micrography of 3D printed PLA and PLA reinforced with short carbon fibers. Compos Part B Eng 124:88–100. https://doi.org/10.1016/j.compositesb.2017.05.013
217. Goh GD, Dikshit V, Nagalingam AP, Goh GL, Agarwala S, Sing SL, Yeong WY (2018) Characterization of mechanical properties and fracture mode of additively manufactured carbon fiber and glass fiber reinforced thermoplastics. Mater Des 137:79–89. https://doi.org/10.1016/j.matdes.2017.10.021
218. Liu Z, Lei Q, Xing S (2019) Mechanical characteristics of wood, ceramic, metal and carbon fiber-based PLA composites fabricated by FDM. J Mater Res Technol 8:3743–3753. https://doi.org/10.1016/j.jmrt.2019.06.034
219. Jiang D, Smith DE (2017) Anisotropic mechanical properties of oriented carbon fiber filled polymer composites produced with fused filament fabrication. Addit Manuf 18:84–94. https://doi.org/10.1016/j.addma.2017.08.006
220. Spoerk M, Savandaiah C, Arbeiter F, Traxler G, Cardon L, Holzer C, Sapkota J (2018) Anisotropic properties of oriented short carbon fibre filled polypropylene parts fabricated by extrusion-based additive manufacturing. Compos Part A Appl Sci Manuf 113:95–104. https://doi.org/10.1016/j.compositesa.2018.06.018
221. Christ JF, Aliheidari N, Ameli A, Pötschke P (2017) 3D printed highly elastic strain sensors of multiwalled carbon nanotube/thermoplastic polyurethane nanocomposites. Mater Des 131:394–401. https://doi.org/10.1016/j.matdes.2017.06.011
222. Dul S, Fambri L, Pegoretti A (2018) Filaments production and fused deposition modelling of ABS/carbon nanotubes composites. Nanomaterials. https://doi.org/10.3390/nano8010049

223. Hymas DM, Arle MA, Singer F, Shooshtari AH, Ohadi MM (2017) Enhanced air-side heat transfer in an additively manufactured polymer composite heat exchanger. Proceedings of the 16th InterSociety Conference on Thermal and Thermomechanical Phenomena in Electronic Systems, ITherm 2017:634–638. https://doi.org/10.1109/ITHERM.2017.7992546
224. Wong M, Tsopanos S, Sutcliffe CJ, Owen I (2007) Selective laser melting of heat transfer devices. Rapid Prototyp J 13:291–297. https://doi.org/10.1108/13552540710824797
225. Arie MA, Shooshtari AH, Tiwari R, Dessiatoun SV, Ohadi MM, Pearce JM (2017) Experimental characterization of heat transfer in an additively manufactured polymer heat exchanger. Appl Therm Eng 113:575–584. https://doi.org/10.1016/j.applthermaleng.2016.11.030
226. Doganay D, Coskun S, Kaynak C, Unalan HE (2016) Electrical, mechanical and thermal properties of aligned silver nanowire/polylactide nanocomposite films. Compos Part B Eng 99:288–296. https://doi.org/10.1016/j.compositesb.2016.06.044
227. DI Stepashkin C, Senatov FS, Salimon AI, Korsunsky AM, Kaloshkin SD (2018) 3D-printed PEEK-carbon fiber (CF) composites: structure and thermal properties. Compos Sci Technol 164:319–326. https://doi.org/10.1016/j.compscitech.2018.05.032
228. Espera AH, Valino AD, Palaganas JO, Souza L, Chen Q, Advincula RC (2019) 3D printing of a robust polyamide-12-carbon black composite via selective laser sintering: thermal and electrical conductivity. Macromol Mater Eng 304:1–8. https://doi.org/10.1002/mame.201800718
229. Waheed S, Cabot JM, Smejkal P, Farajikhah S, Sayyar S, Innis PC, Paull B (2019) Three-dimensional printing of abrasive, hard, and thermally conductive synthetic microdiamond-polymer composite using low-cost fused deposition modeling printer. ACS Appl Mater Interfaces 11:4353–4363. https://doi.org/10.1021/acsami.8b18232
230. Guiney LM, Mansukhani ND, Jakus AE, Wallace SG, Shah RN, Hersam MC (2018) Three-dimensional printing of cytocompatible, thermally conductive hexagonal boron nitride nanocomposites. Nano Lett 18:3488–3493. https://doi.org/10.1021/acs.nanolett.8b00555
231. Nikzad M, Masood SH, Sbarski I (2011) Thermo-mechanical properties of a highly filled polymeric composites for fused deposition modeling. Mater Des 32:3448–3456. https://doi.org/10.1016/j.matdes.2011.01.056
232. Zhao Z, Teng K, Li N, Li X, Xu Z, Chen L, Liu Y (2017) Mechanical, thermal and interfacial performances of carbon fiber reinforced composites flavored by carbon nanotube in matrix/interface. Compos Struct 159:761–772. https://doi.org/10.1016/j.compstruct.2016.10.022
233. Vinyas M, Athul SJ, Harursampath D, Nguyen Thoi T (2019) Experimental evaluation of the mechanical and thermal properties of 3D printed PLA and its composites. Mater Res Express. https://doi.org/10.1088/2053-1591/ab43ab
234. Hassouna F, Raquez JM, Addiego F, Dubois P, Toniazzo V, Ruch D (2011) New approach on the development of plasticized polylactide (PLA): grafting of poly(ethylene glycol) (PEG) via reactive extrusion. Eur Polym J 47:2134–2144. https://doi.org/10.1016/j.eurpolymj.2011.08.001
235. MacDonald E, Salas R, Espalin D, Perez M, Aguilera E, Muse D, Wicker RB (2014) 3D printing for the rapid prototyping of structural electronics. IEEE Access 2:234–242. https://doi.org/10.1109/ACCESS.2014.2311810
236. Aslanzadeh S, Saghlatoon H, Honari MM, Mirzavand R, Montemagno C, Mousavi P (2018) Investigation on electrical and mechanical properties of 3D printed nylon 6 for RF/microwave electronics applications. Addit Manuf 21:69–75. https://doi.org/10.1016/j.addma.2018.02.016
237. Jakus AE, Secor EB, Rutz AL, Jordan SW, Hersam MC, Shah RN (2015) Three-dimensional printing of high-content graphene scaffolds for electronic and biomedical applications. ACS Nano 9:4636–4648. https://doi.org/10.1021/acsnano.5b01179
238. Leigh SJ, Bradley RJ, Purssell CP, Billson DR, Hutchins DA (2012) A simple, low-cost conductive composite material for 3D printing of electronic sensors. PLoS One 7:1–6. https://doi.org/10.1371/journal.pone.0049365
239. Farahani RD, Dalir H, Le Borgne V, Gautier LA, El Khakani MA, Therriault LMD (2012) Direct-write fabrication of freestanding nanocomposite strain sensors. Nanotechnology. https://doi.org/10.1088/0957-4484/23/8/085502
240. Tian X, Jin J, Yuan S, Chua CK, Tor SB, Zhou K (2017) Emerging 3D-printed electrochemical energy storage devices: a critical review. Adv Energy Mater 7:1–17. https://doi.org/10.1002/aenm.201700127
241. Flowers PF, Reyes C, Ye S, Kim MJ, Wiley BJ (2017) 3D printing electronic components and circuits with conductive thermoplastic filament. Addit Manuf 18:156–163. https://doi.org/10.1016/j.addma.2017.10.002
242. Kim H, Johnson J, Chavez LA, Rosales CAG, Tseng TLB, Lin Y (2018) Enhanced dielectric properties of three phase dielectric MWCNTs/BaTiO3/PVDF nanocomposites for energy storage using fused deposition modeling 3D printing. Ceram Int 44:9037–9044. https://doi.org/10.1016/j.ceramint.2018.02.107
243. Zang X, Shen C, Chu Y, Li B, Wei M, Zhong J, Lin L (2018) Laser-induced molybdenum carbide–graphene composites for 3D foldable paper electronics. Adv Mater 30:1–8. https://doi.org/10.1002/adma.201800062
244. Wang Z, Zhang Q, Long S, Luo Y, Yu P, Tan Z, Bai H (2018) Three-dimensional printing of polyaniline/reduced graphene oxide composite for high-performance planar supercapacitor. ACS Appl Mater Interfaces 10:10437–10444. https://doi.org/10.1021/acsami.7b19635
245. Han T, Kundu S, Nag A, Xu Y (2019) 3D printed sensors for biomedical applications: a review. Sensors (Switzerland). https://doi.org/10.3390/s19071706
246. Yoo DJ (2011) Computer-aided porous scaffold design for tissue engineering using triply periodic minimal surfaces. Int J Precis Eng Manuf 12:61–71. https://doi.org/10.1007/s12541-011-0008-9
247. Placone JK, Engler AJ (2018) Recent advances in extrusion-based 3D printing for biomedical applications. Adv Healthc Mater 7:1–11. https://doi.org/10.1002/adhm.201701161
248. Xu C, Dai G, Hong Y (2019) Recent advances in high-strength and elastic hydrogels for 3D printing in biomedical applications. Acta Biomater 95:50–59. https://doi.org/10.1016/j.actbio.2019.05.032
249. Alam F, Shukla VR, Varadarajan KM, Kumar S (2020) Micro-architected 3D printed polylactic acid (PLA) nanocomposite scaffolds for biomedical applications. J Mech Behav Biomed Mater 103:103576. https://doi.org/10.1016/j.jmbbm.2019.103576
250. Mondal S, Nguyen TP, Pham VH (2020) Hydroxyapatite nano bioceramics optimized 3D printed poly lactic acid scaffold for bone tissue engineering application. Ceram Int 46:3443–3455. https://doi.org/10.1016/j.ceramint.2019.10.057
251. Wang W, Caetano G, Ambler WS, Blaker JJ, Frade MA, Mandal P, Bártolo P (2016) Enhancing the hydrophilicity and cell attachment of 3D printed PCL/graphene scaffolds for bone tissue engineering. Materials (Basel). https://doi.org/10.3390/ma9120992
252. Bayer IS (2017) Thermomechanical properties of polylactic acid-graphene composites: a state-of-the-art review for biomedical applications. Materials (Basel). https://doi.org/10.3390/ma10070748
253. Rasoulianboroujeni M, Fahimipour F, Shah P, Khoshroo K, Tahriri M, Eslami H, Tayebi LJMS (2019) Development of 3D-printed PLGA/TiO 2 nanocomposite scaffolds for bone tissue

engineering applications. Mater Sci Eng C 96:105–113. https://doi.org/10.1016/j.msec.2018.10.077
254. Chen X, Gao C, Jiang J, Wu Y, Zhu P, Chen G (2019) 3D printed porous PLA/nHA composite scaffolds with enhanced osteogenesis and osteoconductivity in vivo for bone regeneration. Biomed Mater 14. https://doi.org/10.1088/1748-605X/ab388d
255. Huang B, Vyas C, Roberts I, Poutrel QA, Chiang WH, Blaker JJ, Bártolo P (2019) Fabrication and characterisation of 3D printed MWCNT composite porous scaffolds for bone regeneration. Mater Sci Eng C 98:266–278. https://doi.org/10.1016/j.msec.2018.12.100
256. Manzoor F, Golbang A, Jindal S, Dixon D, McIlhagger A, Harkin-Jones E, Mancuso E (2021) 3D printed PEEK/HA composites for bone tissue engineering applications: effect of material formulation on mechanical performance and bioactive potential. J Mech Behav Biomed Mater 121:104601. https://doi.org/10.1016/j.jmbbm.2021.104601
257. Han X, Yang D, Yang C, Spintzyk S, Scheideler L, Li P, Rupp F (2019) Carbon fiber reinforced PEEK composites based on 3D-printing technology for orthopedic and dental applications. J Clin Med 8:1–17. https://doi.org/10.3390/jcm8020240
258. Ryan KR, Down MP, Banks CE (2021) Future of additive manufacturing: overview of 4D and 3D printed smart and advanced materials and their applications. Elsevier BV
259. Valino AD, Dizon JRC, Espera AH, Chen Q, Messman J, Advincula RC (2019) Advances in 3D printing of thermoplastic polymer composites and nanocomposites. Prog Polym Sci 98:101162. https://doi.org/10.1016/j.progpolymsci.2019.101162
260. Kalsoom U, Nesterenko PN, Paull B (2016) Recent developments in 3D printable composite materials. RSC Adv 6:60355–60371. https://doi.org/10.1039/c6ra11334f
261. Shemelya C, De La Rosa A, Torrado AR, Yu K, Domanowski J, Bonacuse PJ, Roberson DA (2017) Anisotropy of thermal conductivity in 3D printed polymer matrix composites for space based cube satellites. Addit Manuf 16:186–196. https://doi.org/10.1016/j.addma.2017.05.012
262. Wang X, Jiang M, Zhou Z, Gou J, Hui D (2017) 3D printing of polymer matrix composites: a review and prospective. Compos Part B Eng 110:442–458. https://doi.org/10.1016/j.compositesb.2016.11.034
263. Gibbons GJ, Williams R, Purnell P, Farahi E (2010) 3D Printing of cement composites. Adv Appl Ceram 109:287–290. https://doi.org/10.1179/174367509X12472364600878
264. Zareiyan B, Khoshnevis B (2017) Interlayer adhesion and strength of structures in contour crafting - effects of aggregate size, extrusion rate, and layer thickness. Autom Constr 81:112–121. https://doi.org/10.1016/j.autcon.2017.06.013
265. Zhang W, Melcher R, Travitzky N, Bordia RK, Greil P (2009) Three-dimensional printing of complex-shaped alumina/ glass composites. Adv Eng Mater 11:1039–1043. https://doi.org/10.1002/adem.200900213
266. Le Duigou A, Castro M, Bevan R, Martin N (2016) 3D printing of wood fibre biocomposites: from mechanical to actuation functionality. Mater Des 96:106–114. https://doi.org/10.1016/j.matdes.2016.02.018
267. Paul SC, Tay YWD, Panda B, Tan MJ (2018) Fresh and hardened properties of 3D printable cementitious materials for building and construction. Arch Civ Mech Eng 18:311–319. https://doi.org/10.1016/j.acme.2017.02.008
268. Minas C, Carnelli D, Tervoort E, Studart AR (2016) 3D printing of emulsions and foams into hierarchical porous ceramics. Adv Mater 28:9993–9999. https://doi.org/10.1002/adma.201603390
269. Zou R, Xia Y, Liu S, Hu P, Hou W, Hu Q, Shan C (2016) Isotropic and anisotropic elasticity and yielding of 3D printed material. Compos Part B Eng 99:506–513. https://doi.org/10.1016/j.compositesb.2016.06.009
270. Guessasma S, Belhabib S, Nouri H, Ben Hassana O (2016) Anisotropic damage inferred to 3D printed polymers using fused deposition modelling and subject to severe compression. Eur Polym J 85:324–340. https://doi.org/10.1016/j.eurpolymj.2016.10.030
271. Jagadeesh P, Thyavihalli Girijappa YG, Puttegowda M, Rangappa SM, Siengchin S (2020) Effect of natural filler materials on fiber reinforced hybrid polymer composites: an overview. J Nat Fibers 00:1–16. https://doi.org/10.1080/15440478.2020.1854145
272. Niendorf T, Leuders S, Riemer A, Richard HA, Tröster T, Schwarze D (2013) Highly anisotropic steel processed by selective laser melting. Metall Mater Trans B Process Metall Mater Process Sci 44:794–796. https://doi.org/10.1007/s11663-013-9875-z
273. Mühler T, Gomes CM, Heinrich J, Günster J (2015) Slurry-based additive manufacturing of ceramics. Int J Appl Ceram Technol 12:18–25. https://doi.org/10.1111/ijac.12113
274. Zocca A, Colombo P, Gomes CM, Günster J (2015) Additive manufacturing of ceramics: issues, potentialities, and opportunities. J Am Ceram Soc 98:1983–2001. https://doi.org/10.1111/jace.13700
275. He Z, Chen Y, Yang J, Tang C, Lv J, Liu Y, Hui D (2017) Fabrication of polydimethylsiloxane films with special surface wettability by 3D printing. Compos Part B Eng 129:58–65. https://doi.org/10.1016/j.compositesb.2017.07.025
276. Quan Z, Suhr J, Yu J, Qin X, Cotton C, Mirotznik M, Chou TW (2018) Printing direction dependence of mechanical behavior of additively manufactured 3D preforms and composites. Compos Struct 184:917–923. https://doi.org/10.1016/j.compstruct.2017.10.055
277. Coniglio N, Sivarupan T, El Mansori M (2018) Investigation of process parameter effect on anisotropic properties of 3D printed sand molds. Int J Adv Manuf Technol 94:2175–2185. https://doi.org/10.1007/s00170-017-0861-5
278. Yin S, Jacobsen AJ, Wu L, Nutt SR (2013) Inertial stabilization of flexible polymer micro-lattice materials. J Mater Sci 48:6558–6566. https://doi.org/10.1007/s10853-013-7452-0
279. Maskery I, Aboulkhair NT, Aremu AO, Tuck CJ, Ashcroft IA (2017) Compressive failure modes and energy absorption in additively manufactured double gyroid lattices. Addit Manuf 16:24–29. https://doi.org/10.1016/j.addma.2017.04.003
280. Jagadeesh P, Puttegowda M, Mavinkere Rangappa S, Siengchin S (2021) Influence of nanofillers on biodegradable composites: a comprehensive review. Polym Compos 42:5691–5711. https://doi.org/10.1002/pc.26291
281. Harris JA, Winter RE, McShane GJ (2017) Impact response of additively manufactured metallic hybrid lattice materials. Int J Impact Eng 104:177–191. https://doi.org/10.1016/j.ijimpeng.2017.02.007
282. Goyanes A, Det-Amornrat U, Wang J, Basit AW, Gaisford S (2016) 3D scanning and 3D printing as innovative technologies for fabricating personalized topical drug delivery systems. J Control Release 234:41–48. https://doi.org/10.1016/j.jconrel.2016.05.034
283. Ursan I, Chiu L, Pierce A (2013) Three-dimensional drug printing: a structured review. J Am Pharm Assoc 53:136–144. https://doi.org/10.1331/JAPhA.2013.12217
284. Hossainy S, Prabhu S (2008) A mathematical model for predicting drug release from a biodurable drug-eluting stent coating. J Biomed Mater Res Part A 87:487–493. https://doi.org/10.1002/jbm.a.31787
285. Campbell I, Bourell D, Gibson I (2012) Additive manufacturing: rapid prototyping comes of age. Rapid Prototyp J 18:255–258. https://doi.org/10.1108/13552541211231563
286. Sharma R, Singh R, Penna R, Fraternali F (2018) Investigations for mechanical properties of Hap, PVC and PP based 3D porous structures obtained through biocompatible FDM filaments.

Compos Part B Eng 132:237–243. https://doi.org/10.1016/j.compositesb.2017.08.021
287. Burn MB, Ta A, Gogola GR (2016) Three-dimensional printing of prosthetic hands for children. J Hand Surg Am 41:e103–e109. https://doi.org/10.1016/j.jhsa.2016.02.008
288. Mannoor MS, Jiang Z, James T, Kong YL, Malatesta KA, Soboyejo WO, McAlpine MC (2013) 3D printed bionic ears. Nano Lett 13:2634–2639. https://doi.org/10.1021/nl4007744
289. Edgar J, Tint S (2015) Additive manufacturing technologies: 3D printing, rapid prototyping, and direct digital manufacturing. 2nd Edition. Johnson Matthey Technol Rev 59:193–198. https://doi.org/10.1595/205651315X688406
290. Turco E, Golaszewski M, Giorgio I, D'Annibale F (2017) Pantographic lattices with non-orthogonal fibres: experiments and their numerical simulations. Compos Part B Eng 118:1–14. https://doi.org/10.1016/j.compositesb.2017.02.039
291. Naddeo F, Cappetti N, Naddeo A (2017) Novel "load adaptive algorithm based" procedure for 3D printing of cancellous bone-inspired structures. Compos Part B Eng 115:60–69. https://doi.org/10.1016/j.compositesb.2016.10.033
292. Imbalzano G, Linforth S, Ngo TD, Lee PVS, Tran P (2018) Blast resistance of auxetic and honeycomb sandwich panels: comparisons and parametric designs. Compos Struct 183:242–261. https://doi.org/10.1016/j.compstruct.2017.03.018
293. Imbalzano G, Tran P, Ngo TD, Lee PVS (2017) Three-dimensional modelling of auxetic sandwich panels for localised impact resistance. J Sandw Struct Mater 19:291–316. https://doi.org/10.1177/1099636215618539
294. Ren X, Shen J, Tran P, Ngo TD, Xie YM (2018) Design and characterisation of a tuneable 3D buckling-induced auxetic metamaterial. Mater Des 139:336–342. https://doi.org/10.1016/j.matdes.2017.11.025
295. Parthasarathy J, Starly B, Raman S (2011) A design for the additive manufacture of functionally graded porous structures with tailored mechanical properties for biomedical applications. J Manuf Process 13:160–170. https://doi.org/10.1016/j.jmapro.2011.01.004
296. Bartlett NW, Tolley MT, Overvelde JTB, Weaver JC, Mosadegh B, Bertoldi K, Wood RJ (2015) Robot powered by combustion. Science 80(349):161–165. https://doi.org/10.1126/science.aab0129
297. Zarek M, Layani M, Cooperstein I, Sachyani E, Cohn D, Magdassi S (2016) 3D printing of shape memory polymers for flexible electronic devices. Adv Mater 28:4449–4454. https://doi.org/10.1002/adma.201503132
298. Mohamed OA, Masood SH, Bhowmik JL (2016) Optimization of fused deposition modeling process parameters for dimensional accuracy using I-optimality criterion. Meas J Int Meas Confed 81:174–196. https://doi.org/10.1016/j.measurement.2015.12.011
299. Parandoush P, Lin D (2017) A review on additive manufacturing of polymer-fiber composites. Compos Struct 182:36–53. https://doi.org/10.1016/j.compstruct.2017.08.088